X-RAY AND GAMMA-RAY COMPTON SCATTERING

by

Philip Pattison

A thesis submitted for the degree of
Doctor of Philosophy of the
University of Warwick

Dept. of Physics,
University of Warwick.

April, 1975.

CONTENTS

CHAPTER 1	PRINCIPLES OF COMPTON SCATTERING	1
	1.1 General Introduction	1
	1.2 Photon-electron Scattering	6
	1.3 The Compton Profile	14
	References	22
CHAPTER 2	EXPERIMENTAL METHOD	24
	2.1 General Considerations	24
	2.2 The X-ray Technique	27
	2.2.1 Apparatus	27
	2.2.2 Data processing	30
	2.3 The Gamma-ray Technique	32
	2.3.1 A comparison of x-ray and gamma-ray techniques	33
	2.3.2 Apparatus	36
	2.3.3 Data processing	39
	References	45
CHAPTER 3	INVESTIGATION OF MULTIPLE SCATTERING	46
	3.1 Introduction	46
	3.2 Experimental Investigation	47
	3.2.1 Variation with sample thickness	47
	3.2.2 Offset-beam measurements	48
	3.2.3 Cross section ratio	51
	3.3 Analytical Results for X-rays	52
	3.3.1 Review of DuMond's results for [2.2] scattering by stationary electrons	53
	3.3.2 Extension of DuMond's results to include moving electrons	55
	3.3.3 Calculation of the spectral distribution for [2,1] scattering	57
	3.3.4 Spectral distribution for [2,1] scattering from moving electrons	58
	3.3.5 Limitations of the theory	60
	3.3.6 Conclusions	61
	3.4 The Monte Carlo Approach	63
	3.4.1 The Monte Carlo procedure	65
	3.4.2 Results for stationary electrons	69
	References	72
CHAPTER 4	APPLICATIONS OF THE MONTE CARLO METHOD	73
	4.1 A Survey of Multiple Scattering	74
	4.2 Application to Experimental Compton Profiles	77

4.3 The Cross Section Ratio 80
4.3.1 Total cross sections for inelastic and elastic scattering 82
4.3.2 Experimental 84
4.3.3 Conclusions 86
4.4 Further Developments 87
References 89

CHAPTER 5 THE COMPTON PROFILE OF ALUMINIUM 90

5.1 Background 90
5.2 The X-ray Measurement 93
5.2.1 Experimental 93
5.2.2 Data reduction 94
5.2.3 Discussion 96
5.3 The Gamma-ray Measurement 98
5.3.1 Experimental and data processing 98
5.3.2 Multiple scattering correction 99
5.3.3 Results and discussion 100
References 102

CHAPTER 6 MOLECULAR COMPTON PROFILES 103

6.1 Introduction 103
6.2 Experimental 105
6.3 Results and Discussion 107
6.3.1 Formamide and p-benzoquinone 107
6.3.2 Decaborane 109
References 111

CHAPTER 7 CONCLUSIONS AND DEVELOPMENTS 112

7.1 General Conclusions 112
7.2 Developments in the Experimental Method 117
7.2.1 X-ray experiments
7.2.2 Gamma-ray experiments 118
7.2.3 Alternative experiments 120
7.3 Future Applications 122
References 127

APPENDIX I 128

APPENDIX II 132

References 135

Acknowledgements

I would like to thank my supervisor Dr. Malcolm Cooper for his help and encouragement throughout my period of research. Additionally, I have benefited from valuable contacts with many people whose approach to the work has been stimulating and refreshing.

In particular, I am indebted to Dr. Brian Williams who introduced me to this field, and whose ideas inspired much of the work described in this thesis. I am grateful to both Dr. Joshua Felsteiner and Dr. Seppo Manninen whose friendly cooperation has been invaluable. Dr. Irving Epstein and Dr. Wolf Weyrich assisted me greatly in understanding and interpreting the study of molecular systems, and I am grateful to Dr. Peter Lindner for communicating his theoretical results to me prior to publication. I would also like to thank Prof. Malcolm Wallbridge who prepared the sample of decaborane.

I thank Prof. A.J. Forty for allowing me to use the facilities of the Dept. of Physics, and the Science Research Council for providing a Research Studentship. Finally, I wish to express my gratitude to Mrs. Joan Cooper for her careful typing of the manuscript.

Memorandum

This dissertation is submitted to the University of Warwick in support of my application for admission to the degree of Doctor of Philosophy. It contains an account of my own work performed at the Department of Physics of the University of Warwick in the period from October 1972 to March 1975 under the supervision of Dr. M.J. Cooper. No part of it has been used previously in a degree thesis submitted to this or any other University. The work described in this thesis is the result of my own independent research except where acknowledged in the text. An account of the work on multiple x-ray scattering has been published in Phil. Mag., 30, 307, and the extension to gamma-rays in Phil. Mag., 30, 537. The survey of multiple scattering described in Chapter 4 has been accepted for publication in Nuc. Instrum. Methods. The study of the Compton profile of aluminium has been published in Phil. Mag., 29, 1237, and Phil. Mag., 30, 973. The work on molecular Compton profiles given in Chapter 6 has been submitted for publication to Chem. Phys. Lett., and Chem. Comm. The symmetric method for separating x-ray doublets described in Appendix I has been published in J. Phys. E., 7, 516.

April, 1975. P. Pattison

ABSTRACT

The Compton profile which can be obtained from the energy loss spectrum of inelastically scattered photons provides a measure of the momentum distribution of electrons in matter. The use of a solid state detector to analyze the spectrum of scattered gamma-rays has many advantages over the earlier system which employed an x-ray tube and crystal spectrometer. A description of the experimental arrangement and data processing procedures is given for both techniques, with emphasis on the newer gamma-ray method.

It is shown that the presence of multiple photon scattering has led to serious systematic errors in almost every experimental profile published up to the present time. A theoretical treatment, with the use of approximate analytical formulae, is found to be too limited. Instead a Monte Carlo approach is adopted; this provides a general method for calculating the contribution from multiple scattering in most experimental conditions.

The predictions of the Monte Carlo procedure are tested by removing multiple scattering effects from experimental profiles, and the resulting corrected curves are found to be independent of the sample geometry. Moreover, a corrected Compton profile of water shows very good agreement with a recent near Hartree-Fock calculation. Further confirmation came from a measurement of the ratio of total elastic and Compton cross sections, which provides an experimental figure for the total amount of multiple scattering.

Several experimental profiles are reported, and in each case multiple scattering is important. An x-ray profile of

aluminium shows marked disagreement with theoretical profiles, whereas a corrected profile measured with 60 keV gamma-rays is in excellent agreement with an interacting electron gas model. Gamma-ray profiles are also obtained for several molecular systems (formamide, p-benzoquinone and decaborane) and the data is used to assess the reliability of localised molecular orbital and semi-empirical descriptions of these complex systems.

Author's note

Notation and Units: Symbols are explained where they occur in the text. In general $(E,\bar{p})$ are the electronic and $(\omega,\bar{k})$ are the photon properties of energy and momentum. Subscripts 1 and 2 refer to initial and final states, respectively. For historical reasons atomic units (a.u.) in which $m = e = \hbar = 1$ are normally used in this thesis. Where the text departs from this procedure for reasons of clarity or simplicity, the alternative units are clearly defined.

CHAPTER 1

PRINCIPLES OF COMPTON SCATTERING

1.1 General Introduction

Information on the scattering of x-rays and gamma-rays has profoundly influenced our current concepts concerning the structure and behaviour of matter. The principal mechanism which provides this information is the photon-electron interaction. An x-ray or gamma-ray photon can interact with matter by any one of several competing mechanisms. The interaction can be with the entire atom (e.g. the photoelectric effect and Rayleigh scattering), or with one electron in the atom (e.g. the Compton effect and pair production) or with the atomic nucleus.

In the Compton effect some of the energy is absorbed and appears as kinetic energy of a Compton recoil electron, while the balance of the incident energy emerges as a Compton scattered photon. The energy of the scattered photon will depend on the initial energy and momentum both of the photon and the atomic electron. It is this relation between the initial electron momentum and the final photon energy that enables Compton scattering to probe the behaviour of electrons in matter.

In 1923 Compton[1] demonstrated the essential duality of waves and particles by his interpretation of the wavelength shift observed when x-rays are scattered by atomic electrons. X-rays, whose wave properties accounted for their diffraction in crystals, were shown to possess the properties of energy and momentum associated with particles. Initially Compton interpreted these results in terms of the interaction of a

photon with a free stationary electron. It was soon clear that the energy distribution of the scattered photons was too broad to be explained simply in terms of instrumental resolution. Jauncey[2] first suggested that the line width was related to the initial momentum of the electron. However, it was not until DuMond[3] produced a description of the interaction in terms of a Doppler-broadening that the effects of electron momentum were generally recognised. DuMond has given a review of the experimental and theoretical work up to 1933[4].

Once the influence of the electron momentum on the photon energy distribution had been established, the way was open for a direct comparison between theory and experiment. Accurate wave functions for hydrogen and helium were calculated by Hicks[5] in 1937, and a measurement of the Compton line shape was undertaken by DuMond and Kirkpatrick[6]. These experiments required immense skill and patience (the measurements took 2000 hours). The resulting good qualitative agreement with the theoretical profile confirmed the potential of the technique as a method of studying the electron momentum distribution, and hence the electronic wave function.

Despite these promising results, there followed a dormant experimental period between 1940 and 1965. The daunting practical difficulties were probably responsible in part for this lack of interest in x-ray Compton scattering, coupled with the success of the x-ray technique of structure analysis by diffraction. Following the revival in 1965[7], a series of experiments of a largely qualitative nature demonstrated the wide range of systems which could be studied with the technique. As experience was gained in experimental and analytical procedures, several systematic studies were under-

taken on such systems as metals, ionic solids and molecules. The progress in x-ray Compton scattering during this period has been covered in an extensive review by Cooper[8], which includes a detailed description of the experimental method and a summary of the historical background and development of the technique.

The work which was done at this time was largely directed at 'interesting' but rather complex materials; cyclohexane and polythene are examples[9]. Hence, there was no reliable theory which could provide a means of assessing the accuracy of the experimental results. It was not until 1970 that the experiment of DuMond and Kirkpatrick was repeated, and a careful measurement was made by Eisenberger[10] of the electron momentum density in He and H_2. The results were compared with theoretical calculations based on Hartree-Fock self-consistent-field wave functions. The close agreement between theory and experiment for He justified the accuracy claimed in the experimental results, while for H_2 certain discrepancies were attributed to the effects of binding and the electron-electron interaction.

Thus the technique was developing into a quantitative tool, capable of accurately determining the momentum distribution of atomic electrons. Unfortunately, although the power available from commercial x-ray generators has greatly increased, the x-ray technique is still laborious, requiring long measuring times and substantial processing of the experimental data. Interest in making experimental measurements was therefore confined to a few laboratories. Where there were significant differences in the results obtained by various groups this was generally attributed to the difficulties of the experimental method, or uncertainties in the correct form for

the data processing and deconvolution procedures.

The possibility of using a gamma-ray source in Compton scattering experiments had been suggested by Hulubei[11] as early as 1934. However, the low flux and higher energy which is available from a gamma source makes spectral analysis with a crystal spectrometer quite impractical. It was not until the advent of high resolution solid state detectors that gamma-ray experiments became feasible. An early demonstration of the technique was reported by McIntyre[12] in 1967, using gamma-rays from a Co^{60} source and a Ge(Li) detector. In a series of papers in 1970 and 1971 Felsteiner, Fox and Kahane[13] describe measurements of the electron momentum distribution in graphite and aluminium using an Am^{241} source with an energy of 60 keV. The use of gamma-rays and a solid state detector has many advantages over the older system of an x-ray tube and crystal spectrometer. The technique was therefore soon adopted by several groups, and in 1972 Eisenberger and Reed[14] made a measurement of a series of inert gases in which a 160 keV Te^{123m} source was used. This again gave a basis for evaluating the accuracy of the technique and demonstrated the good agreement between the x-ray and gamma-ray results for He. The experimental methods used in both of these techniques are described in Chapter 2, with particular emphasis on the gamma-ray system which was designed in this laboratory.

The enormous reduction in the length of an experiment is one of the major advantages of the gamma-ray technique. Indeed, because of the large photoelectric absorption, measurements with x-rays ($\sim$20 keV) are mainly limited to systems containing elements with atomic number less than about 13. Since with gamma-rays accurate experimental data

can be obtained in a comparatively short time, it became practical to make a series of measurements on the same material to investigate the effect of varying sample dimensions. In 1972 Reed and Eisenberger[15] reported that the measured line shape could depend strongly on the sample scattering volume and attributed this result to the effect of multiple scattering, i.e. the detection of photons which have suffered more than one collision before leaving the sample. It was soon established that multiple scattering was a major source of systematic error,[16,17] and probably accounted for many of the anomalies in earlier results.

The possibility that multiple scattering could give rise to significant errors in Compton measurements had been pointed out by DuMond[18] in 1930, and in 1934 Hulubei[11] had made an experimental investigation of the multiple scattering of x-rays. The neglect of this source of error prior to 1972 reflects the exploratory nature of the earlier experiments. Efforts were made to compensate for these effects by measuring the variation of the line shape with sample thickness, or by using very thin samples. However, these empirical methods provide no satisfactory means of assessing the reliability of the final result, and the need to repeat measurements or use thin samples greatly increases the length of an experiment. It became necessary therefore to establish a general method for correcting measured profiles for the effects of multiple scattering.

An extension of the theory of DuMond on the multiple scattering of x-rays is given in Chapter 3, where approximate classical formulae are used to produce analytic solutions. Such approximations are not valid at higher energies (where gamma-rays are used), nor is it practical to obtain exact analytic solutions at those energies. Therefore a Monte

Carlo approach has been adopted, with the object of calculating the effect of multiple scattering with sufficient accuracy to enable a reliable correction to be made directly to the experimental data. The Monte Carlo procedure is described in detail in Chapter 3, and some applications of this method are reported in the following chapter. In the experimental results which are given in Chapters 5 and 6, each of the gamma-ray measurements has been corrected for multiple scattering using the Monte Carlo method. Where a comparison with previous results is possible (e.g. for aluminium), there is a considerable improvement in the agreement with the theoretical model and multiple scattering is shown to be responsible for many effects which were earlier attributed to such physical properties as electron-electron correlations[19].

At the level of accuracy and reliability which can now be obtained in Compton scattering measurements of electron momentum distributions, the technique provides a powerful tool for testing electronic wave function calculations. Much of the recent theoretical work has been concentrated on molecular wave functions, and measurements on a series of molecular systems are described below. The success of Compton scattering as a means of establishing the accuracy of the various wave function representations can be seen from these results.

1.2 Photon-electron scattering

There are many possible interactions between electromagnetic radiation and electrons. In the energy range of interest here (0.01-0.5 MeV) the principal mechanisms are photoelectric absorption, coherent or Rayleigh scattering and Compton scattering. The nature of these interactions is the subject of an extensive review by Evans[20], and a

more rigorous treatment is given by Jauch and Rohrlich[21].

In the case of photoelectric absorption the incident photon disappears and an electron is ejected from the atom. The ejected electron carries away all the energy of the absorbed photon minus the binding energy. The photoelectric cross section is roughly proportional to Z^4/ω_1^3 where Z is the atomic number and ω_1 the incident photon energy. The importance of this process in Compton scattering experiments is mainly seen in its effect on the intensity of the scattered radiation. The photoelectric effect competes with Compton scattering (particularly for materials with high atomic number Z) and removes photons from the incident and scattered beams.

If an electron is assumed to be initially free and at rest, the differential scattering cross section is given by the Klein-Nishina formula[22],

$$d\sigma_{KN}(\omega_1,\Theta) = \frac{1}{4} r_o^2 d\Omega \left(\frac{\omega_2}{\omega_1}\right)^2 \left(\frac{\omega_1}{\omega_2}+\frac{\omega_2}{\omega_1}-2+4\cos^2\Theta\right) \qquad 1\text{-}1$$

where Θ is the angle between the electric vectors of the incident and scattered photons, r_o is the classical electron radius, $d\Omega$ is the element of solid angle through which the photon emerges after the collision and ω_1, ω_2 are the energies of the initial and final photons respectively. The relation between ω_1 and ω_2 is given by

$$\frac{\omega_1}{\omega_2} = 1 + \frac{\omega_1}{m_o c^2}\left(1-\cos\Theta\right) \qquad 1\text{-}2$$

where Θ is the scattering angle and $m_o c^2$ is the electron rest energy. For the case of unpolarized incident radiation, the Klein-Nishina formula reduces to

$$d\sigma_{KN}(\omega_1,\Theta) = \frac{1}{2} r_o^2 d\Omega \left(\frac{\omega_2}{\omega_1}\right)^2 \left(\frac{\omega_1}{\omega_2}+\frac{\omega_2}{\omega_1}-\sin^2\Theta\right) \qquad 1\text{-}3$$

In an atom, however, electrons are bound to the

nucleus. Where the electron recoil energy would be comparable with, or smaller than, the electron binding energy, the electron may fail to be ejected from the atom. Such collisions will reduce the average collision cross section to something less than the Klein-Nishina value. Assuming each electron in the atom acts independently, the scattering per atom is the sum of the intensities of the scattering by individual electrons. The scattering is therefore described as incoherent. The differential incoherent scattering cross section per atom can be written as

$$\frac{d\sigma}{d\Omega}_{incoh} = \left(\frac{d\sigma_{KN}}{d\Omega}\right) Z\, S(q,Z) \qquad 1\text{-}4$$

where S is the incoherent scattering function associated with an element of atomic number Z where there is a momentum transfer q. S represents the probability that the scattered photon will leave the atom in an ionized state. Exceptionally the electron may be raised to an excited state rather than the continuum, and this process is called Raman scattering.

If an electron makes no transition then the atom as a whole takes up the electron recoil momentum and, since the atomic mass is relatively large, this corresponds to negligible energy absorption, i.e. elastic scattering. Under these conditions constructive interference exists between the scattering from individual electrons, and the process is called coherent or Rayleigh scattering. On the other hand, Compton collisions involve only incoherent scattering in which each electron acts entirely independently.

The probability for the whole atom taking up the recoil momentum can be expressed approximately through the use of an atomic form factor $f(q,Z)$. This is the sum of the electronic form factors, and represents the ratio of the amplitude

of the coherent scattering by an entire atom to the amplitude of the scattering by a single free electron. The atomic form factor is related to the electronic wave function $\psi_i(r)$ by

$$f(q,Z) = \sum_i \int |\psi_i|^2 e^{i\bar{q}\cdot\bar{r}_i} d\bar{r}_i \qquad 1\text{-}5$$

where $\bar{r}_i$ is the position of the i^{th} electron and $\bar{q} = \bar{k}_2 - \bar{k}_1$, where $\bar{k}_1$ and $\bar{k}_2$ are the momenta of the incident and scattered photons. This probability amplitude $f(q,Z)$ can be combined with the Klein-Nishina cross section for scattering by a single free electron. For elastic scattering $\omega_1 = \omega_2$ and the resultant differential coherent scattering cross section per atom is given by

$$\frac{d\sigma_{coh}}{d\Omega} = \frac{r_e^2}{2}(1+\cos^2\theta)\left[f(q,Z)\right]^2 \qquad 1\text{-}6$$

The elastic, coherent Rayleigh scattering described above relates only to scattering from randomly positioned atoms. Where there is spatial structure of the type found in crystals then there may be intense scattering in particular directions (Bragg scattering), due to constructive interference of the radiation scattered from different atoms. The high intensity obtained in Bragg scattering makes the technique of x-ray diffraction particularly attractive. The intensity of Bragg reflections depends upon the structure factor, which describes the phase relationship between the scattering from different atoms. However, the scattering from each atom (the atom form factor) depends principally upon the electronic spatial density distribution $|\psi_i|^2$ (see equation 1-5). Since atomic electron density distributions are concentrated around the core, the outer electrons make

little contribution to the Bragg scattering. Fig. 1-1 shows the calculated free atom form factors for the ten 'neon core' electrons of aluminium and the three outer or bonding electrons[23]. The arrow indicates the $(\sin\Theta/\lambda)$ value of the lowest order Bragg reflection (111). For the case of aluminium the form factor of the outer electrons never contributes more than about 1% to the total form factor at the Bragg peaks. Thus, although structure factor measurements can be very successfully used to establish the crystal structure, information about the atomic electrons is mainly limited to those in the region of the core. Moreover, these core electrons are generally unaffected by the atomic environment and can be well described by a free-atom model.

In the derivation of the Klein-Nishina formula (eqn. 1-1), the electron is assumed to be free and at rest. It has proved to be almost impossible to obtain a cross section for Compton scattering from a bound electron without making certain assumptions. A major simplification is contained in the impulse approximation, where the binding energy of the electron E_B is taken to be much smaller than the electron recoil energy E_R gained in the scattering process. It has been pointed out[24] that this is equivalent to assuming that the electron is moving in a constant potential, and can therefore be regarded as free. When the incident photon energy is low, or the scattering angle small, then E_B may be of the same order as E_R and the impulse approximation will break down. This partly explains why measurements with conventional x-ray sources (e.g. MoKα) have been concentrated on systems in the first row of the periodic table where the impulse approximation has been shown to hold reasonably well for typical x-ray

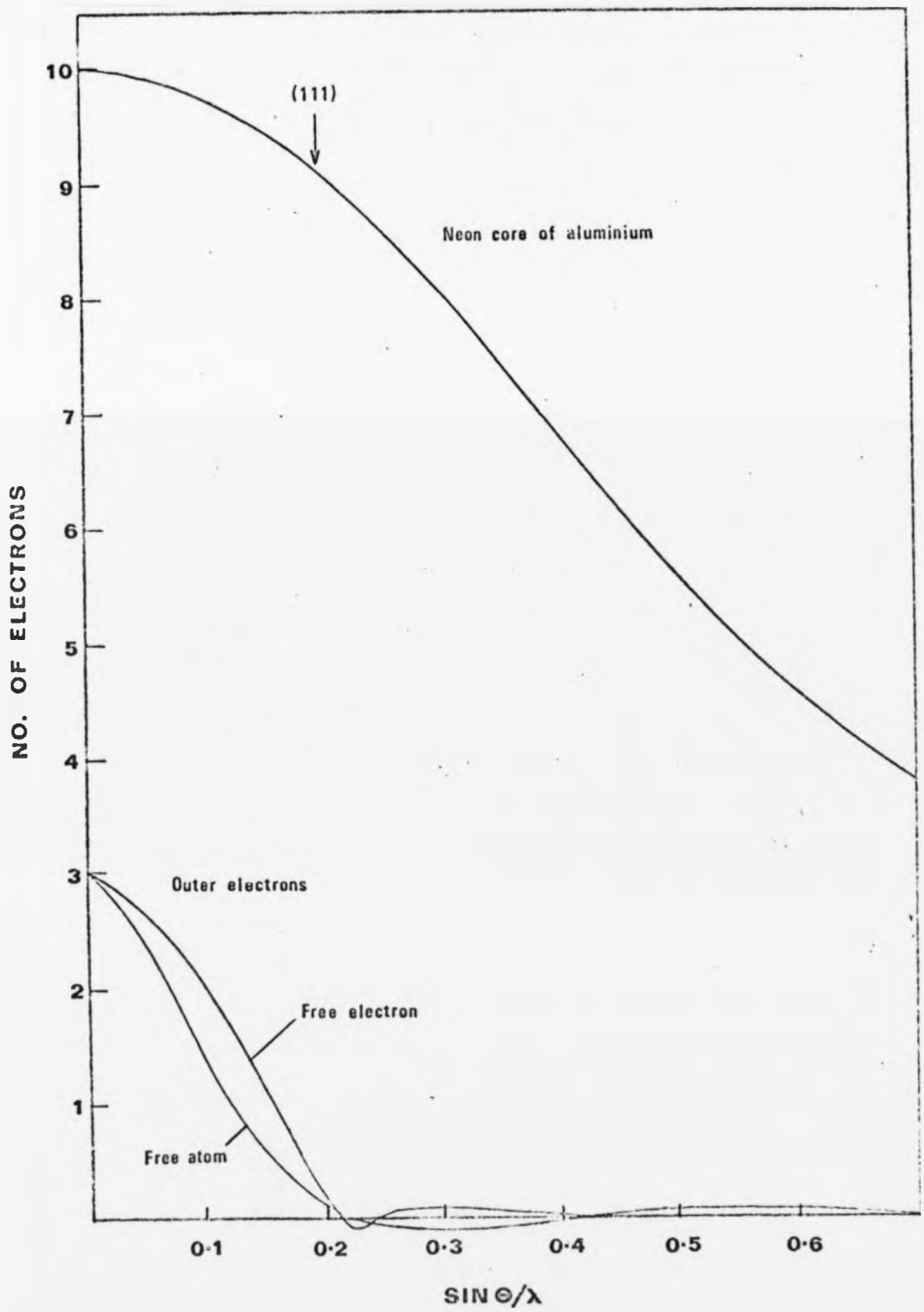

Fig. 1-1: Hartree-Fock free atom form factor curve for aluminium showing the outer and core electron contributions separately. The curve corresponding to three free electrons is also given.

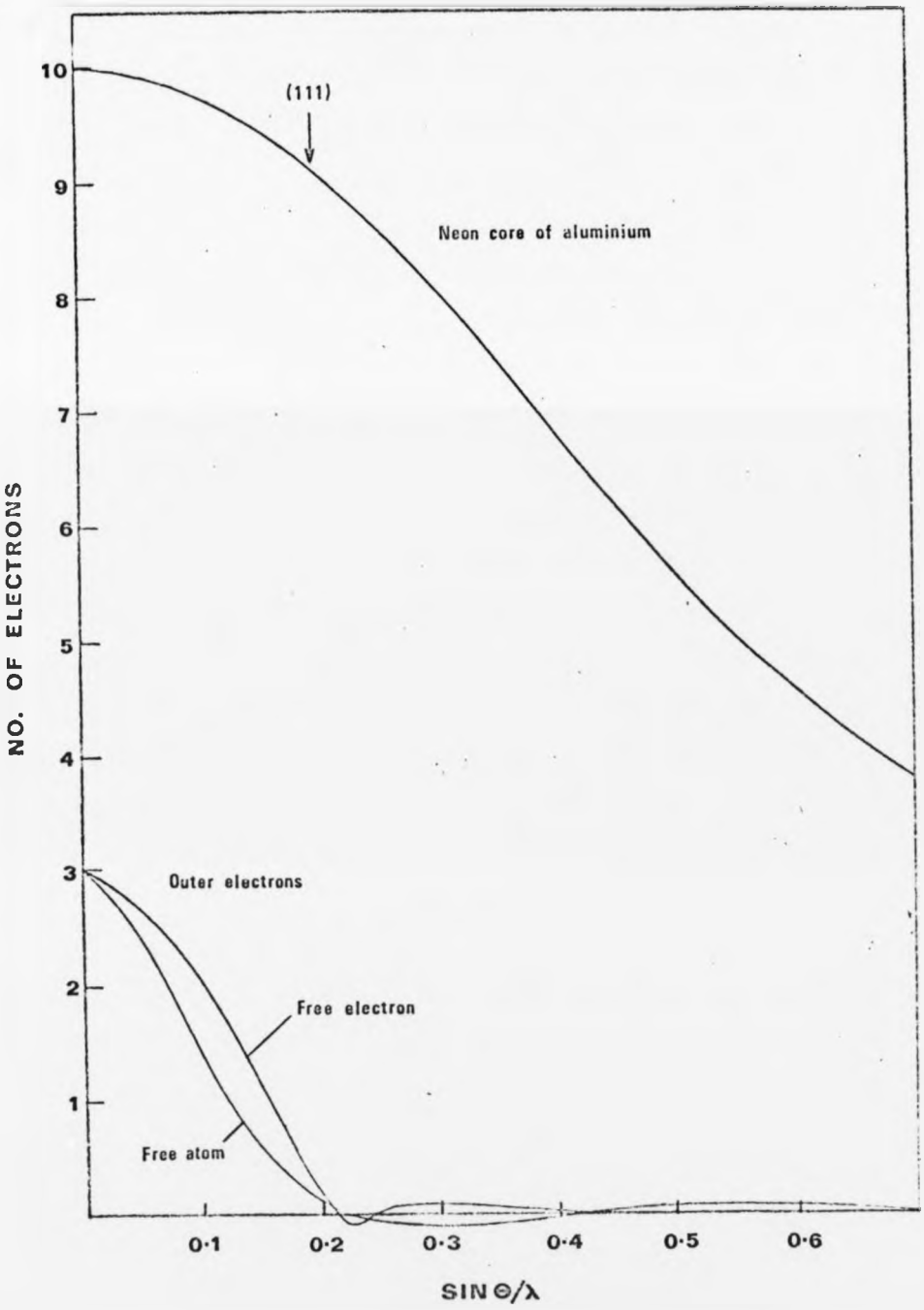

Fig. 1-1: Hartree-Fock free atom form factor curve for aluminium showing the outer and core electron contributions separately. The curve corresponding to three free electrons is also given.

energies (15-25 keV)[24]. Moreover, it will be shown later that the results of a Compton scattering experiment are relatively insensitive to the core electrons (where E_B is greatest), and the major contribution arises from the lightly bound outer electrons. Therefore some breakdown in the impulse approximation can be tolerated for the core electrons without the introduction of serious errors.

Therefore, in the impulse approximation, the required cross section must describe the interaction of photons with electrons which are free but in motion. The Klein-Nishina formula has been generalised by Jauch and Rohrlich[21] to include the case of moving electrons, and later modified to a form suitable for application in Compton scattering experiments[25,26]. Fig. 1-2 shows the geometry of the scattering event, where $(E,\bar{p})$ are electronic and $(\omega,\bar{k})$ are photon properties. Subscripts 1 and 2 refer to initial and final states respectively. The initial motion of the electron is described by $N(\bar{p}_1)$, the probability that the electron has momentum $\bar{p}_1$. The goal of a Compton scattering experiment is to extract from the measured differential cross section a description of the momentum distribution which is independent of the particular experimental conditions. The Compton profile provides such a description and can be defined as

$$J(p_z) = \iint_{-\infty}^{+\infty} \int_{p_z}^{\infty} N(\bar{p}_1)\, dp_x dp_y \qquad 1\text{-}7$$

where p_z is the projection of the initial electron momentum $\bar{p}_1$ onto the scattering vector $\bar{k}_2-\bar{k}_1$. Experimental factors such as the initial photon energy and the scattering angle modify the energy distribution of the differential cross section. These factors must be eliminated from the final result, which should contain only that part of the

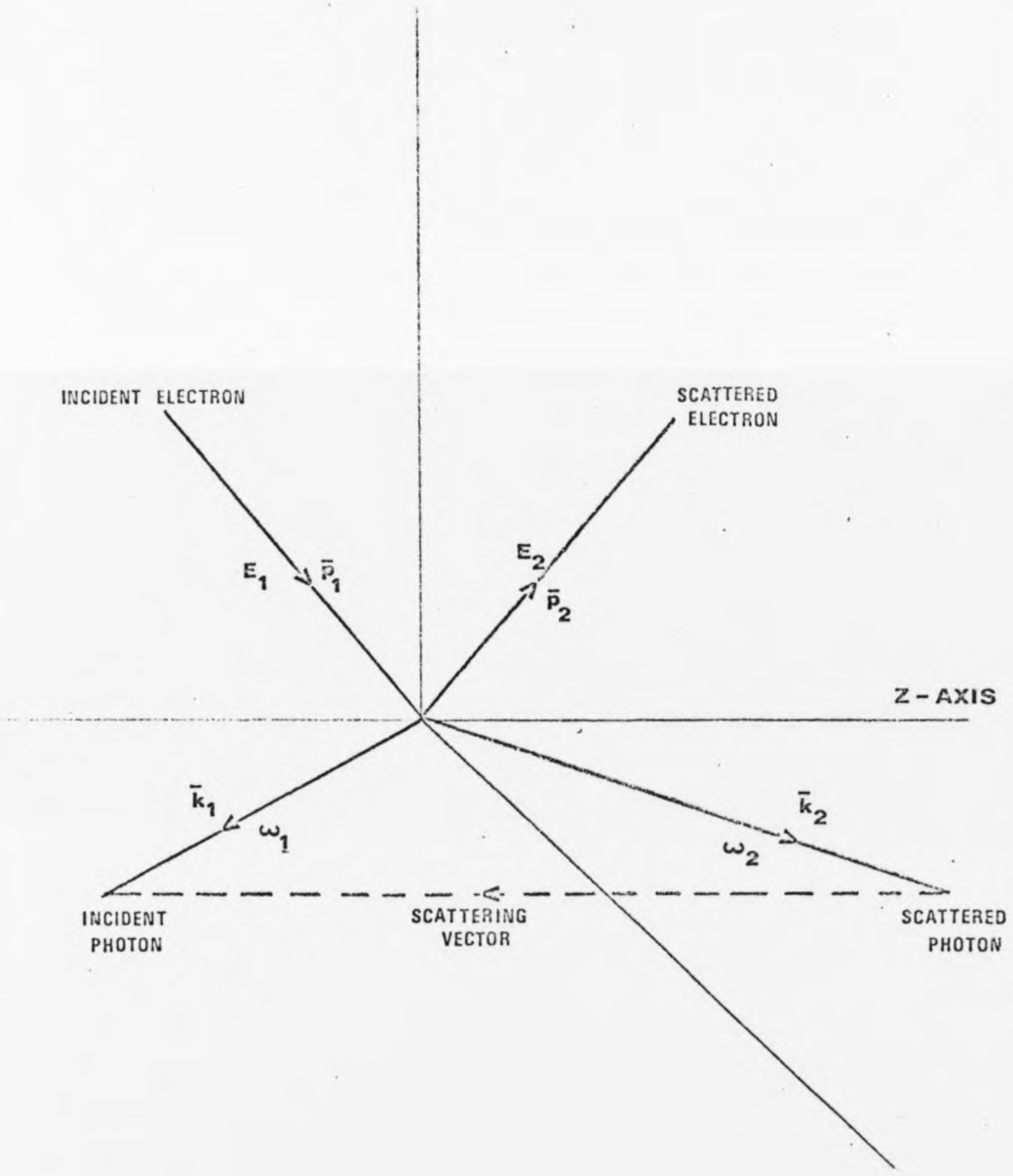

Fig. 1-2: Geometry of the photon-electron scattering event.

cross section which depends on the electron momentum. It is necessary therefore to describe the cross section in the following form:

$$\frac{d^2\sigma}{d\omega_2 d\Omega_2} = C(\omega_1, \omega_2, \theta, p_z)\, J(p_z) \qquad 1\text{-}8$$

The Compton profile, and hence the momentum dependence, may now be obtained directly from the differential Compton cross section. The derivation of this result will be outlined here in order to establish the nature of any further approximations and their effect on the reliability of experimental Compton profiles. A more detailed analysis is given by Eisenberger and Reed[25] and by Manninen, Paakkari and Kajantie[26].

Jauch and Rohrlich[21] consider the scattering of a beam of photons by a beam of moving relativistic electrons. Since in Compton scattering experiments a beam of photons is scattered from moving electrons which have a fixed centre of mass, certain modifications are necessary. If eqn. 11-9 of Jauch and Rohrlich is modified to describe the scattering from atomic electrons, the energy distribution of photons scattered at a fixed angle Θ into a solid angle $d\Omega_2$ can be written as

$$\frac{d^2\sigma}{d\omega_2 d\Omega_2} = \frac{r_e^2 m^2 \omega_2}{2E_2} \int \frac{d^3\bar{p}_1 N(\bar{p}_1)}{\omega_1 E_1} \int d^3\bar{p}_2 \, X \, \delta^4(k_1 + p_1 - k_2 - p_2) \qquad 1\text{-}9$$

where k_1, k_2, p_1 and p_2 are four-momenta, and $\hbar = c = 1$. The X is a spin factor and the δ-function arises from energy and momentum conservation. Integrating over p_2 gives,

$$\frac{d^2\sigma}{d\omega_2 d\Omega_2} = \frac{r_e^2 m^2 \omega_2}{2E_2} \int \frac{d^3\bar{p}_1 N(\bar{p}_1) X}{\omega_1 E_1} \delta\left(\omega_1 + E_1 - \omega_2 - \left[\bar{p}_1^2 + |\bar{k}_1 - \bar{k}_2|^2 + 2p_z|\bar{k}_1 - \bar{k}_2| + m^2\right]^{1/2}\right) \qquad 1\text{-}10$$

Now p_z can be defined from the δ-function in eqn. 1-10 by

$$p_z = \frac{E_1(\omega_2 - \omega_1) + \omega_1\omega_2(1-\cos\Theta)}{(\omega_1^2 + \omega_2^2 - 2\omega_1\omega_2\cos\Theta)^{1/2}} \qquad 1\text{-}11$$

where Θ is the angle between $\bar{k}_1$ and $\bar{k}_2$, the scattering angle. Integration over p_z in eqn. 1-10 leads to

$$\frac{d^2\sigma}{d\omega_2 d\Omega_2} = \frac{r_o^2 m^2 \omega_2}{2\omega_1 E_1(|\bar{k}_1 - \bar{k}_2|) + p_z(\omega_1 - \omega_2)/E_1} \int dp_{1x}\, dp_{1y}\, N(\bar{p}_1) X \qquad 1\text{-}12$$

The formula now includes a distribution of initial electron velocities $N(\bar{p}_1)$. However, this cross section is not in a form appropriate for analysing Compton scattering results, and certain difficulties are met before eqn. 1-12 can be written in the desired form of eqn. 1-8. There are two major problems:

(i) E_1 in eqns. 1-11 and 1-12 depends upon $\bar{p}_1$ rather than p_z.

(ii) The spin factor X in eqn. 1-12 depends upon both E_1 and $\bar{p}_1$.

Therefore, without further approximations, it is not possible to remove X from the integral in eqn. 1-12 and obtain the Compton profile. The necessary approximations are

(i) Replace E_1 by $m c^2$ i.e. neglect terms of order p^2/m^2.

(ii) Solve X for $\Theta = 180^\circ$, for which X depends only upon p_z.

Under these conditions $X(\bar{p}_1)$ is now a constant in the integration and can be written[26]

$$X(\bar{p}_1) = \frac{\omega_1 A_1}{\omega_2 A_2} + \frac{\omega_2 A_2}{\omega_1 A_1} + 2m\left(\frac{1}{\omega_1 A_1} - \frac{1}{\omega_2 A_2}\right) - m^2\left(\frac{1}{\omega_1 A_1} - \frac{1}{\omega_2 A_2}\right)^2 \qquad 1\text{-}13$$

$$= B$$

where $A_1 = (1+p_z/m)$ and $A_2 = (1-p_z/m)$.

The differential cross section is then given by

$$\frac{d^2\sigma}{d\omega_2 d\Omega_2} = \frac{r_0^2 m^2 \omega_2 B}{2\omega_1 E_1(\omega_1+\omega_2+p_z(\omega_1-\omega_2)/E_1)} J(p_z) \qquad 1\text{-}14$$

which is of the required form.

The approximations which were necessary to establish eqn. 1-14 will give rise to errors mainly in the core electron Compton profiles of elements with $Z > 20$ where $v/c > 0.1$. However, as will be discussed in the following section, the Compton profile is relatively insensitive to the core electrons. It is this feature which permits very reliable comparisons to be made with theoretical profiles even when certain of the above approximations may be breaking down for the most tightly bound electrons.

In the above analysis a single photon-electron collision has been investigated, and the final result describes the energy distribution of photons scattered at some angle Θ. However, it is possible that a photon may have suffered more than one collision before emerging with a total scattering angle Θ. This has been a source of considerable error in the interpretation of experimental Compton profiles in the past, and the problem of multiple scattering is the subject of Chapters 3 and 4.

1.3 The Compton Profile

It is therefore possible (with certain approximations) to obtain a description of the electron momentum distribution directly from measured Compton cross sections. This information is contained in the Compton profile (eqn. 1-7) which is the momentum dependent part of the differential cross section. The relationship between the Compton profile and the electron momentum distribution, electron

charge density and other physical parameters is the subject of this section.

The Compton profile (eqn. 1-7) can be written

$$J_j(p_z) = \iint_{-\infty}^{+\infty} \int_{p_z}^{\infty} |\chi_j(\bar{p})|^2 \, dp_x \, dp_y \qquad 1\text{-}15$$

where $J_j(p_z)$ is the Compton profile for each one-electron orbital j, whose ground state momentum wave function is $\chi_j(\bar{p})$. Hence, although the Compton profile does not yield directly any single physical parameter, it can easily be related to the momentum density $|\chi_j(\bar{p})|^2$. Moreover, momentum and position space representation are complementary, and it is possible to transfer from one space to another via a simple Fourier transform (in this context usually called the Dirac transformation[27].) The position space wave function $\psi(\bar{r})$ is related to the momentum wave function $\chi(\bar{p})$ by the transformation:

$$\chi(\bar{p}) = (2\pi)^{-3/2} \int \psi(\bar{r}) \exp(-i\bar{p}.\bar{r}) \, d\bar{r} \qquad 1\text{-}16$$

The electron momentum distribution or momentum density $N(\bar{p})$ is obtained from the momentum wave function $\chi(\bar{p})$, where

$$N(\bar{p}) = |\chi(\bar{p})|^2 \qquad 1\text{-}17$$

For an isotropic momentum distribution $N(\bar{p}) = N(p)$, and the Compton profile is given by

$$J(p_z) = 2\pi \int_{p_z}^{\infty} N(p) \, p \, dp \qquad 1\text{-}18$$

A radial momentum distribution I(p) can be defined such that

$$I(p)dp = N(p) 4\pi p^2 dp \qquad 1\text{-}19$$

The Compton profile for an isotropic medium then reduces to

$$J(p_z) = \frac{1}{2}\int_{p_z}^{\infty} \left[I(p)/p\right] dp \qquad 1\text{-}20$$

which is easily inverted to yield

$$I(p)dp = -2p\,\frac{dJ(p)}{dp} \qquad (p>0) \qquad 1\text{-}21$$

Thus differentiation of the experimental profile yields directly the radial momentum distribution. Epstein[28] has shown that in principle momentum expectation values and total energies may be obtained from Compton scattering data via the relation

$$\langle p^n \rangle = \int_0^{\infty} p^n I(p)\, dp \qquad 1\text{-}22$$

where $\frac{1}{2}\langle p^2 \rangle$ gives the electronic kinetic energy. However, the statistical accuracy obtainable at present and the restricted range of momenta observed in Compton experiments severely limits the accuracy of the resulting atomic or molecular energies. A significant improvement in the experimental technique is necessary before reliable kinetic energies can be obtained in this way. An observable which is directly available from the Compton profile is $\langle p^{-1} \rangle$. From eqn. 1-20 the height of the profile J(0) is seen to be equal to $\frac{1}{2}\langle p^{-1} \rangle$. The correlation between this expectation value and other physical properties is not well understood, and such relationships remain to be developed.

Certain consequences of the Dirac relation make the Compton profile particularly sensitive to the behaviour of the outer electrons in an atom or molecule. These outer electrons have an extensive spatial wave function which leads, after transformation, to a sharp, narrow momentum

wave function and Compton profile. Hence, the entire contribution of these electrons to the Compton profile is confined to regions of low momenta. Conversely, the inner electrons are highly localised around the atomic core with a spatial wave function which is sharply peaked at the nucleus. The Fourier transform of this wave function will lead to a broad and flat Compton profile. This behaviour can be understood in terms of the uncertainty relation between position and momentum, which limits the accuracy which can be obtained in a simultaneous measurement of the two properties. Thus, since the inner electrons are known to be localised in position space, this implies an uncertainty in the electron momentum and hence a delocalised wave function in momentum space. Fig. 1-3 illustrates the effect of transforming from position to momentum space. Gaussian functions are used to represent the electronic wave functions $\psi(x)$ and $\chi(p)$. If the position wave function is written

$$\psi(x) = \frac{1}{(2\pi\sigma^2)^{1/4}} \exp(-x^2/4\sigma^2) \qquad 1\text{-}23$$

then the corresponding momentum wave function is

$$\chi(p) = (8\pi\sigma^2)^{1/4} \exp(-p^2\sigma^2) \qquad 1\text{-}24$$

Fig. 1-3(a) might represent a tightly bound atomic core electron, while fig. 1-3(c) is a suitable function for a weakly bound outer electron. The Gaussian functions have the convenient property of transforming into other Gaussian functions, and are therefore often used in forming basis sets for a momentum wave function.

In the impulse approximation, the area of the profile is normalised to the number of electrons, i.e.

$$\int_{-\infty}^{\infty} J(p_z)\, dp_z = 1 \qquad \text{(per electron)} \quad 1.25$$

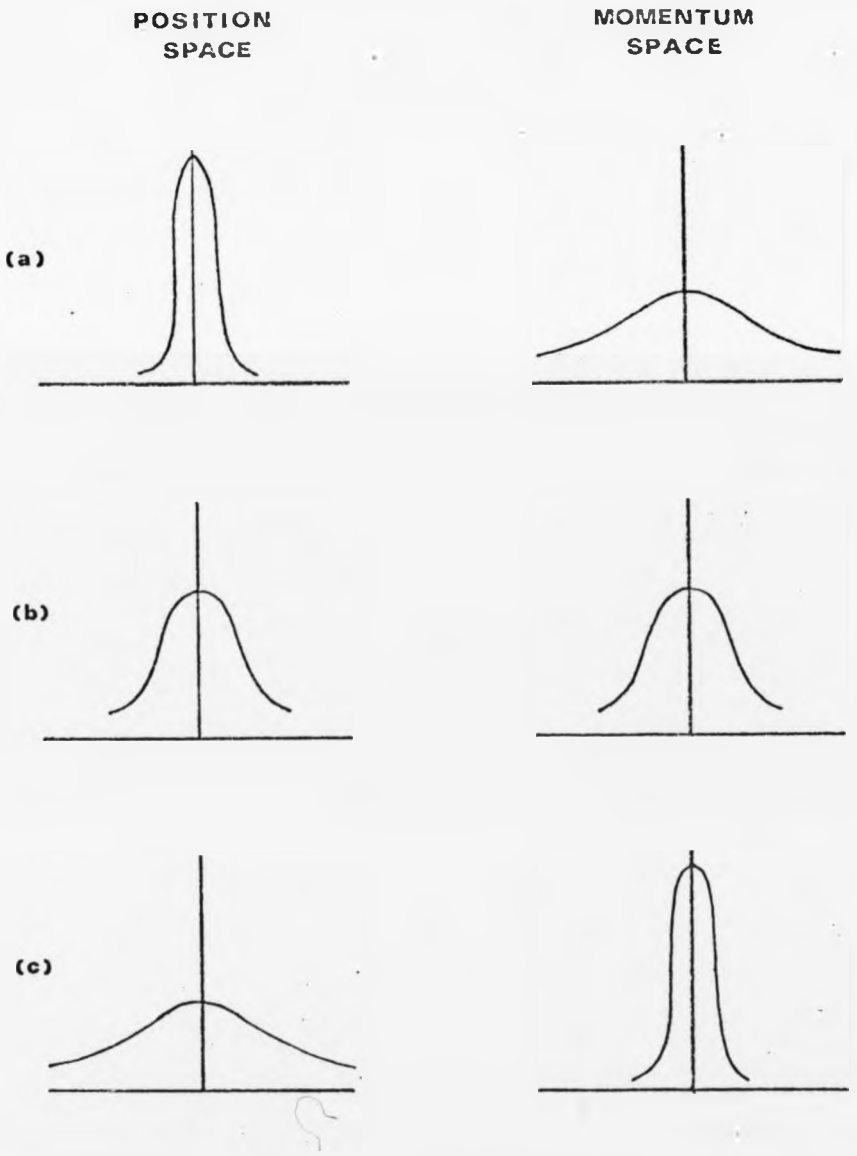

Fig. 1-3: An illustration of the effects of transforming from position to momentum space using Gaussian functions.

Therefore in this approximation each electron contributes the same area to the total profile. However, the contribution from the outer electrons is limited to regions of low momenta and this gives rise to the characteristic profile shape illustrated in fig. 1-4.

As seen in fig. 1-4, the core and outer electron contributions to the Compton profile are superimposed. In order to study the behaviour of the outer electrons, the core profile must be subtracted from the total. Since the core electrons may be expected to be essentially unaffected by the transition to a solid state or molecular environment, it is possible to calculate reliable core electron Compton profiles on the basis of free atom, Hartree-Fock wave functions. Having removed the core contribution from the measured profile, the remaining profile can then be compared with various models for the outer electrons.

The sensitivity of the Compton profile to the outer electrons contrasts with the results of an x-ray diffraction measurement. The intensity of the Bragg peaks depends primarily on the electron density in position space $|\psi|^2$ (see eqn. 1-5 for the atomic form factor). Therefore, the electrons which are concentrated in regions near the atomic cores will dominate the scattering, and the outer electrons will be responsible for little of the observed intensity. The complimentary nature of position and momentum space is reflected in the sensitivity of the two techniques, and gives Compton scattering a considerable advantage when studying the behaviour of the outer electrons. This information is of major interest since these electrons are responsible for the inter-atomic effects which lead to the formation of molecules and solids.

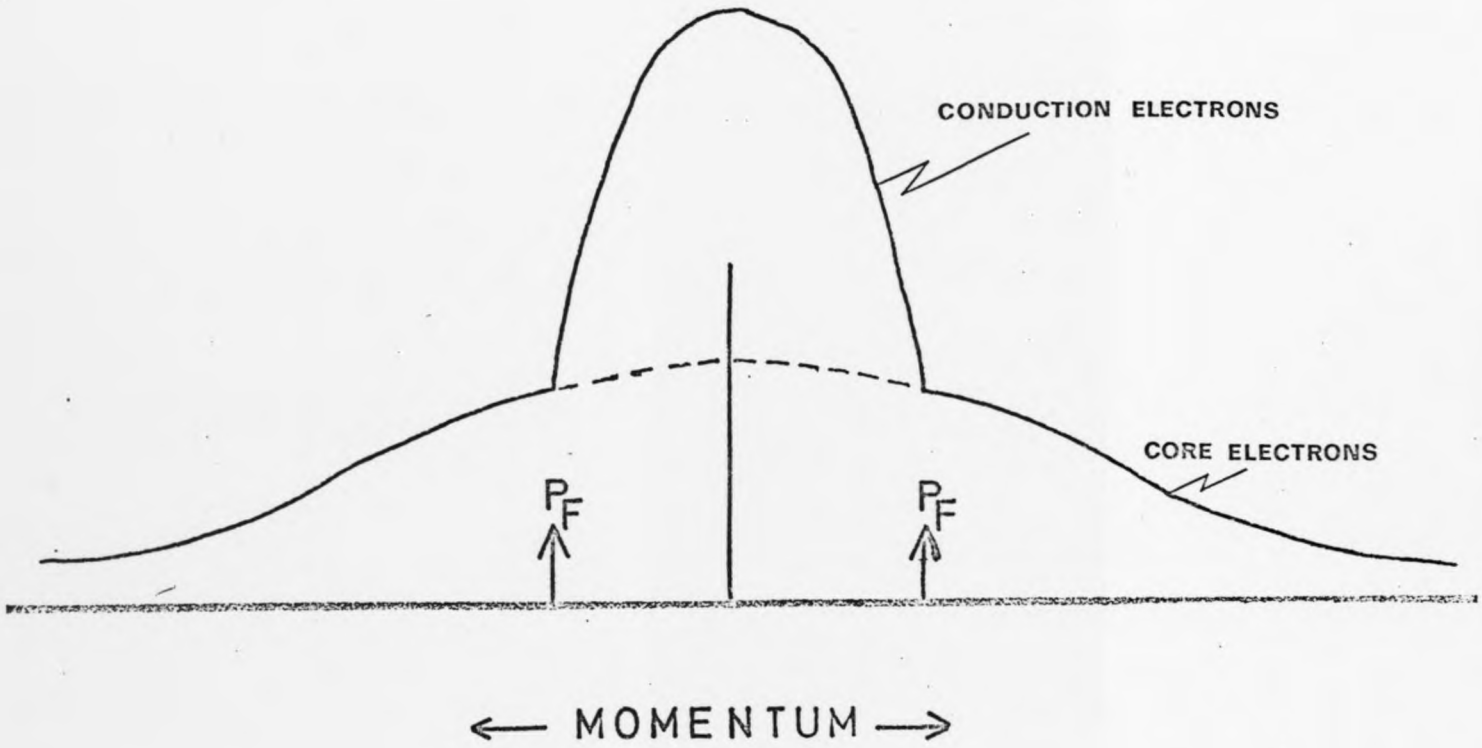

Fig. 1-4: Typical Compton profile for a metallic system.

The behaviour of electrons in metals has been of considerable interest to solid state physicists. The metallic, conduction electrons may be treated, in a first approximation, as a homogeneous non-interacting Fermi gas whose electron momentum distribution N(p) is given by

$$N(p) = \frac{J(p)}{4\pi p^2} = \begin{cases} N(0) & p \leq p_F \\ 0 & p > p_F \end{cases} \qquad 1\text{-}26$$

where p_F is the Fermi momentum. From eqn. 1-20 one can obtain the Compton profile

$$J(p_z) = \begin{cases} \pi N(0)(p_F^2 - p_z^2) & p_z \leq p_F \\ 0 & p_z > p_F \end{cases} \qquad 1\text{-}27$$

The 'free-electron' Compton profile is therefore an inverted parabola, cutting off at the Fermi momentum. Fig-1-4 shows a typical Compton profile for a free-electron metallic system. Where experiments are in disagreement with this elementary result, the model can be refined to include the electron-electron interaction and the required orthogonalization with the core electron wave functions. Such improvements have met with considerable success in explaining the residual discrepancies in some results. The case of aluminium has been investigated in detail and the results are given in Chapter 5.

In general then the Compton profile is used primarily as a tool for testing theoretical wave functions for the outer electrons. The relative simplicity of the experimental method has led to measurements being made on many different systems. Gases, liquids, ionic crystals, metals and even polymers have received attention from the experimental groups which have been formed over the last decade. Occasionally experiments have been made in the absence of any comparable theoretical work, and as the accuracy of the

technique improves it has become increasingly important to have reliable theoretical profiles for quantitative comparison with the experimental results.

The Dirac transformation relationship has been crucial to the development of Compton scattering as a viable technique for testing theoretical wave functions. Attempts to solve the Schrodinger equation in the momentum space description in order to obtain a momentum wave function directly have met serious practical difficulties, and successful calculations have been limited to systems having only one or two electrons[29]. In contrast, an indirect approach in which the solution to the familiar position space equation is transformed to momentum space has enjoyed considerable success for a wide range of systems.

The tremendous advances in computer technology have led to the development of very sophisticated methods for calculating these position space wave functions. Compton scattering offers a stringent test of these wave functions and, despite certain difficulties in applying the Dirac transformation, electron momentum distributions have been calculated for many systems. Much of the work has been concentrated on molecular wave functions, using the self-consistent-field linear-combination-of-atomic-orbitals approach[30]. The hydrocarbons[31] and the boron hydrides[32] have received particular attention, and experimental results for both of these systems are described in Chapter 6.

As experimental results are extended to include the heavier elements, atomic calculations at the non-relativistic Hartree-Fock level[33] will fail to take account of the large

relativistic effects in the wave function, especially of the inner s and p orbitals. Recent relativistic calculations by Mendelsohn, Biggs and Mann[34] have revealed significant effects even for orbitals with large principal quantum number. Investigation of these effects, with both theory and experiment, is a promising line of development.

References for Chapter 1

(1) Compton, A.H., (1923), Phys. Rev. 21, 483

(2) Jauncey, G.E.M., (1924), Phys. Rev., 24, 204

(3) DuMond, J.W.M., (1929), Phys. Rev., 33, 643

(4) DuMond, J.W.M., (1933), Rev. Mod. Phys., 5, 1

(5) Hicks, B., (1937), Phys. Rev., 52, 436

(6) DuMond, J.W.M., and Kirkpatrick, H.A., (1937), Phys. Rev., 52, 419

(7) Cooper, M.J., Leake, J.A., and Weiss, R.J., (1965), Phil. Mag., 17, 1079

(8) Cooper, M.J., (1971), Adv. Phys., 20, 453

(9) Weiss, R.J., (1969), J. Chem. Phys., 52, 2237

(10) Eisenberger, P., (1970), Phys. Rev., A2, 1678

(11) Hulubei, H., (1934), Ann. de. Phys., Ser. XI, 7

(12) McIntyre, J.A., Nha, S.K. and Moreland, R.W., (1967), Bull. Am. Phys. Soc., 12, 177

(13) Felsteiner, J., Fox. R. and Kahane, S., (1970), Phys. Lett., 33A, 442; (1971) Sol. St. Comm., 9, 61; Ibid., 9, 457

(14) Eisenberger, P., and Reed, W.A., (1972), Phys. Rev., A5, 2085

(15) Reed, W.A., and Eisenberger, P., (1972), Phys. Rev., B6, 4596

(16) Felsteiner, J., Fox. R., and Kahane, S., (1972), Sol.St.Comm., 11, 635

(17) Manninen, S., Paakkari, T., Aikala, O., and Mansikka, K., (1973), J. Phys. C., 6, L410

(18) DuMond, J.W.M., (1930), Phys. Rev., 36, 1685

(19) Phillips, W.C., and Weiss, R.J., (1968), Phys. Rev. 171, 790

(20) Evans, R.D., (1955), The Atomic Nucleus (London: McGraw-Hill)

(21) Jauch, J.M., and Rohrlich, F., (1955), The Theory of Photons and Electrons (Cambridge, Mass.: Addison-Wesley)

(22) Klein, O., and Nishina, Y., (1929), Z.Physik, 52, 853

(23) Weiss, R.J., (1963), Solid State Physics for Metallurgists (New York: Pergammon Press)

(24) Eisenberger, P., and Platzman, P.M., (1970), Phys. Rev. B2, 415

(25) Eisenberger, P., and Reed, W.A., (1974), Phys. Rev. B9, 3237

(26) Manninen, S., Paakkari, T., and Kajantie, K., (1974), Phil. Mag., 29, 167

(27) Dirac, P.A.M., (1935) Quantum Mechanics (Oxford: O.U.P.)

(28) Epstein, I.R., (1973), Phys. Rev., A8, 160

(29) McWeeny, R., and Coulson, C.A., (1949), Proc.Phys.Soc, (London), 62A, 509

(30) Roothan, C.C.J., (1951), Rev.Mod.Phys., 23, 69

(31) Epstein, I.R., (1970), J. Chem. Phys., 53, 4425

(32) Epstein, I.R., and Lipscomb, W.N., (1970), J. Chem. Phys., 53, 4418

(33) Weiss, R.J., Harvey, A., and Phillips, W.C., (1968), Phil.Mag., 17, 241

(34) Mendelsohn, L.B., Biggs, F., and Mann, J.B., (1973), Chem. Phys. Lett., 26, 521

CHAPTER 2

EXPERIMENTAL METHOD

2.1 General Considerations

A Compton scattering experiment is designed to measure the differential Compton cross section of inelastically scattered electromagnetic radiation. From this differential cross section it is possible to obtain a Compton profile, and hence the electron momentum distribution. Despite some serious practical difficulties the experimental arrangement is very simple. It consists of:

(i) A source of radiation with a well defined energy.

(ii) A scattering geometry which fixes a scattering angle defined by the source, the sample and the detector.

(iii) A detection system which can analyse the energy spectrum of the scattered radiation.

The range of source energies which can be usefully employed in a Compton scattering experiment is determined by the relative cross sections of the competing processes. Fig. 2-1 provides a guide to the relative importance of the principal interactions for a broad range of incident photon energies, and scattering materials of various atomic number Z. Below about 10 keV photoelectric absorption dominates for all materials, and the intensity of Compton scattered radiation is very small. Although the Compton effect is the major interaction at higher energies (up to about 5 MeV), there is a practical limit at around 500 keV. For gamma-rays with energy above 500 keV the high penetration of the radiation presents major design problems in the scattering geometry. In the energy range (10-500 keV), radiation

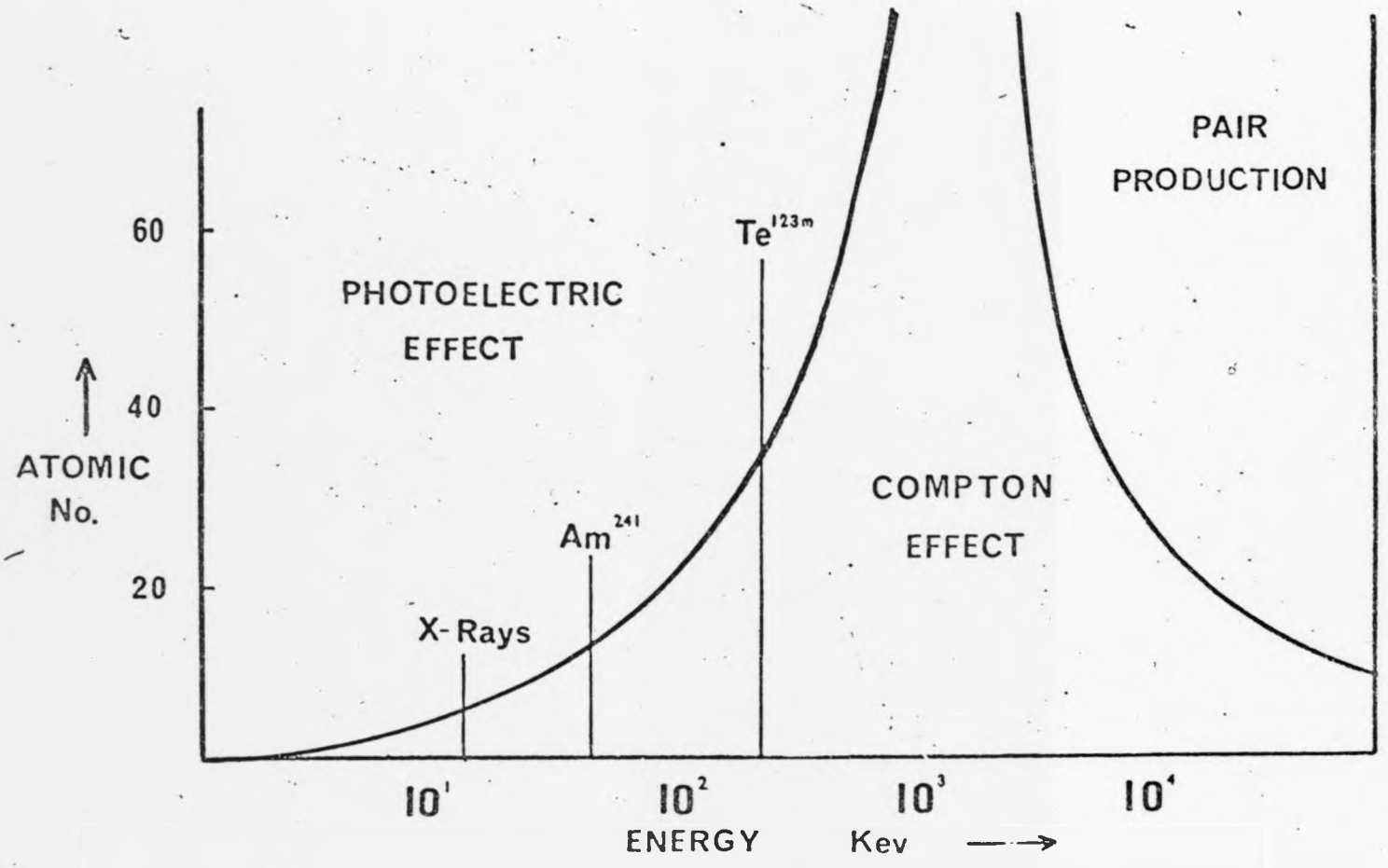

Fig. 2-1: A guide to the relative importance of the principal photon-electron interactions.

at well defined energies can be obtained from an x-ray tube (limited to energies below 100 keV) or a gamma-ray source. Experimental systems employing either MoKα x-rays (17 keV) or Am^{241} gamma-rays (60 keV) are described in the following sections (2.2 and 2.3).

Spectral analysis of the inelastically scattered radiation can be achieved by two methods. On the one hand, there is a dispersive technique, where a crystal spectrometer is employed in conjunction with a scintillation counter. Since the scattered radiation must subsequently be Bragg reflected from the analysing crystal, this technique is suitable for the low energy, high intensity radiation available from an x-ray tube. The method has been used extensively since 1965 and completely replaced the photographic recording technique employed in the earlier experiments. Alternatively, the solid state detector now provides an efficient non-dispersive form of spectral analysis. Lithium drifted silicon detectors (limited to the energy range 0-30 keV) and germanium crystal detectors (covering an energy range up to several MeV) have been developed over the last decade[1]. The energy resolution of a silicon detector (typically 150 ev at 6 keV) is now sufficiently good to challenge the more cumbersome x-ray spectrometers in the field of x-ray fluorescence spectroscopy. A germanium detector, operated at an energy in the range 50-500 keV, can offer comparable resolution to an x-ray spectrometer for the measurement of a Compton profile. A solid state detector linked to a multi-channel analyser generally increases the effective efficiency of the detection system (the two systems are compared in section 2.3.1) which leads to a reduction in measuring times, despite the low intensity available from a gamma-ray source. Moreover, gamma-ray sources can provide

photons of higher energy enabling experiments to be carried out in energy regions where competition from photoelectric absorption is considerably reduced. This extends the range of materials which can be studied to include such systems as the transition metals, where the large photoelectric cross sections make x-ray experiments impractical.

In addition to the practical considerations in Compton scattering experiments, there are certain criteria for assessing the relative merits of various experimental arrangements.

Resolution: Poor instrumental resolution will smooth out details of the measured profile. This is seen particularly in the metals, where there may be a sharp break at the Fermi momentum. Since no method of deconvolution can completely recover this hidden information, the width of the resolution function is an important parameter in Compton profile measurements.

Intensity: The small Compton cross section and consequent low intensity make this a crucial consideration. Early Compton measurements could take around 2000 hours, and even experiments lasting a few days place stringent requirements on the stability of the apparatus. As increased intensity is generally achieved at the cost of lower resolution these two criteria must be carefully optimised.

Profile reliability: In order to derive a direct relation between measured cross section and the Compton profile (eqn. 1-14), certain approximations were necessary. When the incident photon energy is low, or the scattering material is of high atomic number, these approximations could introduce significant errors into a Compton profile which has been obtained from statistically accurate experimental data.

These errors arise from the large binding energy of the core electrons. Binding effects have been neglected in the impulse approximation and, for low energy incident photons, this assumption is unjustified. Even for high energy photons (where the impulse approximation is valid), large core electron binding energies imply high velocities for these core electrons which may introduce errors from neglected relativistic effects. However, since core electrons make a small, slowly varying contribution to the profile in regions of low momenta, considerable errors in the core electron profiles can be tolerated without a serious deterioration in the accuracy of the total profile.

2.2 The x-ray technique

2.2.1 Apparatus

The technique of inelastic x-ray scattering has been described in detail in a recent review by Cooper[2]. Therefore this section will be concerned primarily with certain improvements made to the apparatus and the data processing.

The sample isirradiated with 17 keV molybdenum x-rays from a 2.7 kW spectrometer tube. The incident x-rays are collimated to $\pm 3^{\circ}$, and those with a particular scattering angle exit through a set of fine Soller slits (0.2° total divergence). The spectrometer is designed to work with the largest possible angle of scattering, although in practice $\sim 150^{\circ}$ is the highest which can be obtained without long beam paths, and the consequent serious $1/r^2$ intensity losses. The reason for maximising the scattering angle can be deduced from eqn. 1-11. For low energy radiation ($\omega_1 \approx \omega_2$) the photon energy loss $\Delta\omega$ can be approximated by

$$\Delta\omega = \frac{2\omega_1^2}{mc^2}\sin^2(\theta/2) - \frac{2p_z}{mc}\omega_1 \sin(\theta/2) \qquad 2\text{-}1$$

The first term gives the energy loss after scattering by an electron at rest, and the second term expresses the Doppler broadening due to the finite electron velocity. From the second term it is clear that the higher the scattering angle Θ, the wider the spectral broadening due to the electron momentum component p_z. Hence, for a given energy resolution, an increase in the scattering angle leads to a wider spectral distribution and in turn to an improvement in the momentum resolution.

The finite beam divergence leads to an uncertainty in the scattering angle. This implies some deterioration in the momentum resolution. From eqn. 2-1, it can be shown that

$$\frac{\delta p_z}{p_z} = \cot(\Theta/2)\, \delta\Theta \qquad 2\text{-}2$$

As the scattering angle Θ approaches 180°, the factor $\cot(\Theta/2)$, becomes small and the effect of beam divergence on the momentum resolution is reduced. Therefore a greater tolerance in the collimation, and hence an increase in intensity, can be achieved at high scattering angles.

A spectral analysis of the scattered x-rays is achieved by reflecting them from the plane face of a (100) cleaved LiF crystal into a NaI(Tl) scintillation counter. The counter follows the Bragg reflection from the analysing crystal through a 2 to 1 gearing. A further Soller slit in front of the counter improves the signal to noise ratio. Pulse height analysis cuts out the contributions from high energy x-rays and low energy noise. The layout of the apparatus is shown in Fig. 2-2.

Initially readings were taken of the number of counts measured in a pre-set time at some value of the Bragg angle Θ_B.

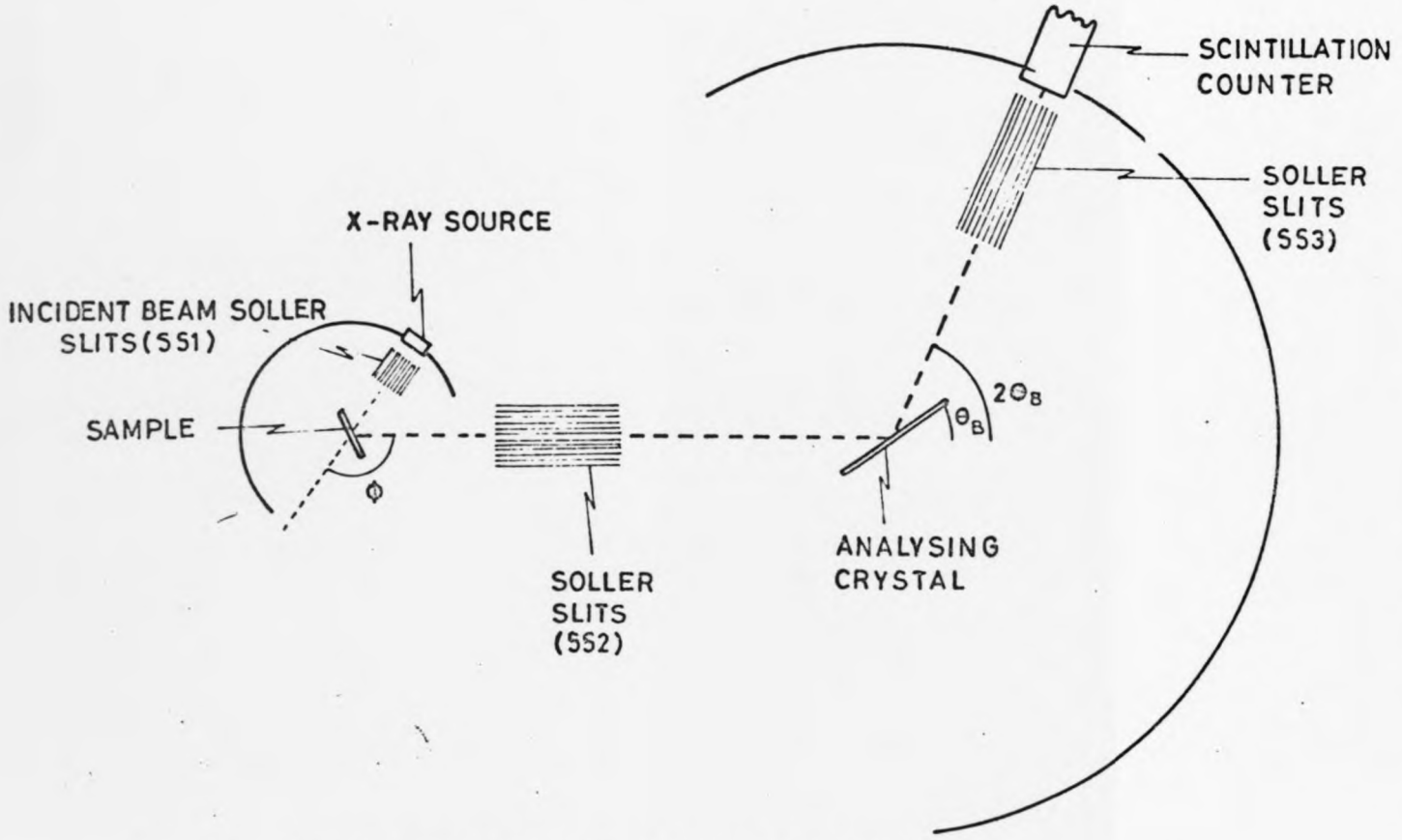

Fig. 2-2: Layout of the x-ray Compton scattering apparatus.

The spectrometer was then turned through a further angle $\Delta\theta_B$(e.g. 0.01°) and the timer restarted. In order to detect instabilities in the system, an experiment would consist of repeated runs across the profile. A comparison was made of each run at the conclusion of the whole experiment, and a statistical test made to ensure that the results of each run were identical to within their statistical accuracy[3].

It was felt that with a system of continuous monitoring one run could replace the series of runs which were necessary earlier. Therefore a further scintillation counter was mounted over the second set of Soller slits (SS2 in Fig. 2-1). In this position the monitor receives Compton scattered radiation directly from the sample and pulse height analysis limits the count to the energy range of the profile. This is possible since the resolution of the NaI(Tl) counter at this energy is about 5 keV, which is roughly the maximum energy loss of the Compton scattered x-rays. The experiment is then controlled by the monitor counter, each point in the profile being measured for a fixed number of monitor counts. This automatically compensates for the small fluctuations in the intensity of the incident x-ray beam.

A sample holder was constructed, comprising a goniometer head which was mounted inside a lead lined steel cylinder with ports for the incident and scattered beams. It was made air-tight so that evacuation would eliminate air scattering. The holder had the added advantage of shielding the x-rays, thereby improving the signal to noise ratio and reducing the safety hazard.

The information from the counters is now printed

directly onto paper tape for processing. In addition a chart recorder is linked to the ratemeter so that the progress of the spectrometer analysis across the profile can easily be followed. Since the count rate in these experiments can be very low (about three counts a second for aluminium), progress across the profile is slow, and a long time constant circuit ($\sim$1000 seconds) is necessary between ratemeter and recorder.

2.2.2 Data processing

The Compton profile may be extracted from the measured differential cross section only after certain systematic corrections have been made. These corrections are:

(a) The removal of the white background

(b) The conversion from a scale of Bragg angle to an energy scale

(c) The correction for the energy dependence of the absorption of x-rays in the sample and in the analysing crystal

(d) The correction for the energy dependence of the x-ray polarization factor.

The appropriate form for these corrections can be found in the review by Cooper[2], and have also been given by Fukamachi and Hosoya[4].

The experimental data should then be deconvoluted. This is to make allowance for the finite width of the apparatus function and the divergence of the incident beam. The deconvolution of experimental x-ray profiles has been discussed by Cheng, Williams and Cooper[5], and the effects of random experimental errors on the deconvoluted line shape have been described by Epstein and Williams[3].

Since the profiles arising from the $K\alpha_1$ and $K\alpha_2$ x-ray

lines are completely overlapped, a correction must be made to separate these profiles. This correction is usually made by the iterative procedure of Rachinger[6]. However, an alternative procedure has recently been described by Cooper, Williams and Pattison[7] which takes advantage of the centro-symmetric nature of the constituent lines. The symmetric method of separation avoids the propagation and amplification of errors, characteristic of the Rachinger method. Details of this deconvolution procedure can be found in appendix (I).

Finally, the Compton profile is obtained from the corrected and deconvoluted data. This is achieved by the following operations:

(a) The conversion from energy to momentum scale

(b) The transformation from differential cross section to Compton profile

(c) The normalization of the resulting profile.

The first two of these operations can be achieved by application of eqns. 1-11 and 1-14, although the accuracy of these equations will be superfluous for x-ray data. Instead, the simpler, non-relativistic form, as given by eqn. 2-1, can be used.

The final step of normalization can lead to some difficulties. In the impulse approximation, the Compton profile is normalised according to the number of atomic electrons, i.e.,

$$\int_{-\infty}^{\infty} J(p_z)\, dp_z = 1 \qquad \text{(per electron)} \qquad 2\text{-}3$$

Since there is a limit to the range of momentum for which experimental data can be obtained, the experimental profile can simply be normalised to the equivalent area of a free-

atom profile calculated in the impulse approximation. Such profiles have been tabulated by Weiss, Harvey and Phillips[8].

However, such a normalisation procedure neglects the effect of electron binding on the experimental profile. When the binding energy is greater than the energy transfer, the electron will not be ejected from the atom and a Compton scattering event cannot occur. This in turn limits the range of p_z for which a particular one-electron profile can be measured, since above a certain momentum (corresponding to an energy transfer equal to the electron binding energy) the electron makes no contribution to the profiles. This cut-off can easily be seen in the measured differential cross section (see e.g. fig. 4-6). When a binding energy cut-off (at momentum p_z binding) falls inside the momentum range of the experimental profile (0-$p_z$max), then the area of each one-electron profile must be calculated on the basis of

$$\int_0^{p_z^{max}} J(p_z)\,dp_z = \int_0^{p_z^{max}} J(p_z)_{Imp}\,dp_z - \int_{p_z\,binding}^{p_z^{max}} J(p_z)_{Imp}\,dp_z \qquad 2\text{-}4$$

The first term gives the area in the impulse approximation, and the second term describes the area lost due to binding effects. The area of the total profile is then the sum of the areas of each one-electron profile.

2.3 The Gamma-ray technique

The experimental arrangement is shown schematically in fig. 2-3. A beam of gamma-rays from a monochromatic radioactive source passes through a lead tunnel and enters an evacuated chamber containing the sample. Photons which are scattered at some fixed angle exit through another tunnel and reach the detection system. The system consists of a

Ge(Li) solid state detector, linked to a multi-channel analyser. Before the components of the experimental apparatus are considered in detail, it is worth comparing the gamma-ray technique with the x-ray system described in the previous section.

2.3.1 A comparison of x-ray and gamma-ray techniques

a) Gamma-ray sources can extend the range of photon energies up to the practical limit of about 500 keV. Unfortunately, few sources have strong, isolated single lines in their energy spectrum, and at present only two are in use. These are Am^{241} at 60 keV, and Te^{123m} at 160 keV. However, the higher energy of these photons (c.f. MoKα at 17 keV) considerably increases the energy transfer $\Delta\omega$ and improves the accuracy of the impulse approximation ($\Delta\omega \gg E_B$).

b) For photon energies in the range 15-150 keV the Compton cross section is roughly proportional to atomic number Z, and the photoelectric cross section to Z^4/ω_1^3, where ω_1 is the incident photon energy. This implies a ratio of Compton to photoelectric of ω_1^3/Z^3. The factor Z^{-3} highlights the difficulties encountered when making Compton scattering measurements on high Z materials, where photoelectric absorption becomes increasingly competitive. The situation improves at higher photon energies and, for example, the use of Te^{123m} gamma-rays produces a gain of about a factor of 10^3 in Compton scattered intensity over Mo x-rays. This can be seen in fig. 2-1, which illustrates how relative Compton and photoelectric cross sections vary with incident photon energy and atomic number of the scattering body.

c) The multi-channel analyser, in conjunction with the Ge(Li)

detector, measures all points on the profile simultaneously, instead of sequentially. This is because the detector is a proportional counter, and analyses the energy of each photon received. Since in an x-ray experiment some 400 points must be measured, point by point, this leads to a further intensity factor of about 400 in favour of the gamma-ray system.

d) The flux from a gamma-ray source is much lower than that obtained with an x-ray tube. A one curie source produces 4×10^{10} photons per second compared with a typical 5×10^{14} photons per second flux from an x-ray tube. Since one curie is the maximum source strength easily handled, the x-rays have an advantage of $\sim 10^4$. However, the two factors in favour of gamma-rays (lower absorption and simultaneous measurement of all points) easily compensate for the lower flux.

e) The points which have been made so far have been mainly concerned with the intensity which can be expected in a gamma-ray experiment. However, the gamma-ray beam has the further advantage of a strong, single line with a low background. This contrasts sharply with the x-ray case where the beam has an $\alpha_1 - \alpha_2$ doublet on a bremsstrahlung background. The step of separating out the double profile is avoided, and the errors inherent in the background subtraction are much reduced.

f) The simple experimental geometry permits a higher angle of scattering in the gamma-ray system ($\sim 170^\circ$ as compared to 150°), which improves the momentum resolution. Moreover, for photon energies approaching 500 keV, the assumptions made in the derivation of the relativistic cross section relation (eqn. 1-14) will be valid only at the higher scattering angle. In practice, however, in order to reduce

the background, experiments at 60 keV are normally made with a scattering angle around 150°.

g) Fukamachi et al.[9] have compared the relative resolutions of a solid state detector and a crystal spectrometer. The momentum resolution which can be obtained with MoKα radiation using the 400 reflection of LiF (~ 0.2 a.u.) is about three times as good as can be obtained with a solid state detector and Am^{241} gamma-rays. Even using Te^{123m}, the x-ray system has about twice the momentum resolution obtained with the Ge(Li) detector. The energy of the incident gamma-rays must be above 300 keV before the resolution of the two systems is comparable.

Clearly the gamma-ray energy should be as close to 500 keV as possible in order to achieve the optimum resolution. Unfortunately, the number of sources with a strong, single line in the energy range 50-500 keV is extremely limited, and at present only two are in use: Am^{241} (60 keV) and Te^{123m} (160 keV). Although the higher energy of the gamma-rays from Te^{123m} lead to a significant improvement in the momentum resolution, the use of this source has been complicated by certain technical difficulties. The production of the isotope requires a period of neutron irradiation in a reactor, and data on the relevant neutron cross sections has not been available. Consequently, development work at the Radiochemical Centre, Amersham has proceeded only on an empirical basis and no useful sources have yet been produced. In this country then the procedure has not, to date, resulted in a source of the necessary strength or purity, although several measurements with Te^{123m} have been reported by Eisenberger and Reed[10]. If the source strength is low there is a consequent increase in the measuring time, while the isotope itself has a half-life of

only about three months. The existence of other high energy impurity lines in the energy spectrum leads to an increase in the background, and there is also some difficulty in shielding the detector from direct irradiation by the source. For these reasons, despite the lower resolution, the Am^{241} source has been used in the gamma-ray Compton profile measurements described below.

2.3.2 Apparatus

A collimated beam of photons impinges on the sample, and at some fixed scattering angle a solid state detector, coupled to a multi-channel analyser, measures the photon energy distribution. The description of the system is divided into two parts; the scattering geometry and the detection system. Data processing is discussed in the following section (2.3.3)

a) Scattering geometry

The experimental arrangement is shown in fig. 2-3. 59.54 keV gamma-ray from a 300 mCi Am^{241} source with an active diameter of 1.2 cm. are first collimated by a lead tunnel of length 13 cm. and diameter 1.2 cm. After scattering in a vacuum chamber through a mean angle of 150^{o} the scattered gamma-rays are collimated by a second lead tunnel (length 15 cm, diameter 1.2 cm). The angle of 150^{o} was chosen so that no part of the walls of the scattering chamber could be seen by both source and detector. Therefore the scattering volume contained only the sample. As a further precaution the inside of the chamber was lined with lead and, since the chamber could be evacuated, air scattering was negligible. With these precautions Compton peak to background ratios of about 1000 to 1 could easily be achieved. The effect of beam divergence on the total resolution will

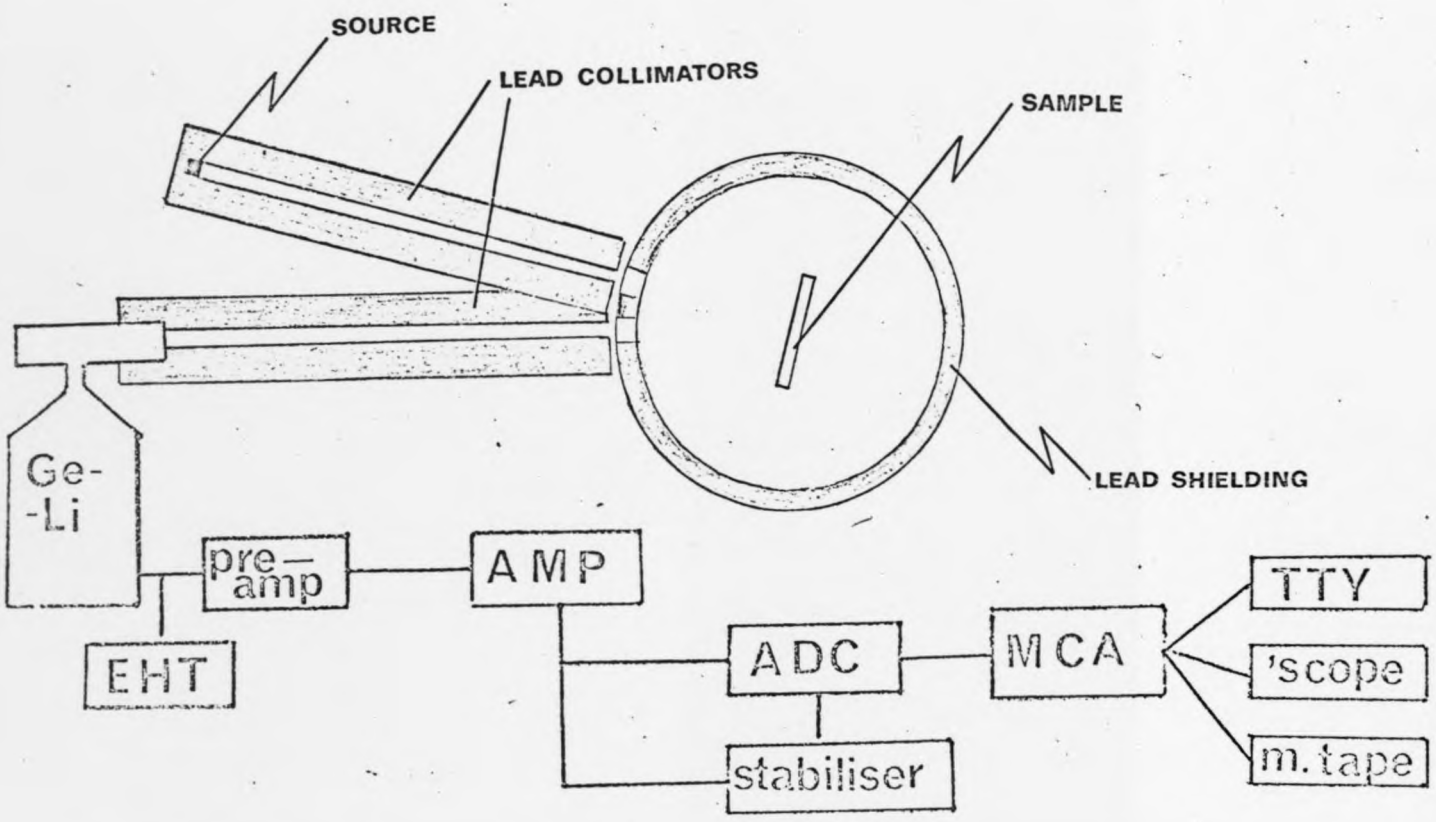

Fig. 2-3: Layout of the gamma-ray Compton scattering apparatus and associated electronics.

be considered in the following section.

b) Detection system

The system consists of a Ge(Li) solid state detector (S.S.D.) linked to a multi-channel analyser (M.C.A.) via an anologue-to-digital converter and pulse-height-analyser. The layout of the detection system is illustrated in fig. 2-3.

One can consider the process by which radiation induces charge in a S.S.D. and is collected and analysed as occuring in two stages. Firstly, the gamma-rays interact with the lithium drifted germanium semi-conductor crystal to produce electrons and holes. The statistical fluctuations produced in $\bar{N}$, the average yield of ion pairs, is given by[1]

$$\sigma^2 = F\bar{N} \qquad 2\text{-}5$$

where F is the Fano factor and σ is the variance. In the second state, the charge carriers are collected at the detector electrodes and the charge converted to a voltage pulse in the pre-amplifier.

The intrinsic resolution of the S.S.D. is given in terms of the full width at half maximum (FWHM) as[9]

$$\Delta E_{FWHM} = 2.355(F\varepsilon\omega_1)^{1/2} \sim \omega_1^{1/2} \qquad 2\text{-}6$$

where ε is the average energy needed to produce an electron-hole pair, and ω_1 is the energy of the incident photons. In order to keep ε as low as possible the crystal is cooled with liquid nitrogen. The resolution function at 60 keV can be measured with a low intensity AM^{241} source, and the function is well represented by a Gaussian line shape with a small ($\sim 1\%$) low energy tail. The resolution function, measured with an Am^{241} source, is shown in fig. 2-4. The intensity is given in logarithmic scale to illustrate clearly the shape

Fig. 2-4: The instrumental resolution function shown on a logarithmic scale. On this scale the asymmetry of the function is clear, showing a pronounced tail on the low energy side of the spectrum.

COUNTS

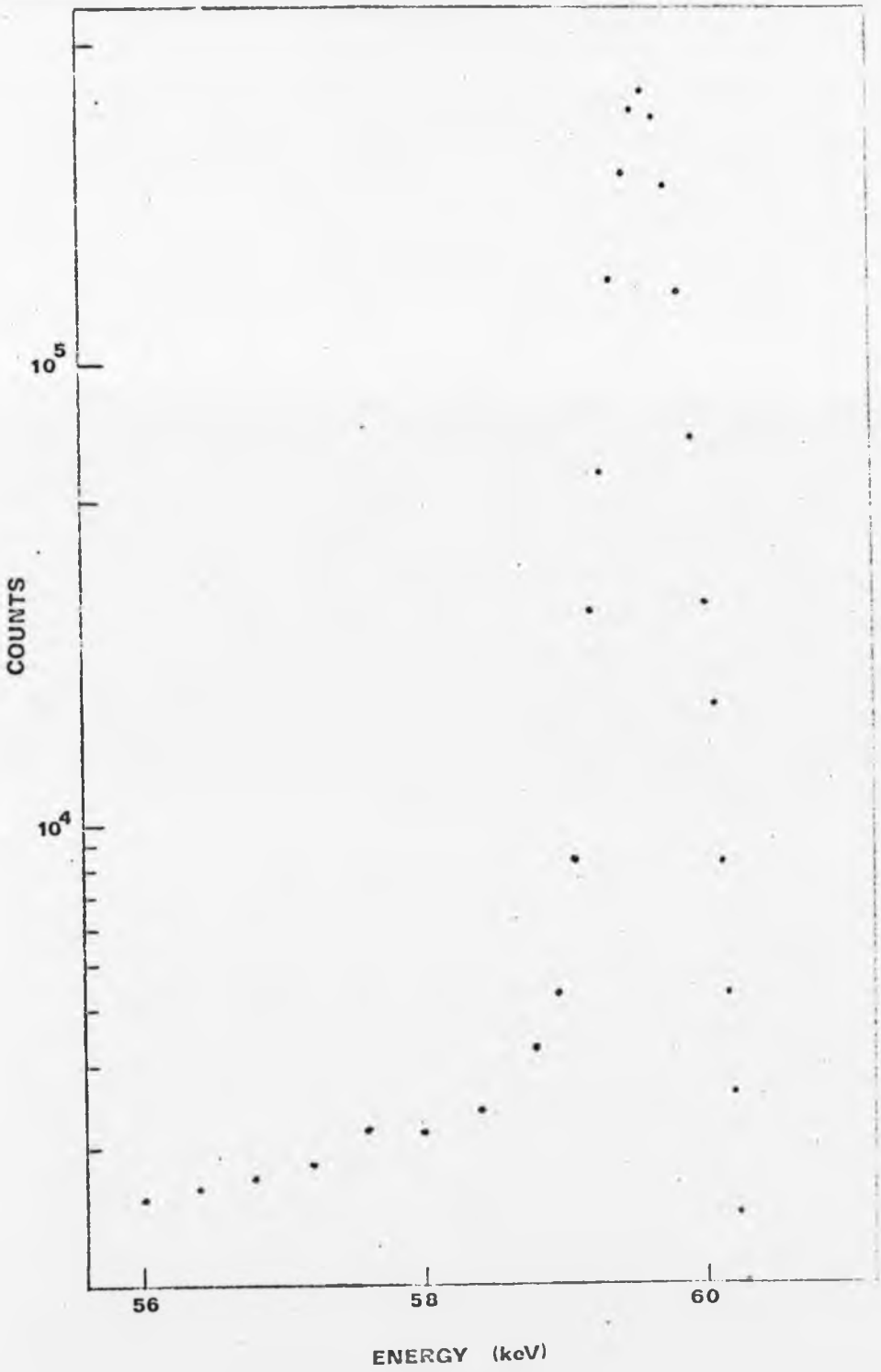
10^5
10^4
COUNTS
56
58
60
ENERGY (keV)

of the tail. The tail arises from detector inefficiency e.g. incomplete photon energy absorption due to the escape of secondary electrons from the surface of the crystal, and the recombination of electron-hole pairs. However, the efficiency of the detector for total photon absorption is very close to unity over the range 30-60 keV, and varies by less than ½% in this range. Therefore no energy dependent correction for detector efficiency is needed over this energy range, although the effect of the tail must be incorporated into any deconvolution procedure. The necessary tail-stripping procedure is described in the next section.

From the S.S.D. the voltage pulse is transmitted to an analogue-to-digital converter (A.D.C.) where the pulse is converted into a digital representation as a function of pulse amplitude. This is achieved by charging a capacitor to a voltage proportional to the analogue pulse and timing the linear discharge, the duration of which is a linear function of the peak voltage amplitude. A clock scales the periodic pulses into an address scalar and the accumulated count is stored in the memory of the M.C.A. The process is repeated every time an input pulse is presented to the A.D.C., with the eventual count being a histogram of the number of counts accumulated versus the input voltage pulse amplitude. The ferrite core memory has 4096 channels, with a memory cycle time of three microseconds. The M.C.A. incorporates an oscilloscope to simultaneously display the number of counts in each of the 4096 channels at any time during the experiment. Once an experiment is complete the data in the core can be stored on magnetic tape and the memory cleared for the next experiment. A Teletype is coupled to the M.C.A. so that the data can be transferred onto paper tape for processing.

2.3.3. Data processing

Typical raw experimental data are shown in fig. 4-6, where a measurement was made on aluminium. The Compton peak-to-background ratio is approximately 1500 to 1 and the background is essentially linear.

The intensity measured at some energy ω_2 can be expressed as[10]

$$I(\omega_2) = D(\omega_2)\, A(\omega_2)\, C \left.\frac{d^2\sigma}{d\omega\, d\Omega}\right|_{\omega_2} + B(\omega_2) \qquad 2\text{-}7$$

where 'D' is the efficiency of the detection system, 'A' is the effect of absorption in the sample, 'C' depends upon source strength, collimation and channel width, and 'B' is the background.

For a detector of thickness t_d and linear absorption coefficient μ_d the efficiency of the detector for total absorption is given approximately by

$$D(\omega_2) = 1 - \exp\left[-\mu_d(\omega_2)\, t_d\right] \qquad 2\text{-}8$$

For a germanium detector of thickness 0.5 cm, the efficiency is almost unity and does not vary appreciably across the energy range of the profile (30 keV - 60 keV). Since the final profile will be renormalised, factors which are constant across the profile can be neglected. This is also true for the factor C which is not energy dependent.

The effect of absorption at high angles of scattering, for a sample of thickness t_s and linear absorption coefficient μ_s, is

$$A(\omega_2) = \frac{1 - \exp\left\{-t_s\left[\mu_s(\omega_2) + \mu_s(\omega_1)\right]\right\}}{\mu_s(\omega_2) + \mu_s(\omega_1)} \qquad 2\text{-}9$$

where ω_1 is the incident photon energy.

The background $B(\omega_2)$ can be divided into two parts:

a) The scattering from the lead directly between the source and the detector, plus the cosmic ray background. This can be measured by plugging the exit from the source holder.
b) The scattering from the sample holder and lead shielding, which can be measured by removing the sample.

When the background has been subtracted (if necessary) and a correction made for sample absorption, the data should be deconvoluted to remove the effects of instrumental resolution. As discussed in the previous section the resolution function has two parts:
a) A Gaussian line shape arising from the statistical nature of the charge generation process in the detector, and further broadened by beam divergence.
b) A low energy tail due to some detector inefficiency.

The problem of the deconvolution of Compton profile data has been analysed by Paatero, Manninen and Paakkari[11] where details of several computational procedures can be found. The effect of the asymmetric part of the resolution function is first removed by a tail-stripping procedure, achieved by applying a simple recursive calculation to each point in the measured profile. An exponentially decreasing function was found to give the best fit to the tail (see fig. 2-4) but the particular response function depends on the geometry of the detector and should be measured for each detector. This can be done by irradiating the detector directly with a source which has a line in the energy region of interest. The source must be of low intensity, since the lineshape and detector resolution is very sensitive to 'build-up' which can occur when the count-rate and the percentage dead-time are high.

The iterative procedure for stripping an exponential tail

from the data can be described by[11]

$$l_i = k_i - \epsilon \sum_{j=i+1} \delta^{j-i} l_j \qquad 2\text{-}10$$

where k_i is the measured data in n channels (i = 1,n), and l_i is the corresponding corrected data. The value of δ is determined by inspection of the tail: if k_a and k_b are two points on the exponential tail, then $\delta^{b-a} = k_a/k_b$. The value of the adjustable parameter ϵ is determined by first attempting to strip the tail from the measured resolution function. With the appropriate value for ϵ, the resolution function should be symmetric following this correction. This can be achieved after a few trial runs. When the values for δ and ϵ have been established by testing the procedure on the resolution function itself, the correction can then be applied, point by point, to the measurement proper.

The remaining symmetrical instrumental broadening can be removed in a variety of ways, and a comparison of the various techniques has been made by Paatero et al.[11]. Lloyd's method[12] of deconvolution has been used in the experimental work reported below. Instrumental broadening arises from both the detector resolution and beam divergence. The FWHM of the detector resolution function at the Compton peak energy (50 keV) is calculated from the measured width at 60 keV (390 eV) according to eqn. 2-6, i.e. the FWHM varies as the square root of the energy. The figure of 390 eV at 60 keV compares with resolution functions of width 360 eV[13] and 400 eV[14] reported elsewhere. The small variation reflects recent developments in the design of solid state detectors.

The increase in the width due to divergence in the

incident and scattered beams can be calculated from the uncertainty in the scattering angle Θ. This uncertainty $\Delta\Theta$ is approximated by

$$(\Delta\Theta)^2 = \left(\frac{d_S}{R_{TS}}\right)^2 + \left(\frac{d_D}{R_{TD}}\right)^2 \qquad 2\text{-}11$$

where d_S and d_D are the source and detector diameters respectively. R_{TS} and R_{TD} are the source-to-target and target-to-detector distances. This uncertainty in Θ gives rise to an additional smearing of the energy resolution. At the Compton peak energy ω_c this is given by

$$\Delta\omega = \frac{\omega_c^2}{mc^2} \sin\Theta \, \Delta\Theta \qquad 2\text{-}12$$

For the scattering geometry described in the previous section (see fig. 2-3), the effect of $\Delta\omega$ is to increase the FWHM of the instrumental function by 10%.

The purpose of the deconvolution (and the various corrections) is to remove any 'experiment dependent' effects from the final Compton profile. This is essential if direct comparisons with theoretical profiles are to be valid. Unfortunately, no deconvolution scheme can recover all of the physical details concealed in the smoothed experimental profile. It is therefore necessary to define a 'residual instrumental function' (RIF) which can be obtained by applying the process of measurement and deconvolution to a delta function. The effect of this residual smearing can be seen by convoluting a theoretical profile with the instrumental function and applying the same deconvolution procedure as used on the experimental data. This procedure has been followed in all the gamma-ray Compton profile measurements which are described in this thesis. The deconvolution procedure is discussed in Appendix II.

A Compton profile can now be obtained from the differential cross section by application of eqns. 1-11 and 1-14. The energy scale is converted to a momentum scale via the relation,

$$p_z = mc \frac{\omega_2 - \omega_1 + \omega_2\omega_1(1-\cos\theta)/mc^2}{(\omega_1^2 + \omega_2^2 - 2\omega_1\omega_2\cos\theta)^{1/2}} \qquad 2\text{-}13$$

The average scattering angle θ used in this equation is determined by measuring the energy shift from the incident energy to the peak of the Compton profile. At the peak $p_z = 0$ and from eqn. 2-13

$$\cos\theta = 1 - \frac{mc^2}{\omega_1\omega_c}(\omega_c - \omega_1) \qquad 2\text{-}14$$

where in this case $\omega_2 = \omega_c$, the Compton peak energy.

After conversion to an electron momentum scale the position of this peak is checked by integrating the profile in the ranges -0.5 to 0.0 a.u. and 0.0 to 0.5 a.u. These areas should agree to within about 0.1% - 0.2%.

The Compton profile $J(p_z)$ can then be related to the differential cross section by

$$\frac{d^2\sigma}{d\omega_2 d\Omega_2} = \frac{r_o^2}{2}\frac{\omega_2}{\omega_1}\frac{mc\,B\;\;J(p_z)}{(\omega_1^2+\omega_2^2-2\omega_1\omega_2\cos\theta)^{1/2}+p_z(\omega_1-\omega_2)/mc} \qquad 2\text{-}15$$

The approximations necessary to derive this relation have been discussed in section 1.2, where a definition of the various parameters can also be found.

The final step, in which the profiles are normalised, follows the same procedure as described for the x-ray technique (section 2.2.2). The profile is normalised to the equivalent area of a free atom profile, calculated in the impulse approximation. Since the energy transfer at the profile peak when using Am gamma-rays will be about 10 keV, core electrons in materials such as transition metals

will contribute to the Compton profile. These contributions will be cut off at the appropriate binding energies and this must be taken into account when calculating the total area for the experimental profile (see eqn. 2-4).

By the procedures outlined above, Compton scattering data obtained by x-ray or gamma-ray techniques, can be corrected for all the systematic errors except those which arise from multiple scattering of the photons in the sample. This important topic is the subject of the next two chapters.

References for Chapter 2

(1) Dearnaley, G. and Northrop, D.C., (1968), Semi-conductor Counters, (New York: Pergamon Press).

(2) Cooper, M.J., (1972), Ad. Phys., 20, 453.

(3) Epstein, I.R., and Williams, B.G., (1973), Phil.Mag. 27, 311.

(4) Fukamachi, T., and Hosoya, S., (1970), J. Phys. Soc. Japan, 29, 736.

(5) Cheng, R., Williams,B.G., and Cooper, M.J., (1971), Phil. Mag., 23, 115.

(6) Rachinger, W.A., (1948), J. Scient. Instrum., 25, 254.

(7) Cooper, M.J., Williams, B.G., and Pattison, P., (1974), J. Phys. E., 7, 516.

(8) Weiss, R.J., Harvey, A., and Phillips, W.C., (1968), Phil. Mag., 17, 241.

(9) Fukamachi, T., Hosoya, S., Hosokawa, Y., and Hirata, H., (1972), Phys. Stat. Sol.,(a), 10, 437.

(10) Eisenberger, P. and Reed, W.A., (1972), Phys.Rev. A5, 2085.

(11) Paatero, P., Manninen, S., and Paakkari, T., (1974), Phil. Mag., 30, 1281.

(12) Lloyd, K.H., (1969), Am.J. Phys., 37, 329.

(13) Paakkari, T., Kohonen, E.L., Aikala, O., Manisikka, K., and Mikkola, S., (1974), Phys. Fennica, 9,207.

(14) Felsteiner, J., Fox.,R., and Kahane, S., (1971), Sol.St. Comm., 9, 61.

CHAPTER 3

INVESTIGATION OF MULTIPLE SCATTERING

3.1 Introduction

If a significant number of photons involved in a Compton scattering experiment suffer more than one photon-electron collision before reaching the detector, then the description of the differential cross section developed in Chapter 1 will no longer be valid. There were early indications from both theory[1] and experiment[2] pointing to multiple scattering as a major source of error. However, the problem was largely neglected until, in 1972, Reed and Eisenberger[3] reported that the experimental profile of silicon measured with Te^{123m} gamma-rays showed a clear dependence upon sample thickness. Efforts to avoid the problem by using thin samples, or by measuring a series of profiles with samples of varying thickness, have been of limited success. The results of these experiments highlighted the sensitivity of the measured profiles to sample size and demonstrated that without an accurate description of the effects of multiple scattering, it is impossible to make a reliable assessment of the errors in experimental Compton profiles. In order to remove the effects of a particular experimental geometry (sample thickness, radius, etc.), it is necessary to reproduce the energy distribution of multiple scattered photons and subtract this contribution from the measured profile.

The possible methods of determining the multiple scattered photon energy distributions, both experimentally and theoretically, are described in this Chapter and the next. Initially, a series of qualitative results are used

to illustrate some general features of multiple scattering. The analytic approach on which these results are based is only valid for low energy photons which are scattered in materials of low absorption. In order to obtain a quantitative description of x-ray and gamma-ray scattering, a Monte Carlo procedure was adopted with the aim of calculating the effect of multiple scattering sufficiently accurately for a reliable correction to be made directly to experimental data. In this Chapter this procedure is given in detail and the method is employed to determine the angular and energy distributions of gamma-rays scattering from free, stationary electrons. In the next Chapter, the method is extended to include the case of moving electrons and several applications are described.

3.2 Experimental investigation

The first objective of this work was to establish the manner in which the Compton line shape varies with sample geometry. The results indicated the extent of the problem, and showed that multiple scattering could give rise to systematic errors far greater than the statistical accuracy claimed in published experimental profiles. Therefore experiments were designed to isolate the multiple scattering (using offset-beam geometry) and measure its spectral distribution. It is also possible, by studying the total Compton cross section (compared with the elastic cross section), to determine the intensity of multiple scattering present in a Compton scattering experiment.

3.2.1 Variation with Sample Thickness

In 1972 Reed and Eisenberger[3] reported that the Compton line shape of silicon measured with Te^{123m} gamma-rays

varied with the volume of the sample. It was shown that an increase in scattering volume led to a broadening of the Compton profile, and this effect was attributed to multiple scattering. Measurements were made on samples of various thickness, and the distortion in the Compton profile was found to vary approximately linearly with the sample thickness. This broadening of the profile implies that the spectral distribution arising from multiple scattering is wider than the single distribution, and the multiple intensity increases roughly linearly with the thickness of the sample. On this basis each point in the data was linearly extrapolated to zero scattering volume over the whole range of the measured momentum distribution. This procedure was adopted in several other reported measurements where the distortion was assumed to vary either linearly[4], or possibly as the square root[5] of sample thickness. Although it is clear that such empirical methods provide a means of compensating for some of the effects of multiple scattering, it is difficult to establish a reliable criterion for the accuracy of the final profile. Since the measurements on samples of various thicknesses are time consuming and lead to results which are possibly unreliable, experiments were designed to determine both the spectral distribution and total intensity of multiple scattered photons.

3.2.2 Offset-beam Measurements

In order to obtain information about multiple scattering, an experiment was designed to exclude single scattering events. Using a scattering angle of $\Theta = 0^{o}$, the scattering factor reduces the intensity of single Compton scattered radiation to zero. In order to eliminate the contribution

of unscattered and elastically scattered radiation, the x-ray tube is displaced relative to the spectrometer as shown in fig. 3-1. This experimental arrangement was first used by Hulubei in 1934[2]. The sample, a polycrystalline block of lithium (5 x 3 x 2 cm) was covered in a thin film of oil to prevent oxidization and contained in a polythene bag. A lead shield with two windows enclosed the sample which was irradiated by a 2.4 kW Mo x-ray fluorescence tube. The spectrometer has been described in Chapter 2, but here the 200 reflection of the lithium fluoride analysing crystal was used as this results in an increase in the intensity of the radiation reaching the scintillation counter, while the lower resolution has little effect on the wide double profile.

Fig. 3-2 shows the profile measured as a function of the Bragg angle Θ_B. The positions of the α_1 and α_2 lines in the incident beam were determined by spectral analysis. The absence of these lines in the measured spectrum indicates that there is no significant contribution from twice elastically scattered radiation.

For low energy radiation the expression for the wavelength shift following a single inelastic collision is (see DuMond[1] and also eqn. 2-1)

$$\Delta\lambda = 2\lambda_c \sin^2(\Theta/2) + 2\lambda_o p_z \sin(\Theta/2)/137 \qquad 3\text{-}1$$

where λ_o is the incident wavelength, λ_c the Compton wavelength and p_z the projection of the initial electron momentum on the scattering vector (in a.u.).

For double scattered radiation eqn. 3-1 becomes

$$\Delta\lambda = 2\lambda_c\left[\sin^2(\Theta_1/2) + \sin^2(\Theta_2/2)\right] + (2\lambda_o/137) \left[p_{z1}\sin(\Theta_1/2) + p_{z2}\sin(\Theta_2/2)\right] \qquad 3\text{-}2$$

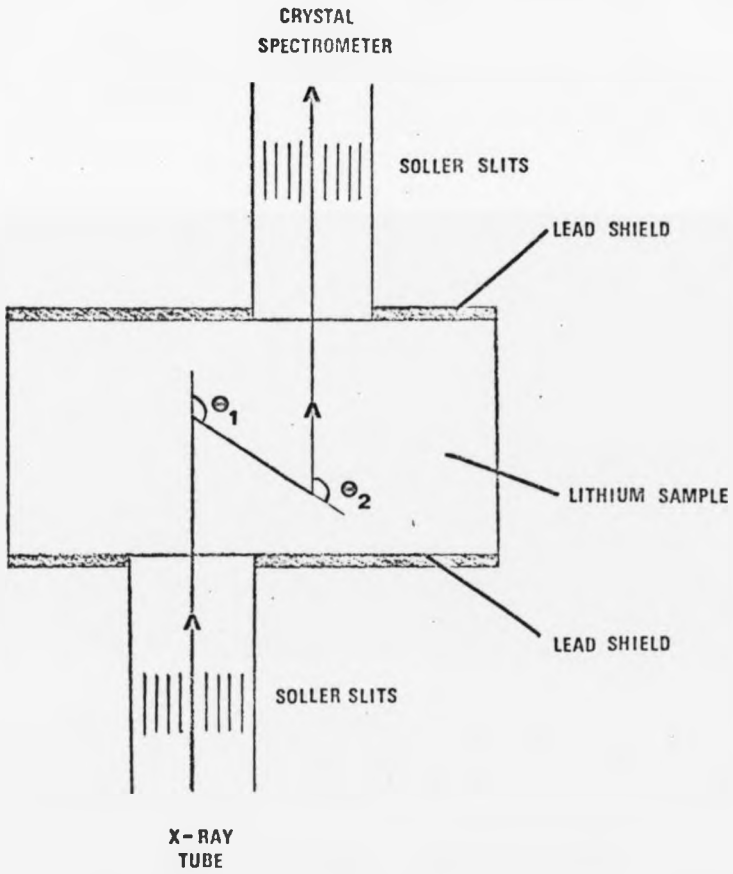

Fig. 3-1: Offset-beam geometry.

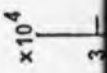

Fig. 3-2: The profile arising from multiple scattered x-rays measured in the offset-beam geometry as a function of the Bragg angle of the LiF analysing crystal. The inset shows the MoKα lines on the same spectral scale.

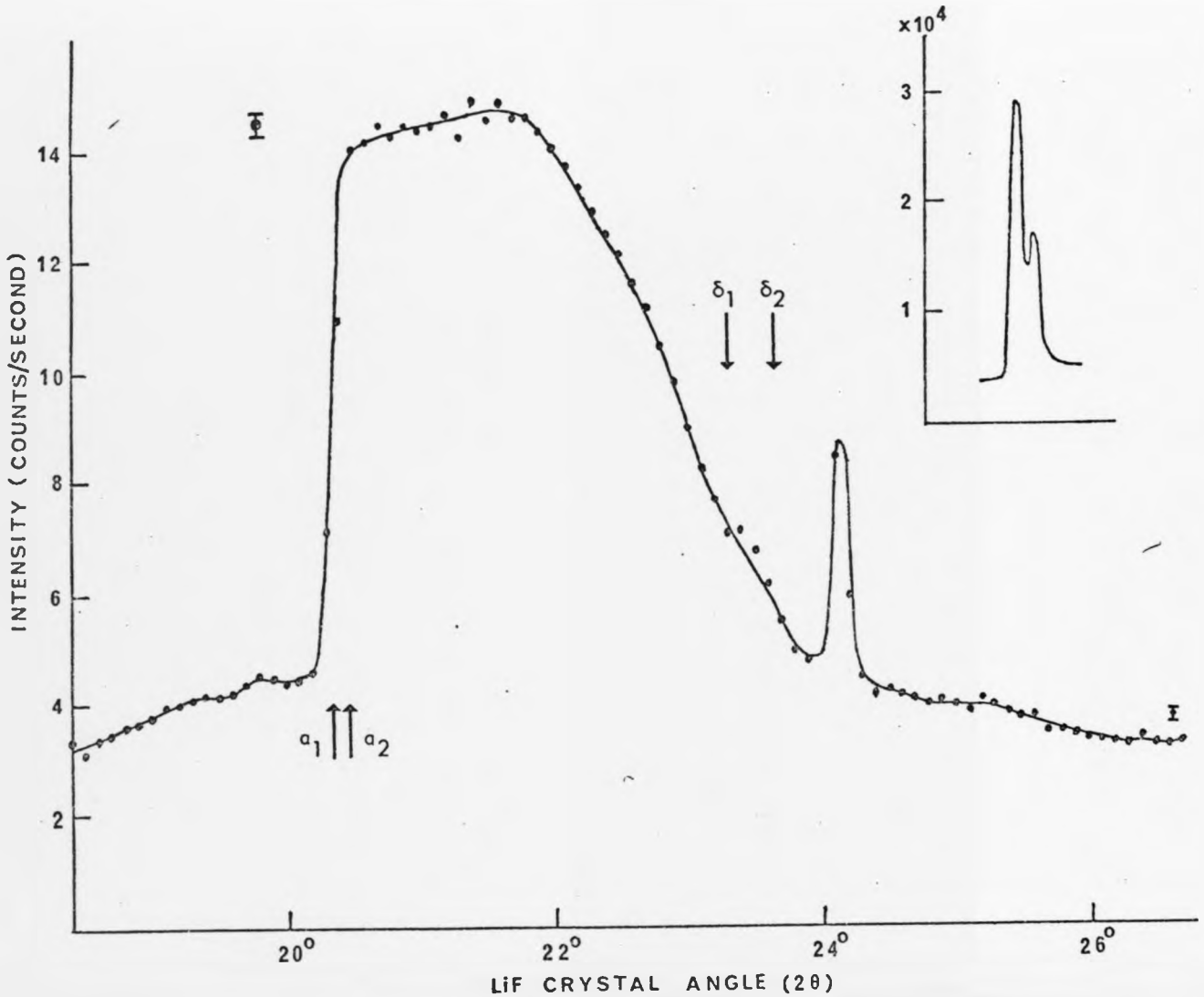
INTENSITY (COUNTS/SECOND)
14
12
10
8
6
4
2
20°
22°
24°
26°
LiF CRYSTAL ANGLE (2θ)
α_1
α_2
δ_1
δ_2
×10⁴
3
2
1

provided $\Delta\lambda \ll \lambda_o$. Subscripts 1 and 2 refer to the first and second scattering respectively. For a total scattering angle $\Theta = 0^o$, $\Theta_1 = \Theta_2 = \Theta_s$ (see fig. 3-1), then eqn. 3-2 reduces to

$$\Delta\lambda = 4\lambda_c \sin^2(\Theta_s/2) + (2\lambda_o/137)\sin(\Theta_s/2)[p_{z1} + p_{z2}] \qquad 3\text{-}3$$

For stationary electrons the second term in eqn. 3-3 is zero (since $p_{z1} = p_{z2} = 0$) and the maximum wavelength shift occurs when $\Theta_s = 180^o$, so that

$$\Delta\lambda_{max} = 4\lambda_c = 0.098\text{Å} \qquad 3\text{-}4$$

This is indicated δ_1 in fig. 3-2

For a free electron gas the maximum wavelength shift is obtained when $\Theta_1 = \Theta_2 = 180^o$ and $p_{z1} = p_{z2} = 0.59$ a.u. of momentum, the Fermi momentum of lithium. In this case

$$\Delta\lambda_{max} = 4\lambda_c + (4\lambda_o/137)(0.59) = 0.110\text{Å} \qquad 3\text{-}5$$

This is indicated δ_2 in fig. 3-2.

The spectral distribution given in fig. 3-2 is thus seen to be consistent with a model based on double Compton scattering. The tail beyond can be attributed partly to contributions from high momentum core electrons which cause wavelength shifts greater than those predicted on the free electron model. Also any triple, or higher order, scattering events could contribute to this tail.

Phillips and Chin[6] obtained a spectral distribution of multiple x-ray scattering in beryllium with the use of a similar scattering geometry which excluded single scattering. By comparing the geometry of such an experiment with that employed in standard Compton profile measurements, they were able to estimate the contribution of

multiple scattering in their experimental profile. The result was consistent with the amount of multiple scattering ($\sim 14\%$) required to account for the differences between a thick-sample and a thin-sample Compton profile. Their experiment served as a clear demonstration of the effects of multiple scattering. However, the use of such a method for correcting Compton profiles involves unjustified assumptions about the behaviour of photons scattering in two different geometries.

It is therefore possible to isolate and measure profiles arising from photons which have scattered more than once, and explain these profiles in a qualitative way. Furthermore these profiles can account for qualitatively the differences in experimental results obtained with thick and thin samples. However, to accomplish this it has been necessary to design scattering geometries which are very different from those employed in Compton experiments. It remains impossible to isolate the spectral distributions of multiple scattered photons obtained in an actual Compton profile measurement.

3.2.3 Cross Section Ratio

In the high momentum transfer region (high $\sin\Theta/\lambda$), it is possible to calculate the ratio of elastic to inelastic cross sections unambiguously; any deviation of the measured ratio from its theoretical value can be directly related to the multiple scattering contribution. In this way, the total intensity of multiple scattering (relative to single Compton scattering) present in a particular Compton profile measurement can be measured in that experiment. This provides a stringent test of any theoretical predictions of

multiple scattering and the application of such a test is described in Chapter 4, section 4.3.

3.3 Analytical Results for X-rays

As early as 1930, DuMond[1] predicted that for an experiment using a spherical graphite sample of 1 cm radius and Mo Kα radiation, the contribution from events involving two collisions would be about 14% of the contribution from single scattering events. The results of the experimental investigations described in the previous section confirm the presence of a significant multiple scattering contribution to experimental Compton profiles. Therefore it is important to establish a qualitative understanding of the physical processes which determine the energy distributions of multiple scattered photons.

The analytical results derived below enable experiments to be designed with a view to minimising multiple scattering. The results also show the limiting conditions where a purely analytic approach may be successfully employed. In this section the results of DuMond are extended to the case of moving electrons and also the case in which one of the collisions is elastic. Experiments using the displaced beam technique described in the previous section are compared with these theoretical predictions.

Notation: Each scattering event in a multiple scattering process is either elastic or inelastic. For this reason, multiple scattering events are referred to as [m,n] scattering events, where m is the total number of times the photon is scattered and n is the number of inelastic collisions. Single Compton scattering is therefore referred to as a [1,1] event. 'Compton units' will be used in which

case $h = m = c = 1$ and the unit of length is $\lambda_c = h/mc = 0.0242\text{Å}$, which results in a considerable simplification (e.g. the peak shift for 180° scattering is 2 Compton units).

3.3.1 Review of DuMond's results for [2,2] scattering by Stationary Electrons

Following DuMond[1] consider a photon scattered through an angle Θ as in fig. 3.3. Let the scattering angle for the first collision be Θ_1 and for the second Θ_2. Θ_1 and Θ_2 may be expressed in terms of spherical coordinates α and φ where α is the angle between the bisector of Θ and the direction of the photon after the first collision, and φ is the angle between the direction of the incident photon and the direction of the photon after the first collision measured about the bisector of the angle Θ. The angles are related by the following expressions:

$$\cos\Theta_1 = \cos\alpha\cos(\Theta/2) + \sin\alpha\sin(\Theta/2)\cos\varphi$$
$$\cos\Theta_2 = \cos\alpha\cos(\Theta/2) - \sin\alpha\sin(\Theta/2)\cos\varphi \qquad 3\text{-}6$$

DuMond considered, initially, the expression for the scattering of radiation by a classical Thompson electron

$$E' = \frac{e^2}{mc^2}\,\vec{\epsilon}_1\cdot\vec{\epsilon}_2\,\frac{E}{r} \qquad 3\text{-}7$$

where e, m and c have their usual meaning, $\vec{\epsilon}_1$ and $\vec{\epsilon}_2$ are the polarization vectors for the incident and scattered photons, E and E' are the amplitudes of the incident and scattered photons and r is the distance from the scattering event at which E' is measured. This expression allows the scattered intensity to be calculated to within about 1% provided the wavelength of the incident photon is greater than about 0.5 Å. Using eqs. 3-6 and 3-7, DuMond then

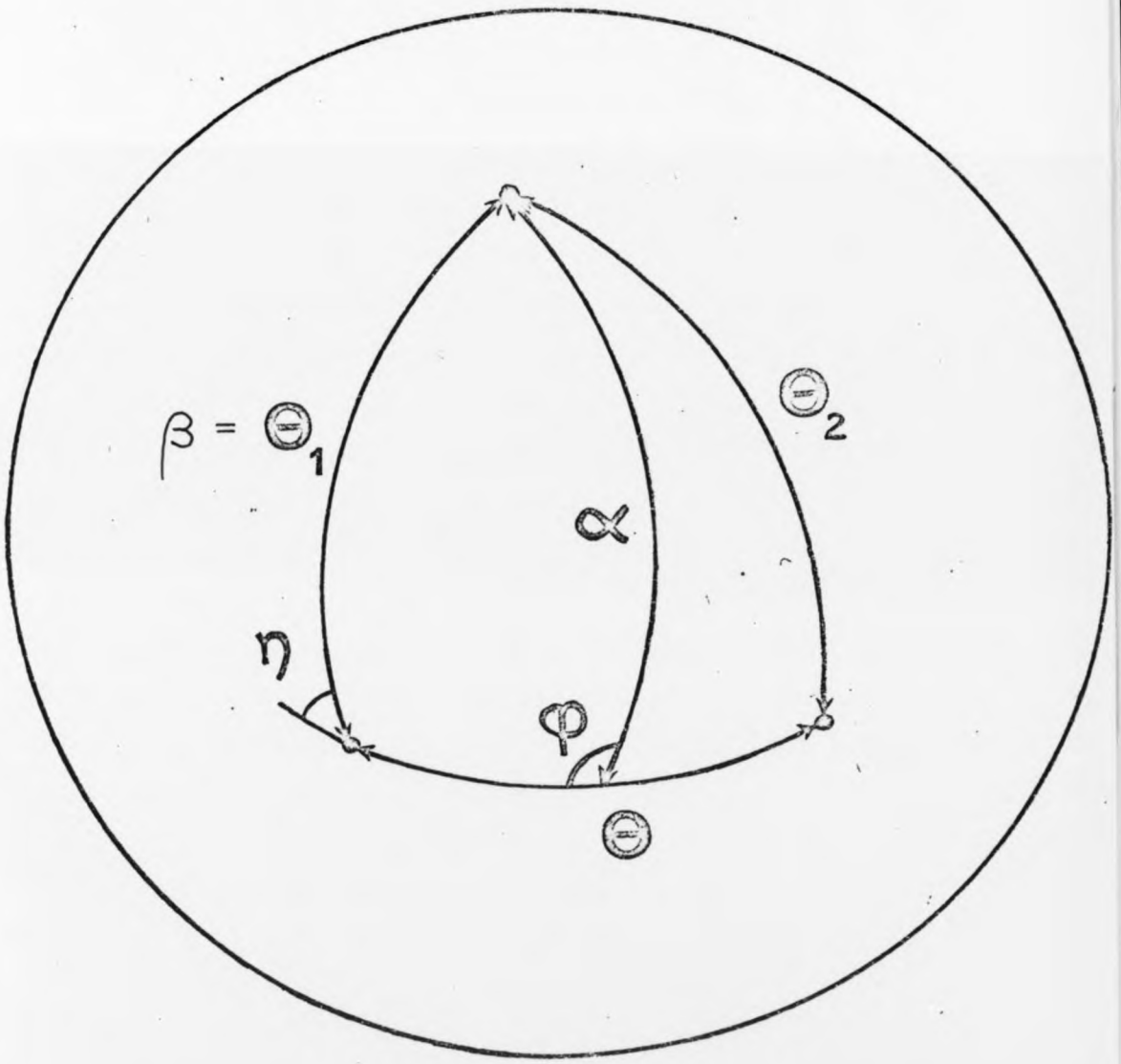

Fig. 3-3: The spherical coordinate systems used in the discussion of double scattering are shown drawn on a sphere.

derived an expression for the ratio of the intensity of double scattering from all electrons in the intermediate solid angle α to $\alpha+d\alpha$, φ to $\varphi+d\varphi$, to the intensity of single scattering. This ratio, R, is

$$R = 3\sigma Y(\alpha,\varphi,\Theta)\sin\alpha\, dr_1 / [8\pi(1+\cos^2\Theta)] \qquad 3\text{-}8$$

where $Y(\alpha,\varphi,\Theta) = \cos^2\Theta + 2(1-\cos\Theta)\cos^2\alpha\cos^2(\Theta/2)$
$+ 2(1+\cos\Theta)\sin^2\alpha\sin^2(\Theta/2)\cos^2\varphi$
$+ [\cos^2\alpha\cos^2(\Theta/2) - \sin^2\alpha\sin^2(\Theta/2)\cos^2\varphi]^2$

and $\sigma = 8\pi e^4/3m^2c^4$ is DuMond's 'scattering coefficient', and dr_1 is a small increment of length in the direction $r_{\alpha\varphi}$. At this point DuMond assumed zero absorption and this enabled him to carry out the integration on dr_1 for all electrons along the direction $r_{\alpha\varphi}$. The Compton shift for a stationary electron in terms of Θ and α is then easily shown to be

$$x = 2[1-\cos(\Theta/2)\cos\alpha] \qquad 3\text{-}9$$

where x is the wavelength shift in Compton units. (Note that this x, in Compton units, is equal to twice DuMond's x). Since the shift is independent of φ, DuMond integrated eqn. 3-8 over φ and substituted x for α using eqn. 3-9 to obtain (with some rearrangement)

$$R = (3/8)\,\sigma r\,[A + B(1-x)^2 + C(1-x)^4] \qquad 3\text{-}10$$

where $A = (19\cos^2\Theta - \cos\Theta + 19)/16$

$B = (1-\cos\Theta)(1+7\cos\Theta)/4(1+\cos\Theta)$

$C = (3\cos^2\Theta + 10\cos\Theta + 19)/4(1+\cos\Theta)^2$

From eqn. 3-10 the spectral distribution for [2,2] scattering from stationary free electrons can be obtained. Finally DuMond integrated eqn. 3-10 all over x to obtain the ratio of the intensity of total double to single scattering as a function of the scattering angle Θ. DuMond's

rather complicated expression can be considerably simplified to give

$$R = (3/8)\sigma\, dr_1\, (28\cos^2\Theta + 44)/[15(1+\cos^2\Theta)] \qquad 3\text{-}11$$

The spectral distribution, given by eqn. 3-10, is illustrated by figs. 3-4a, b and c which are essentially the same as DuMond's figs. 4 to 9. The main feature to be noted is the width of the double scattered profile which decreases from 4 Compton units at $\Theta = 0^\circ$ to zero at $\Theta = 180^\circ$.

3.3.2 Extension of DuMond's Result to include Moving Electrons

For moving electrons some form must be assumed for the electronic wavefunction and hence the Compton profile. A useful, simple form, which is a reasonable approximation in many cases, is to assume a Gaussian Compton profile

$$J(q) = M\exp(-q_\parallel^2/2\gamma^2) \qquad 3\text{-}12$$

where $M = 1/\gamma\sqrt{2\pi}$ normalises the area of J(q) to unity. Consider now a [2,2] scattering event in which the two partial scattering angles are Θ_1 and Θ_2. If the Compton shift λ is measured from the centre of the twice modified peak

$$\lambda = \lambda_1 + \lambda_2 \qquad 3\text{-}13$$

where $\lambda_1 = a_1 p_1 \sin(\Theta_1/2)$

$\lambda_2 = a_2 p_2 \sin(\Theta_2/2)$

and $a_1 = 2\lambda_0/\lambda_c$

$a_2 = 2\lambda_1/\lambda_c$

In eqn. 3-13 λ_1 is the wavelength of the intermediate x-ray, λ_0 is the wavelength of the incident x-ray, and p_1 and p_2 are the component momenta of the scattering electrons resolved along the direction of each x-ray scattering vector. If it is assumed that $\Delta\lambda \ll \lambda_0$ then $\lambda_1 \approx \lambda_0$ and $a_1 \approx a_2$.

Fig. 3-4: The spectral distribution for double [2,2] scattering from stationary electrons for total scattering angles of (a) 0°, (b) 90° and (c) 177°. The wavelength scale is in Compton units (h/mc). The intensity scales are arbitrary.

uble
for
and
ton
bi-

This assumption introduces an error of not more than 10% provided the initial wavelength is greater than about 0.5Å, and furthermore, allows the term $[1 + \frac{\Delta\lambda}{\lambda_o} + (\frac{\Delta\lambda}{2\lambda_o})^2 / \sin^2(\theta/2)]^{1/2}$ which occurs in the full expression for the wavelength shift given by Cooper and Williams[7] to be neglected. The error introduced by this assumption is less than about 5% for wavelengths greater than about 0.5Å.

With these approximations the [2,2] profile is then

$$P(\ell)d\ell = \int_{\ell_1} P(\ell_1)\, P(\ell_2)\, d\ell_1\, d\ell_2 \qquad 3\text{-}14$$

where $P(\ell)d\ell$ is the probability that the wavelength shift lies in the range $d\ell$ at ℓ, and the integral is over all ℓ_1. Using eqn. 3-13 to express ℓ_2 in terms of ℓ_1 and ℓ

$$P(\ell)d\ell = M \int_{\ell_1} J[\ell_1/a\sin(\theta_1/2)]\, J[(\ell-\ell_1)/a\sin(\theta_2/2)]\, d\ell_1 d\ell \qquad 3\text{-}15$$

so that the [2,2] profile for an event (θ_1,θ_2) for a sample whose Compton profile is J(q), is given by the convolution of $J[\ell/a\sin(\theta_1/2)]$ with $J[\ell/a\sin(\theta_2/2)]$. Thus, if the Compton profile is a Gaussian of width γ the [2,2] profile due to an event (θ_1,θ_2) is a Gaussian of width γ_d where

$$\gamma_d/\gamma = 2(\lambda_o/\lambda_c)[\sin^2(\theta_1/2) + \sin^2(\theta_2/2)]^{1/2}$$
$$= \lambda_o/\lambda_c \sqrt{2x} \qquad 3\text{-}16$$

where x, defined in eqn. 3-9, is the wavelength shift for a stationary electron in Compton units.

Now since, from eqn. 3-16 the width of the [2,2] profile is independent of ϕ, the spectral distribution can be calculated as a function of x using eqn. 3-10 and a broadened profile of width proportional to $\sqrt{x}$ can then be included at each point.

From eqns. 3-9 and 3-16 an interesting and important result follows. For $\theta = 180^\circ$ the peak shift for all [2,2]

Fig. 3-5: The spectral distribution of single [1,1] and double [2,2] scattering from moving electrons for which the single scattered profile is a Gaussian of full width at 1/e height = 0.86 a.u. In (a) the scattering angle is 3^{o} leading to a very narrow single scattered profile and a broad double scattered profile. (b) corresponds to a 90^{o} scattering angle and the double profile is still considerably broader than the single profile. In (c), at 177^{o}, the profiles are indistinguishable. The relative heights of [1,1] and [2,2] shown here are arbitrary.

Fig. 3-6: The same spectral distributions as in fig. 3-5 except that a broader Gaussian (full width at 1/e height = 3.5 a.u.) has been taken for the single profile.

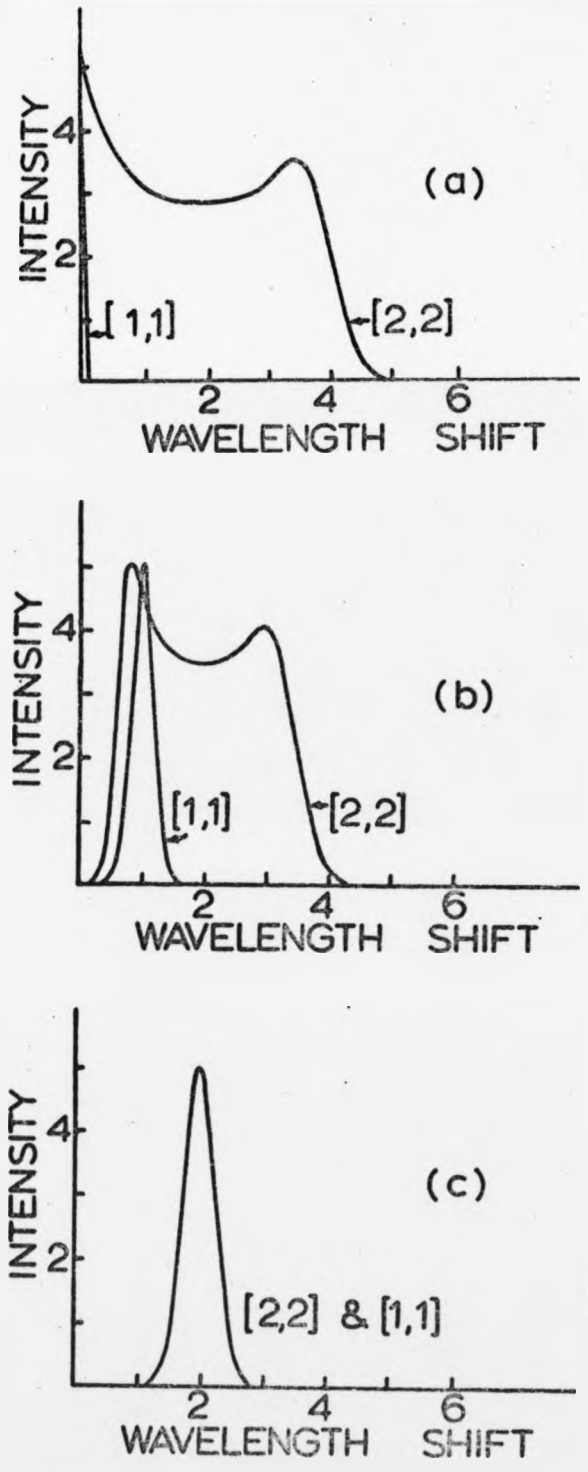
INTENSITY
4
2
(a)
[1,1]
[2,2]
2
4
6
WAVELENGTH SHIFT
INTENSITY
4
2
(b)
[1,1]
[2,2]
2
4
6
WAVELENGTH SHIFT
INTENSITY
4
2
(c)
[2,2] & [1,1]
2
4
6
WAVELENGTH SHIFT

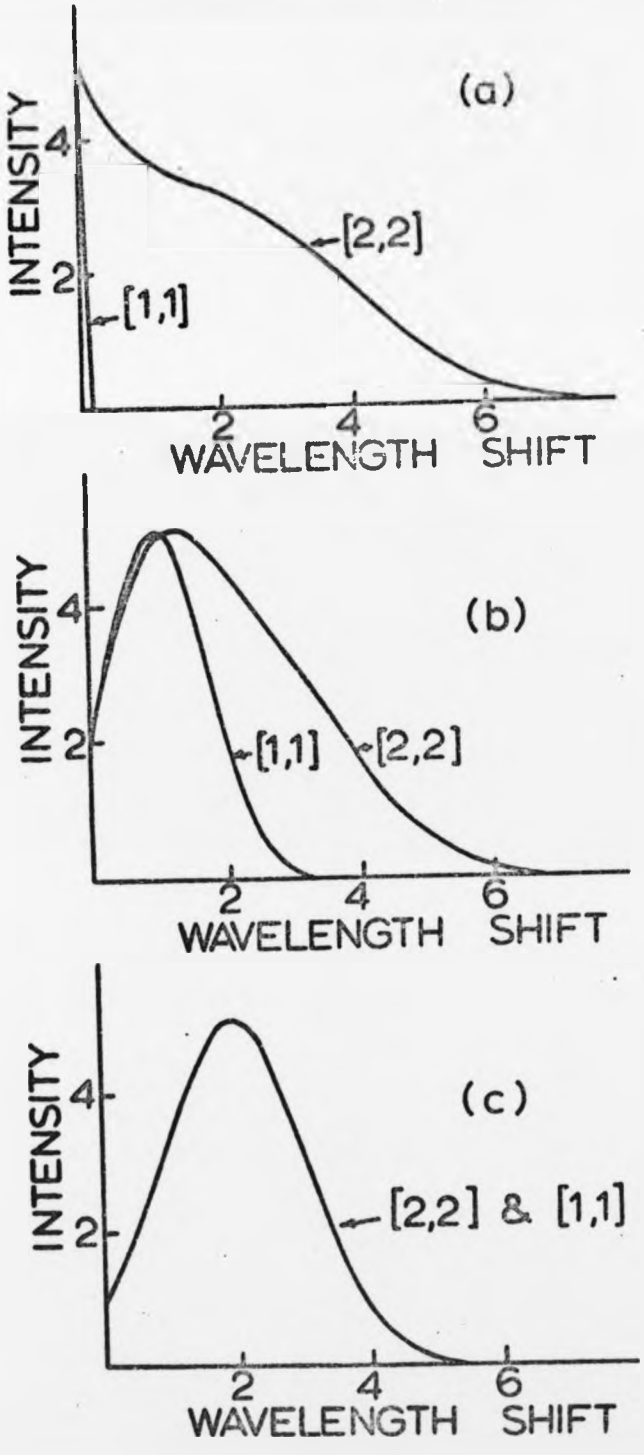
(a)
INTENSITY
4
2
[2,2]
[1,1]
2
4
6
WAVELENGTH SHIFT
(b)
INTENSITY
4
2
[1,1]
[2,2]
2
4
6
WAVELENGTH SHIFT
(c)
INTENSITY
4
2
[2,2] & [1,1]
2
4
6
WAVELENGTH SHIFT

collisions is x = 2 and the width of the profile arising from all [2,2] collisions is $\gamma_d = 2(\lambda_o/\lambda_c)\gamma$. Since these are the same as the peak shift and the width of the profile arising from a single scattered profile for which $\Theta = 180^o$ it follows that for this angle (within the limitations of the approximations used above) the [2,2] and the single scattered profiles are identical if the Compton profile is Gaussian.

The solid lines in figs. 3-5 and 3-6 marked [2,2] show the spectral distribution of double Compton scattering for Gaussian profiles of full width at 1/e height equal to 0.86 a.u. and 3.5 a.u. respectively. The lines marked [1,1] shows the single Compton profile. The broadening, due to the electrons motion, which increases with increasing energy transfer is clearly illustrated. In both cases the shape of the [2,2] profile tends to the shape of the [1,1] or single scattered profile as the total scattering angle tends to 180^o.

3.3.3 Calculation of the Spectral Distribution for [2,1] Scattering

For a [2,1] collision it is convenient to use new polar coordinates β and η as shown in fig. 3-3, since for these coordinates the peak shift and broadening factor are independent of η. (Only the case for which the inelastic collision occurs first is considered. The alternative, in which the second collision is inelastic gives identical results at this level of approximation.)

The equations relating β and η to Θ_1 and Θ_2 are now

$$\Theta_1 = \beta$$

$$\cos\Theta_2 = \cos\beta\cos\Theta - \sin\beta\sin\Theta\cos\eta \qquad 3\text{-}17$$

Using eqn. 3-17, the equivalent of eqn. 3-8 for the

[2,1] case is easily shown to be

$$R = 3\sigma Y(\beta,\eta,\theta)\sin\beta\, d\beta d\eta d\tau/[8\pi(1+\cos^2\theta)] \quad 3\text{-}18$$

where $Y(\beta,\eta,\theta) = \cos^2\theta + \sin^2\theta\cos^2\beta + \cos^2\theta\cos^2\beta$
$- 2\sin\beta\sin\theta\cos^3\beta\cos\theta\cos\eta$
$+ \sin^2\theta\sin^2\beta(1+\cos^2\beta)\cos^2\eta$

The wavelength shift for this [2,1] event is, in Compton units,

$$x = 1 - \cos^2\beta \quad 3\text{-}19$$

As above, since the shift is now independent of η, eqn. 3-18 may be integrated over η and then x substituted for β using eqn. 3-19 to obtain for the spectral distribution for stationary electrons

$$R = (3/8)\sigma[A + B(1-x)^2 + C(1-x)^4] \quad 3\text{-}20$$

where $A = 1 + \cos^2\theta$

$B = 2\sin^2$

$C = 2\cos^2\theta - \sin^2\theta$

If eqn. 3-20 is integrated from x = 0 to 2, i.e. the range of x for all [2,1] events, the ratio of the intensity of total double to single scattering as a function of Θ is found to be the same as for a [2,2] event (see eqn. 3-11). This is to be expected since, at this level of approximation, the cross-section for elastic and inelastic collisions have been taken to be the same.

In fig. 3-7, the spectral distribution for [2,1] scattering from stationary electrons is illustrated. The most important feature of [2,1] scattering is that it gives rise to a distribution which ranges from 0 to 2 Compton units for all values of the total scattering angle and, indeed, is almost independent of the total scattering angle.

3.3.4 Spectral Distribution for [2,1] Scattering from Moving Electrons

Fig. 3-7: The spectral distribution for [2,1] scattering from stationary electrons for total scattering angles of (a) 2^{o}, (b) 90^{o} and (c) 178^{o}. The wavelength scale is in Compton units and the intensity scale is arbitrary.

Fig. 3-8: The spectral distribution of [2,1] scattering from moving electrons for which the single scattered profile is a Gaussian, marked [1,1] .

[2, 1]
otal
c)
units

1]
the
ed

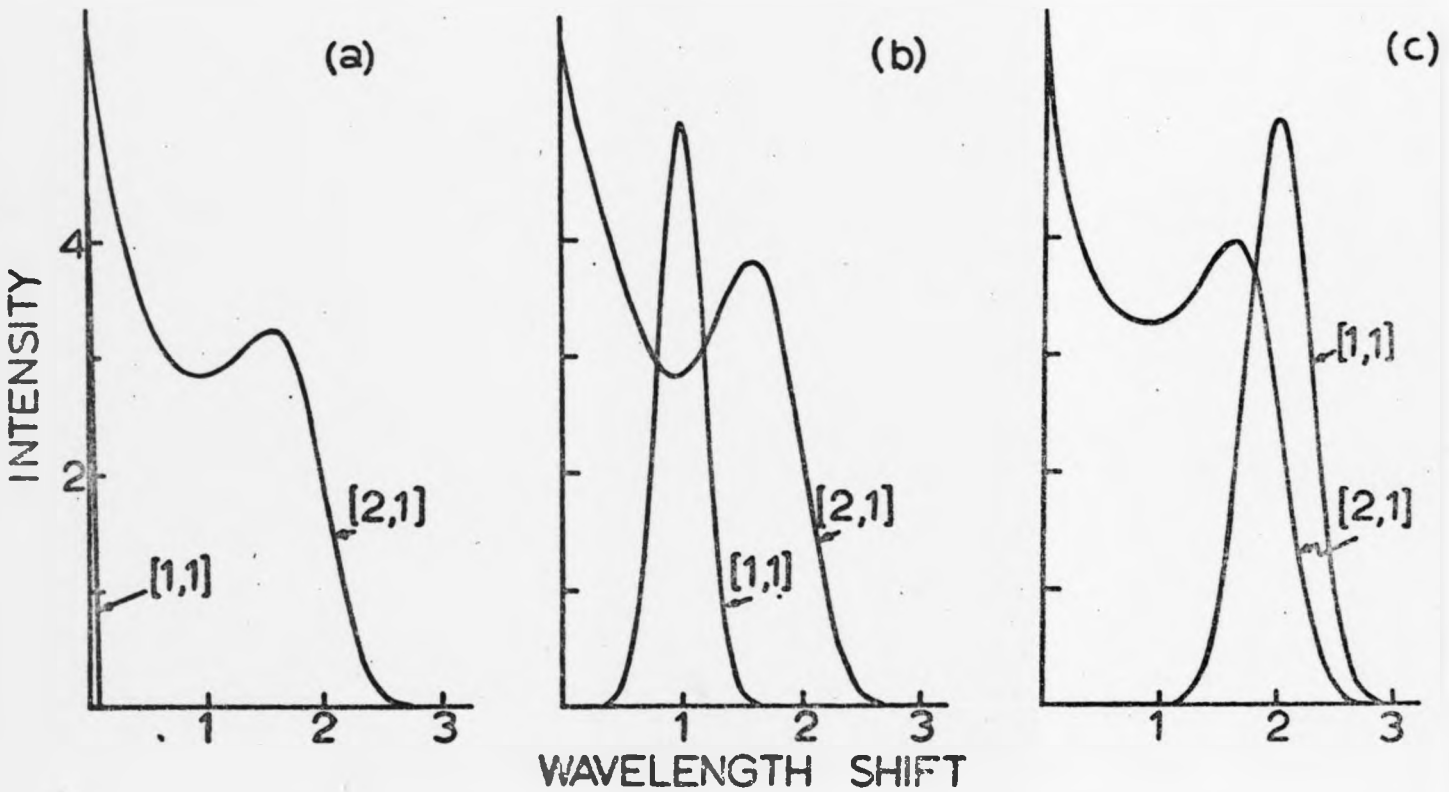
(a)
(b)
(c)
INTENSITY
4
2
[1,1]
[2,1]
1
2
3
WAVELENGTH SHIFT

The spectral distribution for $[2,1]$ scattering by moving electrons may be calculated in the same way as was done for $[2,2]$ scattering. If the Compton profile under consideration is J(q), the $[2,1]$ profile for a collision (β,γ) is $J[q/a \sin(\beta/2)]$. In particular, for the Gaussian Compton profile of eqn. 3-12 the $[2,1]$ profile is a Gaussian of width

$$\sigma_d/\sigma = \sqrt{2x}\,(\lambda_o/\lambda_c) \qquad 3\text{-}21$$

Thus, to calculate the $[2,1]$ profile for a Gaussian Compton profile, eqn. 3-20 can be used to calculate the spectral distribution and then a broadened profile, of width proportional to $\sqrt{x}$, can be included at each point.

Fig. 3-8 shows the spectral distribution for $[2,1]$ scattering for the same Gaussian profile as in fig. 3-5. The singularity at zero wavelength shift corresponds to the situation in which the inelastic scattering is in the forward direction so that $\beta = 0$. However, for bound electrons the cross-section for inelastic forward scattering is zero and this singularity is therefore not present in practice. From fig. 3-8 it is clear that, unlike the $[2,2]$ profile, the $[2,1]$ profile does not tend to the single scattered profile as Θ tends to 180° but is almost independent of the scattering angle. However, for light elements the $[2,1]$ scattering is only expected to amount to a few percent of $[2,2]$ scattering because the elastic scattering cross section is very small compared with the Compton cross section. Where the elastic cross section is significant, say for aluminium and Mo x-rays, then the $[2,1]$ scattering could make a large contribution to the total multiple scattering.

3.3.5 Limitations of the Theory

Throughout this section it has been assumed that the wavelength change, $\Delta\lambda$, in the scattering process is very much less than the initial wavelength λ_o.

This assumption was first used in eqn. 3-7 where the classical Thompson cross-section was used rather than the full relativistic expression. For Mo Kα x-rays ($\lambda \approx 0.7$A) this approximation is adequate. However, for Am^{241} γ-rays ($\lambda \approx 0.2$A) or Te^{123m} γ-rays ($\lambda \approx 0.07$A) the approximation breaks down. Indeed, the complete relativistic expression for the scattering of photons as a function of polarization (see eqn. 1-1) should be used. Unfortunately, this is too complicated to make an analytical treatment of the kind outlined in this chapter possible.

The assumption of negligible wavelength change was next used in eqn. 3-13 where the intermediate wavelength was put equal to the initial wavelength and the correction term $\left[1 + \frac{\Delta\lambda}{\lambda_o} + \left(\frac{\Delta\lambda}{\lambda\lambda_o}\right)^2 / \sin^2(\Theta/2)\right]^{-1/2}$ was put equal to 1. Even for Mo kα x-rays the errors introduced by these approximations are about 5% and 10% respectively and the correction term should therefore be included in any attempt to calculate accurate multiple scattering profiles. These factors could probably be taken into account without much difficulty, provided they are included in eqn. 3-8 before the integration over φ is carried out. For Am^{241} and Te^{123m} γ-rays, this approximation fails completely since for Te^{123m}, say, $\Delta\lambda/\lambda_o$ may be of the order of 1.

From the point of view of x-ray experiments the next most important approximation is the neglect of the binding energy cut-off and the corresponding use of the impulse approximation. To include the binding energy cut-off

requires the use of eqn. 3-8 since the cut-off varies with φ. The broadened profile for each event would be calculated for each α and φ, the binding energy cut-off included and the resulting pairs of profiles convoluted. Finally, the integrations over α and φ would have to be carried out numerically. For the high energy γ-rays the effect of binding energy is less important than it is for the low energy x-rays. The general result however, would be to reduce the profile intensity in the region of small wavelength shift and, in particular, to eliminate the singularity in the $[2,1]$ profiles.

The shape of the multiple scattered profile is also dependent on the sample geometry since this affects the probability of obtaining a given pair of scattering angles. This becomes particularly important if an off-set-beam technique is used to estimate the multiple scattering in an experiment with no offset. A similar problem arises from the photoelectric absorption in the sample, in that this alters the probability of obtaining various paths through the sample.

3.3.6 Conclusions

DuMond integrated eqn. 3-11 over the volume of a spherical sample with the assumption that there is no attenuation of the beam and showed that the ratio of double to single scattering is proportional to r, the radius of the scatterer. From this two important observations follow..

First of all, it is clear that multiple scattering is more important in experiments using high energy gamma-rays rather than x-rays. For x-rays the large photoelectric absorption cross sections produce a geometric constraint on the possible photon paths, and hence reduce the effective

sample size. Secondly, it is clear that the use of a small spherical sample is not a particularly good way of eliminating multiple scattering since the intensity of single scattering will decrease as r^3, while the amount of double scattering will only decrease with r. However, for a disc of thickness 1 and constant radius the single scattering only decreases as 1, and this is therefore a more favourable geometry.

From the results presented in this section it is clear that the width of the $[2,2]$ profile, and hence its effect on the total profile, can be minimised to some extent by using a scattering angle as close to 180° as possible. However, this is not the case for $[2,1]$ scattering and this may have a more pronounced effect on the shape of the experimental profile for x-rays, particularly for the heavier materials for which the elastic scattering is more intense, than the Compton scattering.

Currently, the only way of separating the single and multiple scattering experimentally appears to be some type of displaced beam technique. However, this eliminates the single rather than the multiple scattering and various assumptions must be made about the relationship between multiple scattering in a displaced beam experiment and the scattering in the standard experimental geometry if this method is to be used to "subtract out" multiple scattering.

Thus the theory as presented here can be used to make reasonable qualitative predictions of the $[2,2]$ and $[2,1]$ profile shapes for x-ray experiments. In order to establish the total intensity as well as the spectral distributions, the sample geometry and absorption must be taken into account. These factors probably account for the differences between the theoretical profiles for a total scattering angle

$\Theta = 0^{o}$, shown in fig. 3-4a, and the experimental profile obtained with an offset-beam geometry (fig. 3-2).

McIntire[8] has shown that it is possible to include the effects of sample geometry and absorption for the limiting case of 180^{o} backscattering. In an experiment designed with a scattering angle close to 180^{o} the finite beam divergence prevents the use of the cross-over beam technique described in Chapter 2. This results in a large background and poor signal/background ratio. Therefore a scattering angle closer to 150^{o} is normally chosen for a gamma-ray experiment, while for x-rays the size of the apparatus prevents the use of a higher scattering angle. The results of McIntire cannot be used to correct profiles measured at these lower scattering angles.

In conclusion, the analytical approach as described above can be used to establish some useful qualitative results. These provide guide lines for the design of experiments, and indicate those conditions where multiple scattering must be taken into account. Efforts to quantify the shape and intensity of the spectral distributions obtained in an actual experiment have demonstrated the limiting conditions under which analytical results may be applied successfully. A more general approach is required in order to take account of the various geometries, samples and photon energies employed in current experiments.

3.4 The Monte Carlo approach

The passage of a photon through a scattering body can be interpreted in terms of elementary events, with each event having a characteristic probability. The Monte Carlo method is particularly applicable to this type of problem where the 'life-histories' of a large number of test

particles can be followed in a simulation of a real experiment (see e.g. Cashwell and Everett[9] for an introduction to the technique). The method has previously been applied to problems of photon transport such as radiation shielding, dose-rate absorption, detector efficiency, and many others. In particular, the approach described below is similar to that of Lichtenberg and Przybylski[10] who applied the Monte Carlo technique to the problem of multiple scattering in a Compton polarimeter.

The program must describe the behaviour of photons emanating from a given source configuration, which undergo specified processes in a material medium of known geometry and terminate in certain stipulated categories. A possible flow-chart for such a calculation is given in fig. 3-9. However, in this form many 'life histories' may be followed which terminate in categories which provide no useful information for comparing with a Compton scattering experiment (i.e. the photon may be transmitted without scattering or suffer photoelectric capture). In order to avoid these redundant calculations the photon is assigned a 'weight' or probability which is reduced according to the probability of some unproductive process occuring, and the photon is then 'forced' to follow a more useful path. If this technique is used to avoid both transmission and photoelectric capture the resultant flow-chart is given in fig. 3-10.

This chart is the basis of the program adopted to calculate the energy distributions of multiple scattered photons. A mathematical description of each elementary process is given in the next section, and in the final section some preliminary results are given for the case of stationary electrons. The errors which arise from the statistical nature of the calculation are found to be tolerable (compared

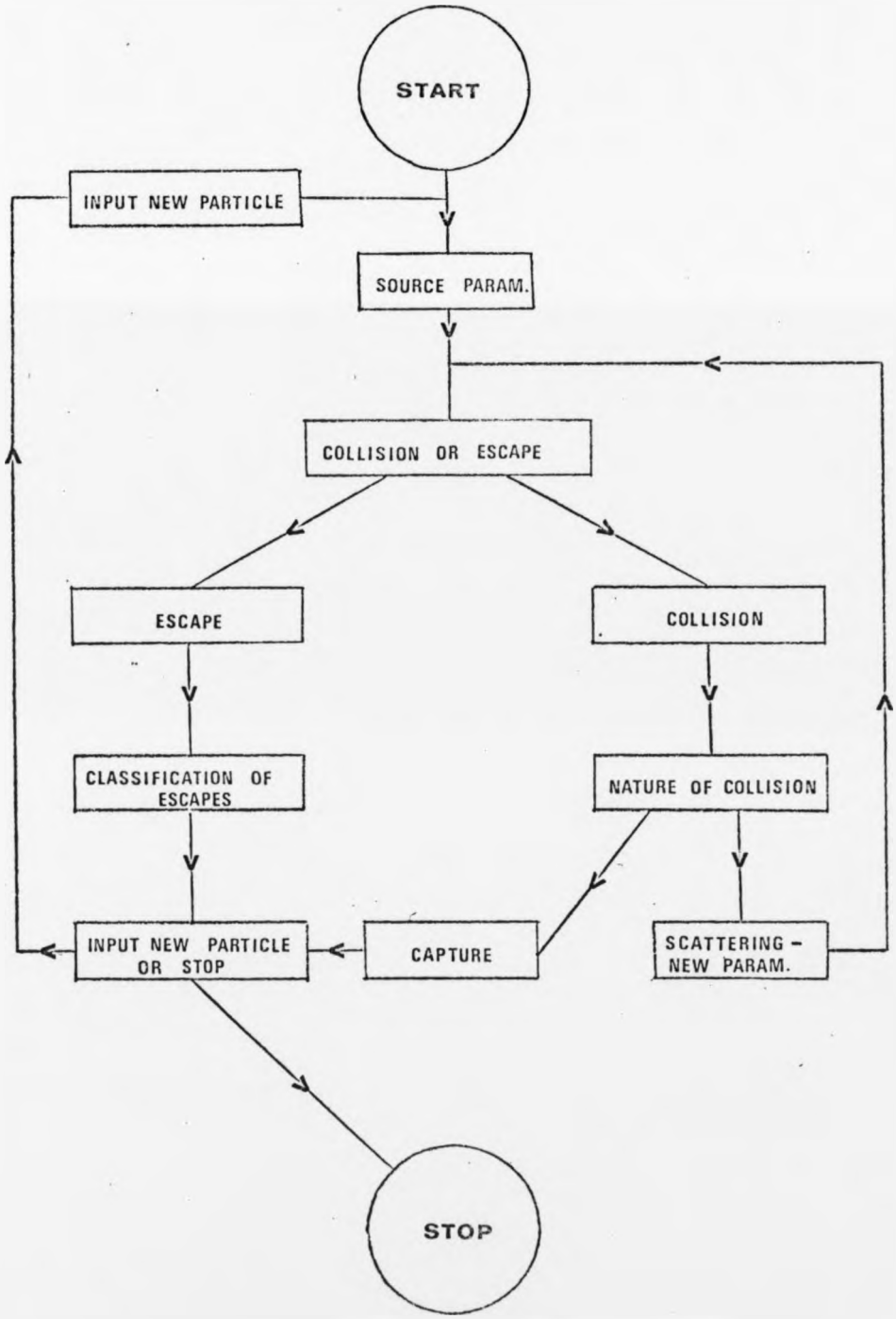

Fig. 3-9: Possible flow-chart for a Monte-Carlo calculation of photon scattering.

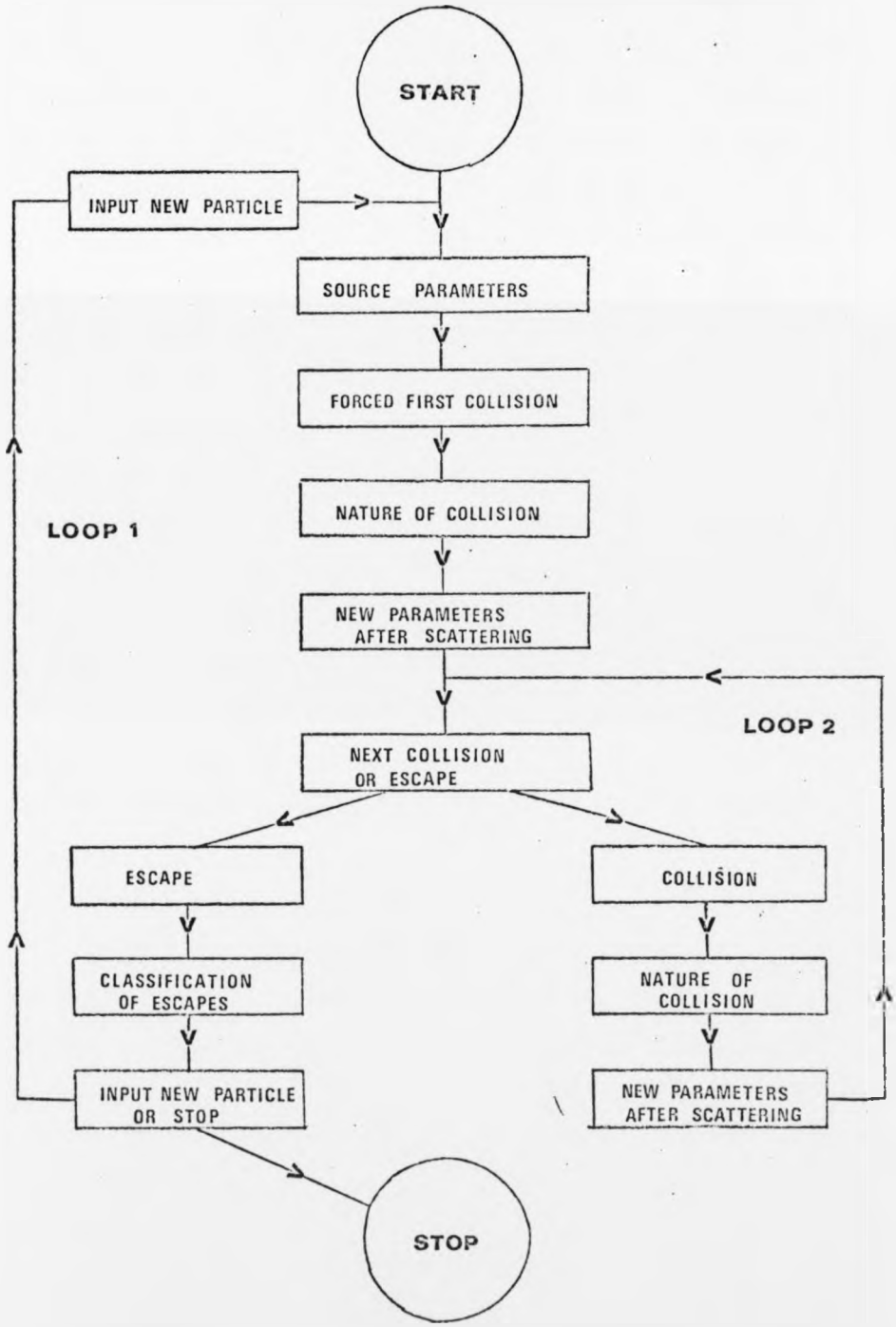

Fig. 3-10: Improved flow-chart for a Monte-Carlo calculation of photon scattering.

with the experimental errors) if some 10^6 test particles are introduced. Up to three photon-electron collisions are followed for each particle, and higher order scattering events are found to play no significant part for any samples and geometries currently employed in Compton experiments.

The computer program is written in FORTRAN and is broken into subroutines according to the flow diagram in fig. 3-10. Each 'photon' follows a cycle shown by loop 1 in fig. 3-10. Up to three collisions are followed for each photon (a collision path is represented by loop 2), and a further terminal category is available for those photons which suffer more than three collisions. These photons represent a very small fraction ($< 1\%$) of the total number of scattered photons in a Compton experiment, and their effect on the final energy distribution can therefore be neglected. The program was run on a CDC 7600 computer (the Manchester Regional Computer), with a CPU time of 450 seconds when 10^6 photon paths are followed. A store of 30K is required.

3.4.1 The Monte Carlo Procedure

In general if a beam of photons is incident upon an assembly of atomic electrons the incoming photons may undergo one of the following interactions: photoelectric absorption, elastic scattering, or Compton scattering. Assuming for the moment linearly-polarised incident radiation interacting with stationary electrons, the differential Compton cross-section is (see eqn. 1-1)

$$d\sigma_{\text{Compton}}(\omega_1,\Theta) = \frac{1}{4} r_0^2 d\Omega \left(\frac{\omega_2}{\omega_1}\right)^2 \left(\frac{\omega_1}{\omega_2} + \frac{\omega_2}{\omega_1} - 2 + 4\cos^2\Theta\right) \quad 3\text{-}22$$

where Θ is the angle between the electric vectors of the incident and scattered photons $\bar{\epsilon}$ and $\bar{\epsilon}'$ respectively, r_0 is

Fig. 3-11: Scattering event at O. ϵ and ϵ' are the electric vectors of the incident and scattered photons. The line O'A' is parallel to OA and makes an angle θ with ϵ'. The various angles are defined in the text.

3'2
A'
O'
I
θ
-3'
C
θ
B
D
A
3
O
3'1

the classical electron radius, $d\Omega$ is the element of solid angle through which the photon emerges after the collision, and ω_1, ω_2 are the energies of the incident and scattered photons, respectively. The relation between ω_1 and ω_2 is given by the well-known expression for the Compton shift (see eqn. 1-2)

$$\frac{\omega_1}{\omega_2} = 1 + \frac{\omega_1}{mc^2}(1 - \cos\Theta) \qquad 3\text{-}23$$

where Θ is the scattering angle, and $m c^2$ is the electron rest energy. Referring to fig. 3-11 we denote by η the azimuthal angle between the primary plane of polarization OAC and the scattering plane ODC, and by β the angle between the plane OADB (defined by $\bar{\epsilon}$ and the direction of scattering) and the plane of polarization after scattering (defined by $\bar{\epsilon}'$ and the direction of scattering). One can then obtain the relationship between the various angles[11]

$$\cos^2\Theta = (1 - \sin^2\Theta\cos^2\eta)\cos^2\beta \qquad 3\text{-}24$$

and eqn. 3-22 becomes

$$d\sigma_{Comp}(\omega,\Theta,\eta,\beta) = \frac{1}{4} r_0^2 d\Omega \left(\frac{\omega_2}{\omega_1}\right)^2 \left(\frac{\omega_1}{\omega_2} + \frac{\omega_2}{\omega_1} - 2 + 4(1 - \sin^2\Theta\cos^2\eta)\cos^2\beta\right) \qquad 3\text{-}25$$

It follows that the scattered radiation is partially polarized. In the case of elastic scattering $(\omega_1 = \omega_2)$ we always have $\beta = 0$, i.e. the scattered radiation is completely polarized and the differential cross-section becomes:

$$d\sigma_{el}(\Theta,\eta) = r_0^2 d\Omega (1 - \sin^2\Theta\cos^2\eta) \qquad 3\text{-}26$$

In the following sections the steps in the Monte-Carlo calculation needed for simulating the path of one photon are described.

(a) Point of entrance into the specimen:

The photon is assumed to arrive at right angles to the

base of a cylindrical specimen, and the point of entrance is selected at random (i.e. the photon flux is considered uniform).

(b) Forced first collision:

In order to save computer time, the photon is forced to have a first collision by using the following Monte-Carlo relation between the depth of penetration ℓ and the total attenuation coefficient μ[9]

$$\ell = -\frac{1}{\mu}\log_e(1 - r[1 - \exp(-\mu L)]) \qquad 3\text{-}27$$

L is the thickness of the specimen, and r is a random number in the interval (0,1). To allow for that part of the flux which would otherwise be transmitted through the specimen without collision, the photon is assigned a weight W according to the expression

$$W = 1 - \exp(-\mu L) \qquad 3\text{-}28$$

(c) The nature of the scattering:

To take account of the possibility that the photon may be photoelectrically absorbed, the weight W given to it is reduced by the ratio, R, of the photoelectric cross-section to the total attenuation coefficient, according to the relationship

$$W' = W(1-R) \qquad 3\text{-}29$$

The type of scattering process is then determined by dividing the random number interval (0,1) in proportion to the fractions of elastic and Compton scattering in the scattering attenuation coefficient (the attenuation coefficients were taken from the tables of Hubbell[12].

(d) Geometrical Considerations:

The scattering angles θ and η following the collision are selected at random in the intervals $(0,\pi)$ and $(0,2\pi)$, respectively, and in the case of Compton scattering the

polarization angle β is also selected at random in the interval $(0,\pi)$. The weight W of the photon is then reduced according to the differential cross-section for either a Compton collision (eqn. 3-25) or an elastic collision (eqn. 3-26), normalised with respect to the total cross-section.

(e) The path after the collision:

The path length ℓ following the collision is then calculated using the formula[9]

$$\ell = -\frac{1}{\mu'} \log_e(r) \qquad 3\text{-}30$$

where μ' is the total attenuation coefficient for the new photon energy and r is a random number in the interval (0,1). The quantity ℓ and the angles Θ and η, are then used to determine whether the photon escapes before suffering another collision, or if not the position of the next scattering is ascertained.

(f) The next collision:

If the photon has another collision the procedure described in sections c, d and e is repeated. This cycle can be continued until the photon leaves the specimen, or can be stopped after an arbitrary number of collisions. (In present calculations up to three collisions are considered). It should be noted that the angles Θ, η and β which described the direction and polarization of the scattered photon are calculated with respect to the coordinate frame of the photon at each collision. This photon frame is not in general equivalent to the laboratory frame and in order to follow the progress of the photon through the specimen these angles must be transformed back to the laboratory frame after each collision.

(g) Exit of photon:

If the photon leaves the specimen, the information relating to its energy and to its scattering angle (in the laboratory frame) is stored by adding the final weight W of the photon into an appropriate register. Several registers were available according to the number and nature of the collisions suffered by the photon. Since the initial beam was considered to be linearly polarized, the intensity of the outgoing photons, at a given angle of scattering Θ, would depend upon the azimuthal angle η. However, as sources used in current experiments provide unpolarized beams of photons, it is necessary to average over all possible directions of the electric vector of the initial photon. Since the assumed experimental geometry has axial symmetry, this can be achieved in the above calculation by averaging the final intensity (for initially polarized radiation) over all angles η for each angle Θ. This imposes certain symmetry conditions on the experimental geometry. In general, however, there is no difficulty in constructing experiments with the required axial symmetry assumed in this calculation.

3.4.2 Results for Stationary Electrons

The angular and energy distributions of the scattered photons were calculated assuming a monochromatic primary photon beam, having an energy of 59.54 keV (^{241}Am gamma source energy), incident upon a cylinder of radius 2.5 cm. and thickness 3.0 cm. with the absorptive properties of water. The paths of 10^6 photons were followed.

Fig. 3-12shows the angular distributions of photons scattered once, twice or three times (single elastic events are not shown). The angular distribution for single Compton scattering is seen to follow the Klein-Nishina formula for

Fig. 3-12: Calculated angular distributions of photons scattered once, twice or three times in a specimen of thickness 3 cm. The energy of the incident photons is 59.54 keV.

INTENSITY
3
2
1
triple
x25
double
x5
single
90°
180°
ANGLE

unpolarized incident radiation (eqn. 1-3) and this serves as an overall check on the Monte Carlo procedure. The good agreement demonstrates how the final averaging removes the polarization condition imposed on the incident photons. Since any total scattering angle for multiple events is made up from many combinations of intermediate angles, a general trend away from any angular dependence for higher order scattering can be expected and this is clearly demonstrated. Furthermore, the angular distribution for double scattering shows qualitative agreement with the distribution predicted analytically by DuMond[1]. (Quantitative agreement would not be expected because DuMond employed a classical cross-section in his calculations.

Fig. 3-13 shows the energy distributions of photons scattered twice and leaving the specimen in three different directions, 5° - 15°, 85° - 95° and 165° - 175°. It can be seen that the double scattering profiles become narrower as the total scattering angle increases. This is to be expected since, for a total scattering angle Θ, the range of angles through which a photon may be deflected ranges from Θ to $(360^\circ - \Theta)$. As the energy loss depends upon the angle of deflection of the photon, this condition will lead to wide profiles at low angles of Θ, and to narrow profiles as Θ approaches 180°. It can also be seen that a region of low and rather uniform intensity extends from the incident photon energy to the main profile. This is due to photons which suffer one Compton and one elastic collision.

Fig. 3-14 shows the same distribution as fig. 3-13 for the case of photons scattered three times. Again, it can be seen that for higher order scatterings there is a loss of angular dependence, as well as a reduction in intensity.

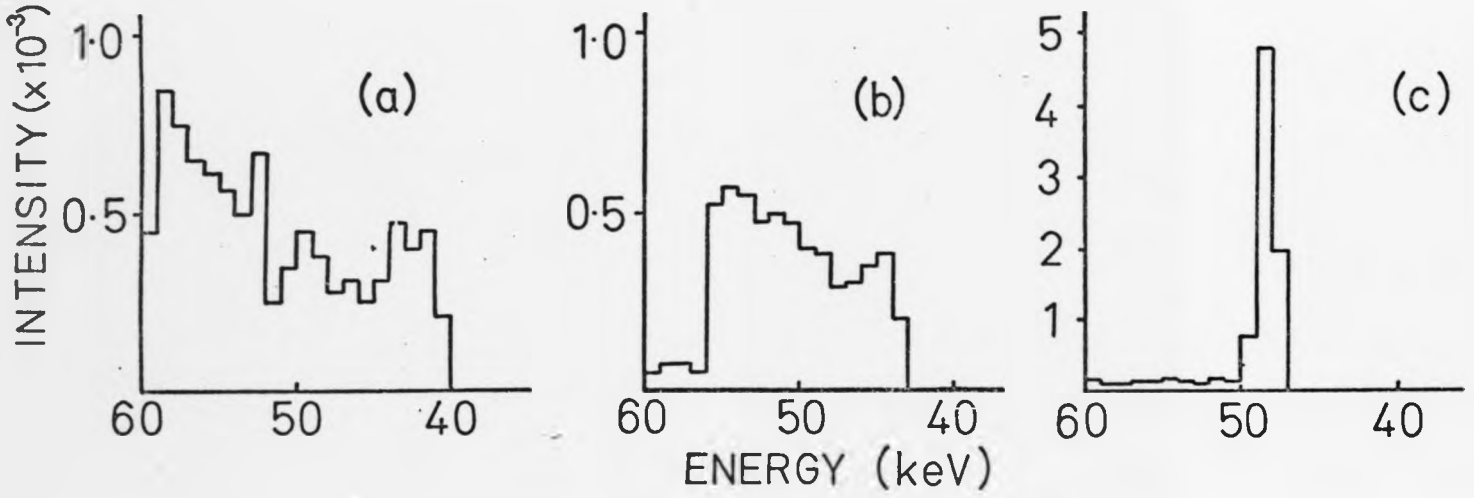

Fig. 3-13: Calculated energy distributions of photons scattered twice and leaving the specimen in the directions (a) 5°-15°, (b) 85°-95° and (c) 165°-175°. The intensity is relative to the incident photon flux.

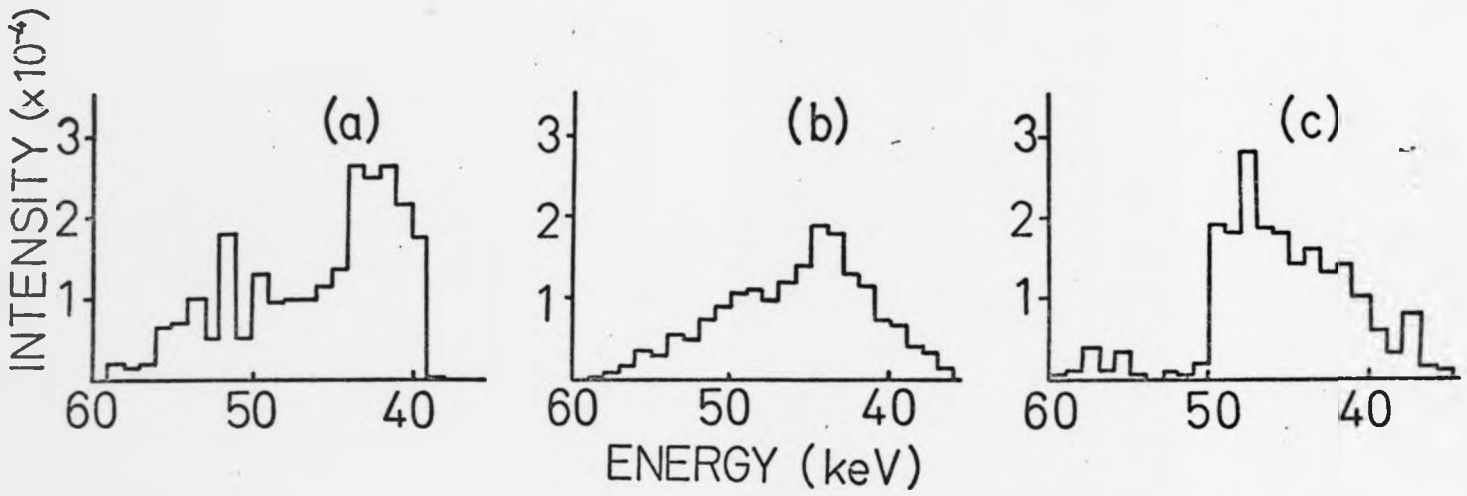

Fig. 3-14: Calculated energy distributions of photons scattered three times and leaving the specimen in the directions (a) 5^{o}-15^{o}, (b) 85^{o}-95^{o} and (c) 165^{o}-175^{o}. The intensity is relative to the incident photon flux.

These Monte Carlo results for scattering by stationary electrons can be compared with the analytic results described in section 3.3. In some general features, such as the profile widths, the two methods predict similar results. However, the effects of absorption and sample geometry have significantly modified the profile shapes. Moreover, the Monte Carlo method provides a means of assessing the relative contributions of multiple and single scattering in any experimental Compton profile.

In the following Chapter the Monte Carlo procedure is used to determine the importance of multiple scattering in various experimental conditions for a range of samples and incident photon energies. Corrections are made directly to measured profiles to remove multiple scattering effects from the differential Compton cross section. Predicted values for the total Compton cross section (compared with the elastic cross section) are found to vary with the amount of multiple scattering, and this behaviour is used to test the Monte Carlo program.

Chapter 3 References

(1) DuMond, J.W.M., (1930), Phys. Rev., 36, 1685.

(2) Hulubei, H., (1934), Ann. de. Phys., Ser. XI, 1, 5.

(3) Reed, W.A., and Eisenberger, P., (1972), Phys. Rev. B6, 4596

(4) see e.g. Felsteiner, J., Fox, R., and Kahane, S., (1972), Solid State Commun., 11, 635; Manninen, S., Paakkari, T., and Kajantie, K., (1974), Phil. Mag., 29, 167.

(5) Paakkari, T., Kohonen, E.L., Aikala, O., Mansikka, K., and Mikkola, S., (1974), Physica Fennica, 9, 207.

(6) Phillips, W.C., and Chin, A.K., (1973), Phil. Mag., 27, 87

(7) Cooper, M.J., and Williams, B., (1972), Phil. Mag., 25, 1499

(8) McIntire, W.R., (1974), Phys. Stat. Sol., 23, 359.

(9) Cashwell, E.D., and Everett, C.J., (1959), The Monte Carlo Method for Random Walk Problems, (London: Pergamon Press).

(10) Lichtenberg, W., and Przybylski, A., (1972), Nucl. Instr. Meth., 98, 99.

(11) see e.g. Evans, R.D., (1955), The Atomic Nucleus (New York: McGraw-Hill).

(12) Hubbell, J.H., (1969), U.S. National Bureau of Standards Circular, NSRDS-NBS 29.

CHAPTER 4

APPLICATIONS OF THE MONTE CARLO METHOD

The investigations described in the previous chapter revealed that a substantial contribution to the Compton profile can arise from photons which have scattered two or more times. Therefore a Monte Carlo technique was developed to calculate the total intensity and spectral distribution of multiple scattered photons. Several applications of the technique are now described in this Chapter.

The results of Monte Carlo calculations for a wide range of experimental conditions are given in the first section. They establish the importance of multiple scattering in various materials for a selection of photon energies commonly used in Compton profile measurements. These results indicate how experiments should be designed in order to reduce multiple scattering to a minimum. In section 4.2 the method is employed to correct measured profiles of water for the effect of multiple scattering, and after correction the profiles appear to be independent of sample thickness, within their statistical error. The variation in the total cross section due to multiple scattering serves as a check on the Monte Carlo procedure and the application of such a test is described in section 4.3.

In all of these calculations the effects of electron binding have been neglected. This should not introduce a serious error since for elements of low atomic number the K-shell binding energies are low in comparison with the incident photon energies, while for high atomic number materials with substantial K-shell binding energies these electrons are a small fraction of the total. However, it

is possible to include the effects of binding through the use of incoherent scattering factors and form factors. These developments are discussed in the final section (4.4).

4.1 A Survey of Multiple Scattering

The dependence of multiple scattering upon photon energy and specimen geometry is described here for three different materials, namely lithium, aluminium and copper. These span the range of atomic numbers (and therefore the range of absorption) of materials presently used in Compton scattering experiments. Incident photon energies of 160 keV (Te^{123m}), 60 keV (Am^{241}) and 17 keV (MoKα) are considered for each of the above three materials. A scattering angle of $150^{\circ} \pm 2^{\circ}$, used in many experiments, was selected, and over 10^6 photon paths were followed in each calculation. Since the collimation system employed in these experiments defines a specimen radius, a radius of 1.0 cm was assumed in all the calculations, leaving the thickness of the specimen as the principal geometric variable.

In some earlier reports of Compton measurements multiple scattering was assumed to vary either linearly[1], or as the square root[2] of sample thickness. The results shown below will clearly indicate that these assumptions were an oversimplification of the true situation.

Fig. 4-1 (a,b,c) shows the variation of multiple scattering with specimen thickness and incident photon energy for the three materials. It is clear from fig. 4-1 that in many cases there is a significant amount of multiple scattering. Experience has shown that if multiple scattering exceeds about 0.05 of the total Compton scattering intensity reaching the detector, then the corrected profile will lie outside the range of statistical error normally quoted in Compton profile results

Table 4-1

Mean free paths (in cm) for different materials and incident photon energies.

	17.5 keV	60 keV	160 keV
Lithium	9.6	12.9	16.5
Aluminium	0.074	1.3	2.75
Copper	0.0023	0.07	0.54

($\sim \pm$ 1% at the peak). In all cases the fraction of multiple scattering increases with thickness until some limit is reached. The reason for this behaviour will be discussed later. The multiple scattering is seen to become far more sensitive to the incident energy when the material is of high atomic number. This would indicate that the variation in multiple scattering stems from the absorption properties of the materials, and table 4-1 gives the mean free paths (m.f.p) for the different materials and incident photon energies. From this table, it can be seen that as the photon energy increases there is little change in the m.f.p. for the light elements, whereas in the case of copper and aluminium the increase is appreciable. In copper the mf.p. of the incident 17.5 keV radiation is very small (0.0023 cm) and hence due to the high probability of photo-electric absorption, there is a severe geometrical constraint upon the available paths which a photon can follow in order to be scattered more than once. The photons see a sample whose effective dimensions are radius 1.0 cm and thickness 0.0023 cm, and increases in the true sample thickness beyond this figure will have little effect on the scattering properties. This constraint is removed at the higher photon energies, where low photoelectric cross-sections lead to a dramatic increase in the maximum possible amount of multiple scattering. Behaviour of this type is not observed in lithium since the m.f.p. is so large that photon absorption never imposes geometrical constraint on the photon paths for any of the incident energies considered.

It is clear from the above considerations that the m.f.p. of the photon in the scattering material plays an important role in determining the amount of multiple scattering for a given geometry. Therefore the results have also been plotted

as a function of the ratio of specimen thickness to m.f.p. for each energy. This is given in fig. 4-2 (a,b,c) which shows that the amount of multiple scattering will depend strongly on sample thickness only when the thickness is smaller than the m.f.p. Beyond this point, increases in thickness will have little effect on the resultant scattering.

These results indicate that careful attention should be paid to the design of a Compton scattering experiment in order to avoid a high contribution from multiple scattered photons. For materials of low atomic number the multiple scattering contributes at most about 10% of the total scattering, and this is largely independent of the incident photon energy. Furthermore, there is no difficulty in reducing the multiple scattering by the use of thin samples, which are still sufficiently thick to provide a reasonable intensity and signal to noise ratio. However, on the other hand, experiments on high atomic number materials can lead to considerable amounts of multiple scattering when using gamma-rays. To reduce this contribution the sample must be thin, compared with the m.f.p. or lower energy photons used where a low m.f.p. itself produces the geometrical constraint on the multiple scattering.

When working with high energy sources such as ^{123m}Te (160 keV), one should be alert to the very large amounts of multiple scattering which can be obtained in some experimental conditions, particularly in materials with high atomic number. Indeed, even in Compton profile anisotropy measurements where samples of the same geometry and material are used, a high multiple scattering contribution will 'wash out' some of the expected anisotropy. This is due to the way in which the measured profiles are normalised with the multiple scattering contribution included in the final profile. For example, in

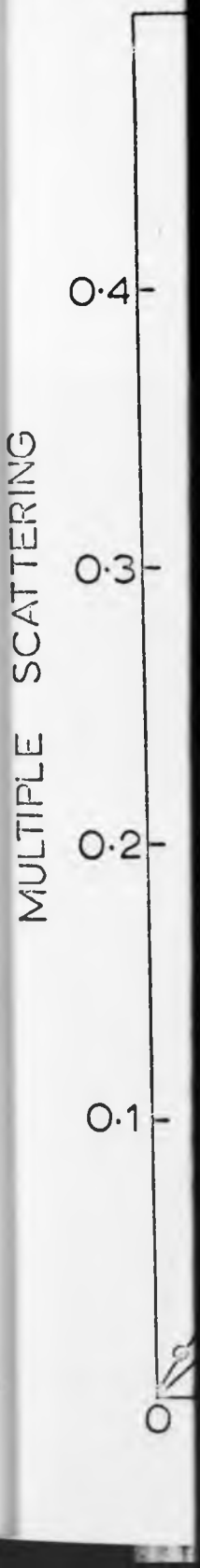

Fig. 4-1: Variation of multiple scattering with sample thickness for incident photons of energy 17.5, 60 and 160 keV. Multiple scattering is given as a fraction of the total inelastically scattered radiation reaching the detector for a scattering angle of $150^{\circ} \pm 2^{\circ}$. Specimens are a) Lithium, b) Aluminium and c) Copper.

ng
s of

total
g the
2°.
d

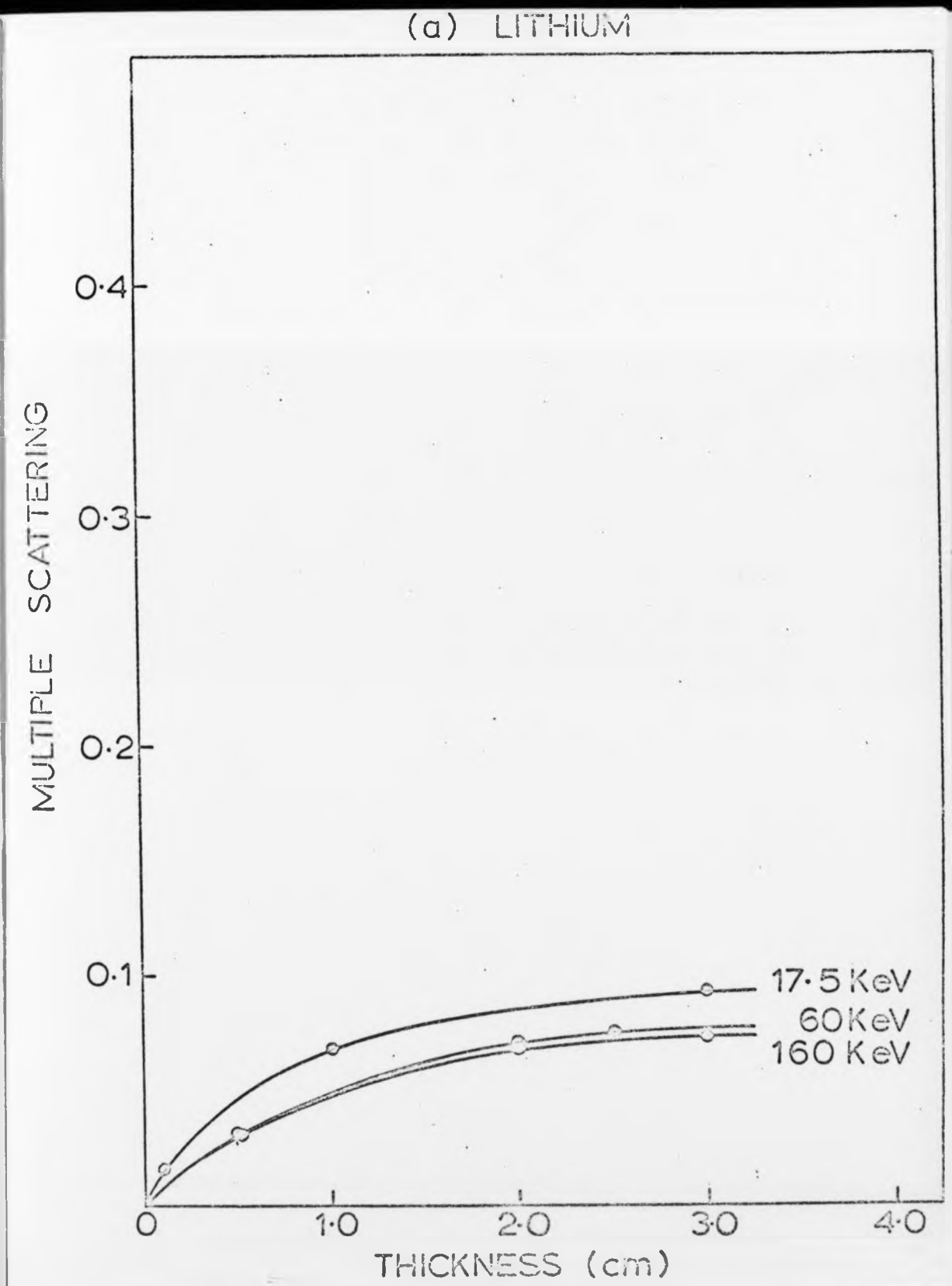

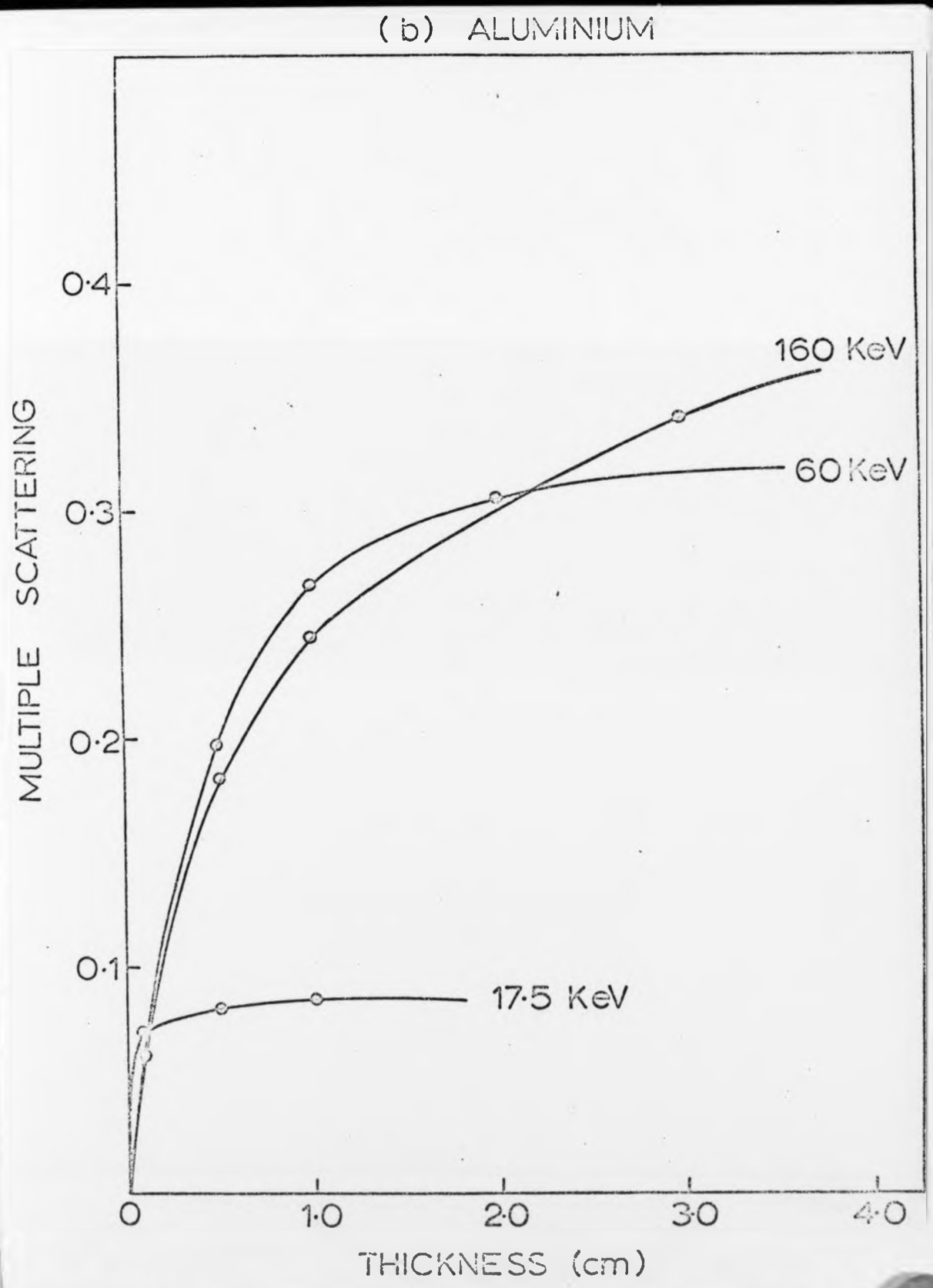
(b) ALUMINIUM
MULTIPLE SCATTERING
0·4
0·3
0·2
0·1
160 KeV
60 KeV
17·5 KeV
0
1·0
2·0
3·0
4·0
THICKNESS (cm)

(c) COPPER

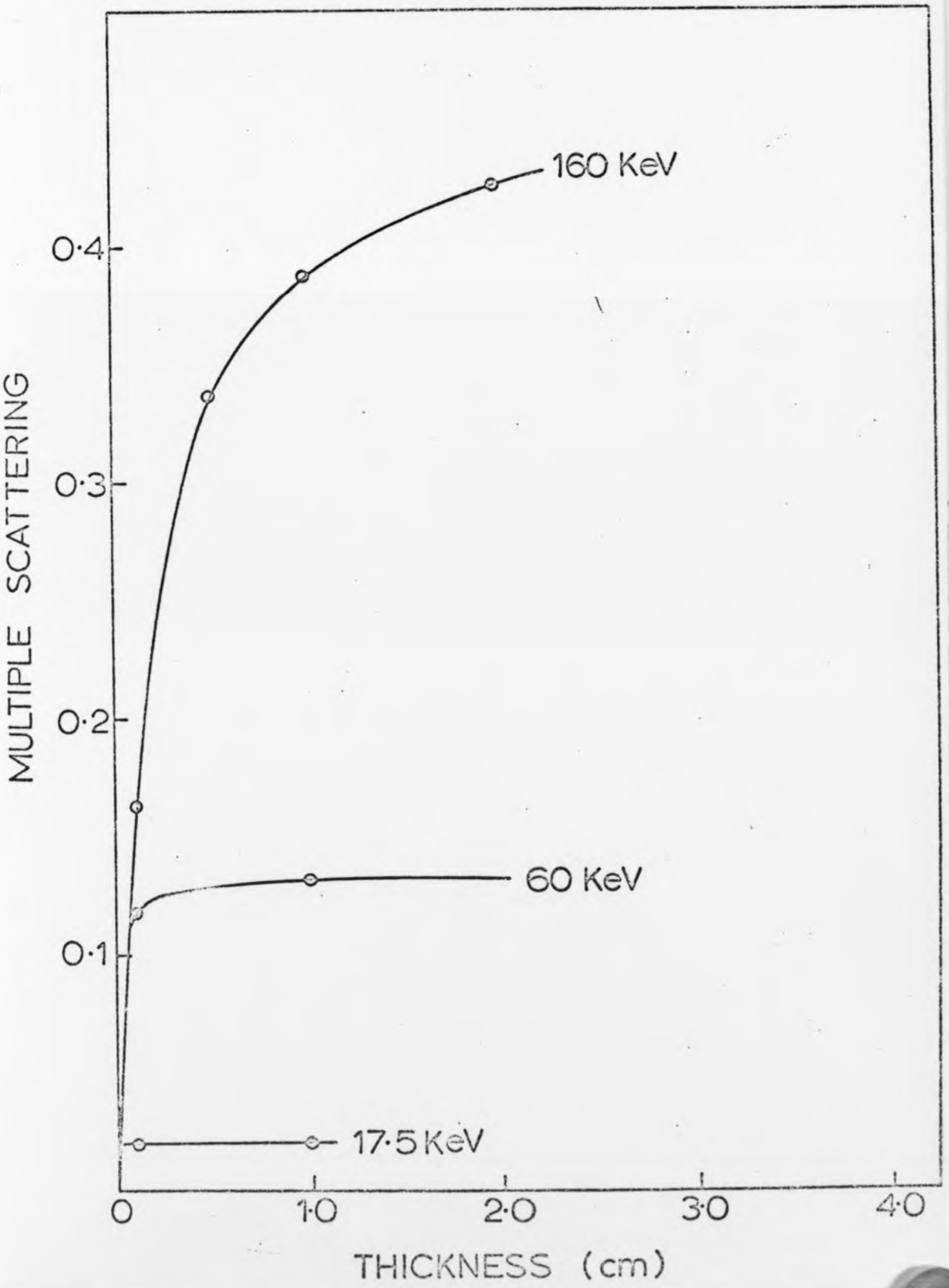
160 KeV
60 KeV
17·5 KeV
MULTIPLE SCATTERING
0·4
0·3
0·2
0·1
0
1·0
2·0
3·0
4·0
THICKNESS (cm)

Fig. 4-2: Multiple scattering shown as a function of the ratio of sample thickness to the incident photon mean free path. The materials and incident photon energies are as in fig. 4-1.

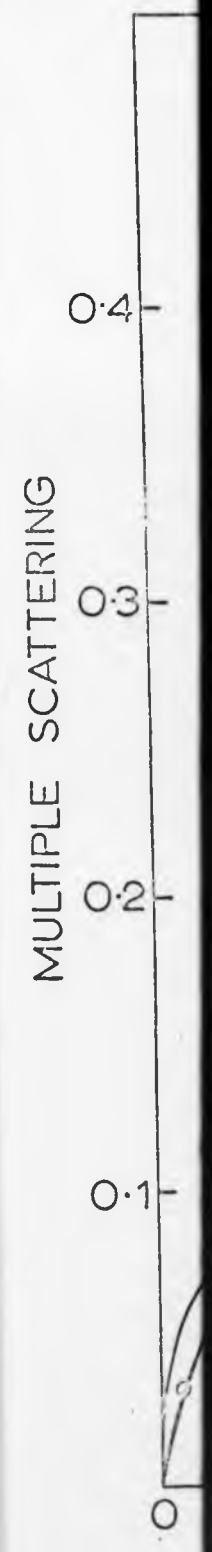

a
ss to the
terials
fig. 4-1.

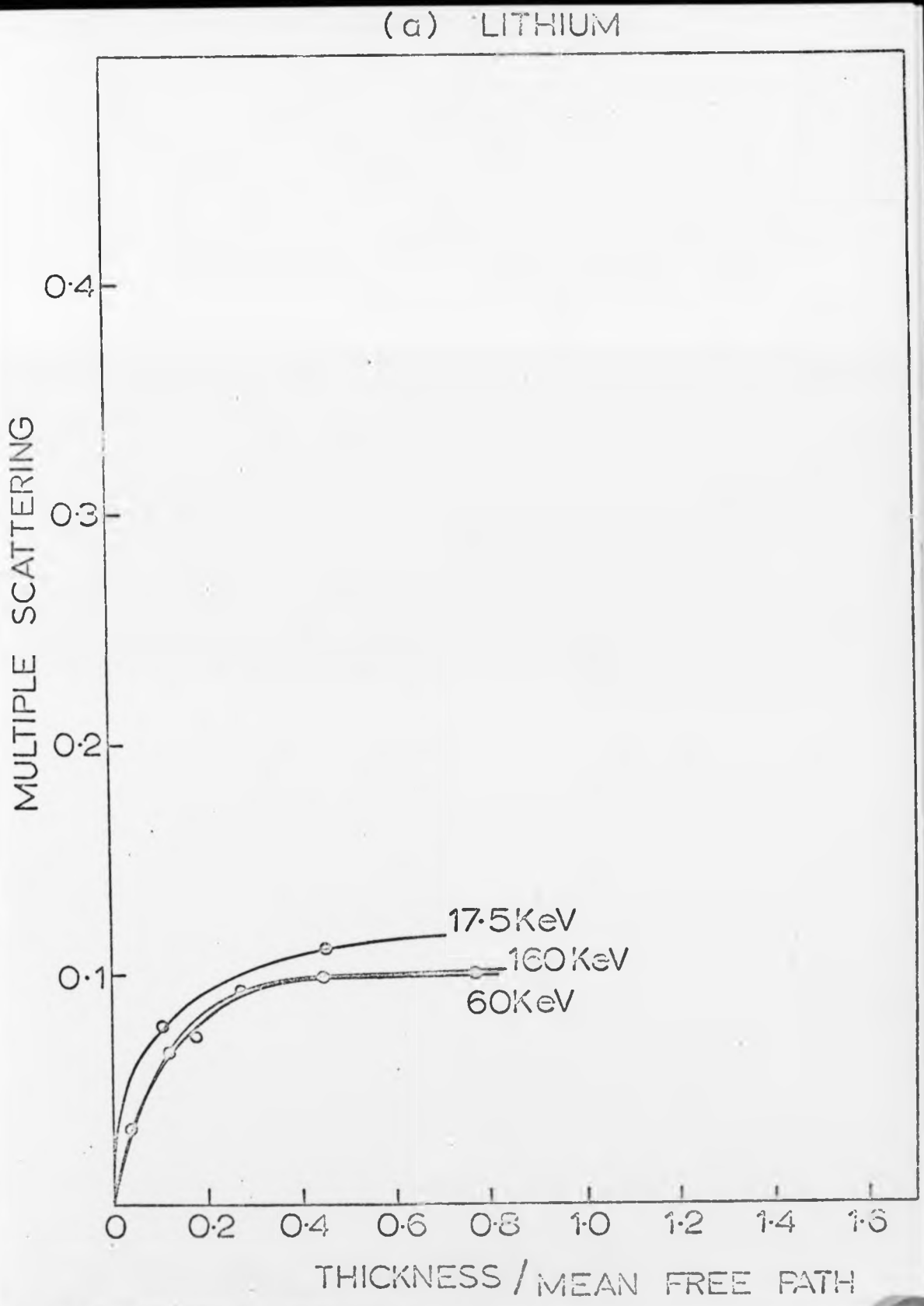

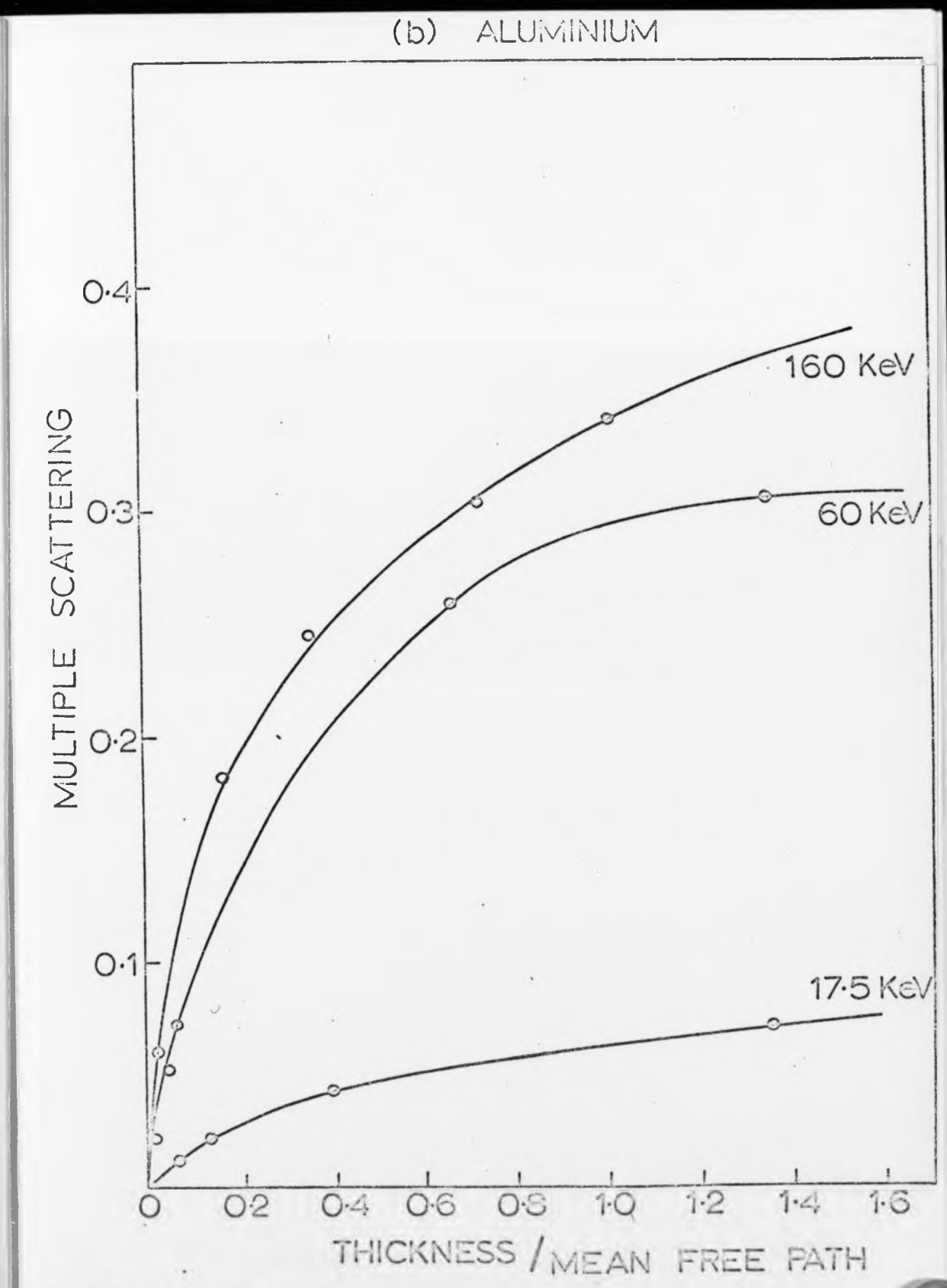
(b) ALUMINIUM
MULTIPLE SCATTERING
0·4
0·3
0·2
0·1
160 KeV
60 KeV
17·5 KeV
0
0·2
0·4
0·6
0·8
1·0
1·2
1·4
1·6
THICKNESS / MEAN FREE PATH

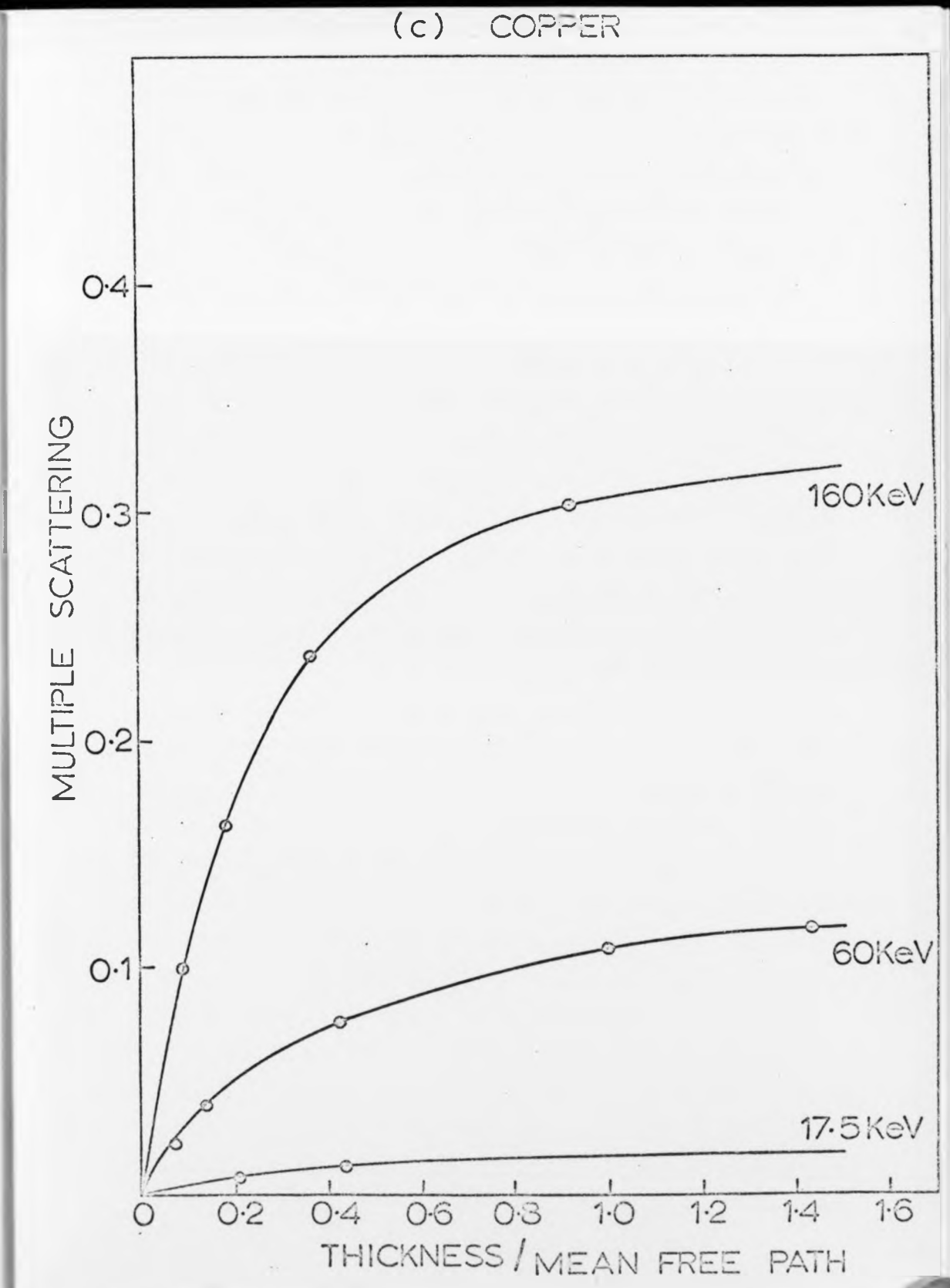
(c) COPPER
MULTIPLE SCATTERING
0·4
0·3
0·2
0·1
160KeV
60KeV
17·5KeV
0
0·2
0·4
0·6
0·8
1·0
1·2
1·4
1·6
THICKNESS / MEAN FREE PATH

a recent report[3] anisotropy measurements were made on copper samples of radius 1.0 cm and thickness 0.6 cm with 160 keV gamma-rays. In these conditions multiple scattering may exceed 30% of the total, leading to a reduction in the sensitivity of the Compton profiles to anisotropy in the samples. The effect of normalising Compton profiles which include multiple scattering is discussed in section 4.3.

4.2 Application to Experimental Compton Profiles

The Monte-Carlo technique described earlier is now used to correct experimental Compton profiles for the effect of multiple scattering. The profiles used were measured in the Technion, Haifa, by Dr. J. Felsteiner for two thicknesses of water, as a part of a current international measurement project organised by the International Union of Crystallography. These profiles (for 1 cm and 3 cm sample thicknesses) are listed in table 4-2 and also shown in fig. 4-3, together with a recent near Hartree-Fock (NHF) calculation by Tanner and Epstein[4]. The measurements were made using 59.54 keV gamma-rays from a 300 mCi ^{241}Am source scattered at an angle of $157^{\circ} \pm 2^{\circ}$ and detected with a Ge (Li) counter. The profile of water (1 cm thickness) has also been measured independently by the author in this laboratory for the same international project. This profile is in good agreement with the 1 cm profile measured in Haifa, and these results are also shown in table 4-2 for comparison.

It is clear that the experimental profiles vary significantly with the sample thickness, and both are in marked disagreement with the NHF theory. Since the measured profiles have already been corrected for sample absorption (and other systematic effects) it is assumed that the depen-

Table 4-2

Experimental and theoretical Compton profiles of water. The experimental profiles are given for two different sample thicknesses and have not been corrected for multiple scattering. The profiles are all normalised to an area of 5.0 in the range 0 - 5 a.u.

	Exp. a)			Exp. b)
p (a.u.)	1 cm.	3 cm.	NHF Theory	1 cm.
0.0	3.666±1%	3.584±1%	3.9546	3.638±1%
0.1	3.635	3.528	3.9354	3.596
0.2	3.574	3.447	3.8749	3.583
0.3	3.432	3.363	3.7673	3.471
0.4	3.303	3.274	3.6087	3.327
0.5	3.147	3.096	3.3997	3.137
0.6	2.929	2.892	3.1491	2.908
0.7	2.682	2.668	2.8700	2.715
0.8	2.502	2.458	2.5779	2.492
0.9	2.227	2.196	2.2872	2.253
1.0	1.939±2%	1.971±2%	2.0097	1.985±2%
1.2	1.551	1.459	1.5223	1.519
1.4	1.199	1.210	1.1422	1.155
1.6	0.911	0.966	0.8627	0.949
1.8	0.752	0.797	0.6636	0.741
2.0	0.650± 3.5%	0.656±3.5%	0.5240	0.629±3.5%
2.5	0.438	0.452	0.3284	0.432
3.0	0.301	0.317	0.2359	0.309
3.5	0.234	0.237	0.1901	0.236
4.0	0.173	0.185	0.1443	0.184
5.0	0.113±7%	0.114±7%	0.0936	0.120±7%

a) Measured by J. Felsteiner, Technion, Haifa, Israel.

b) Measured by the author.

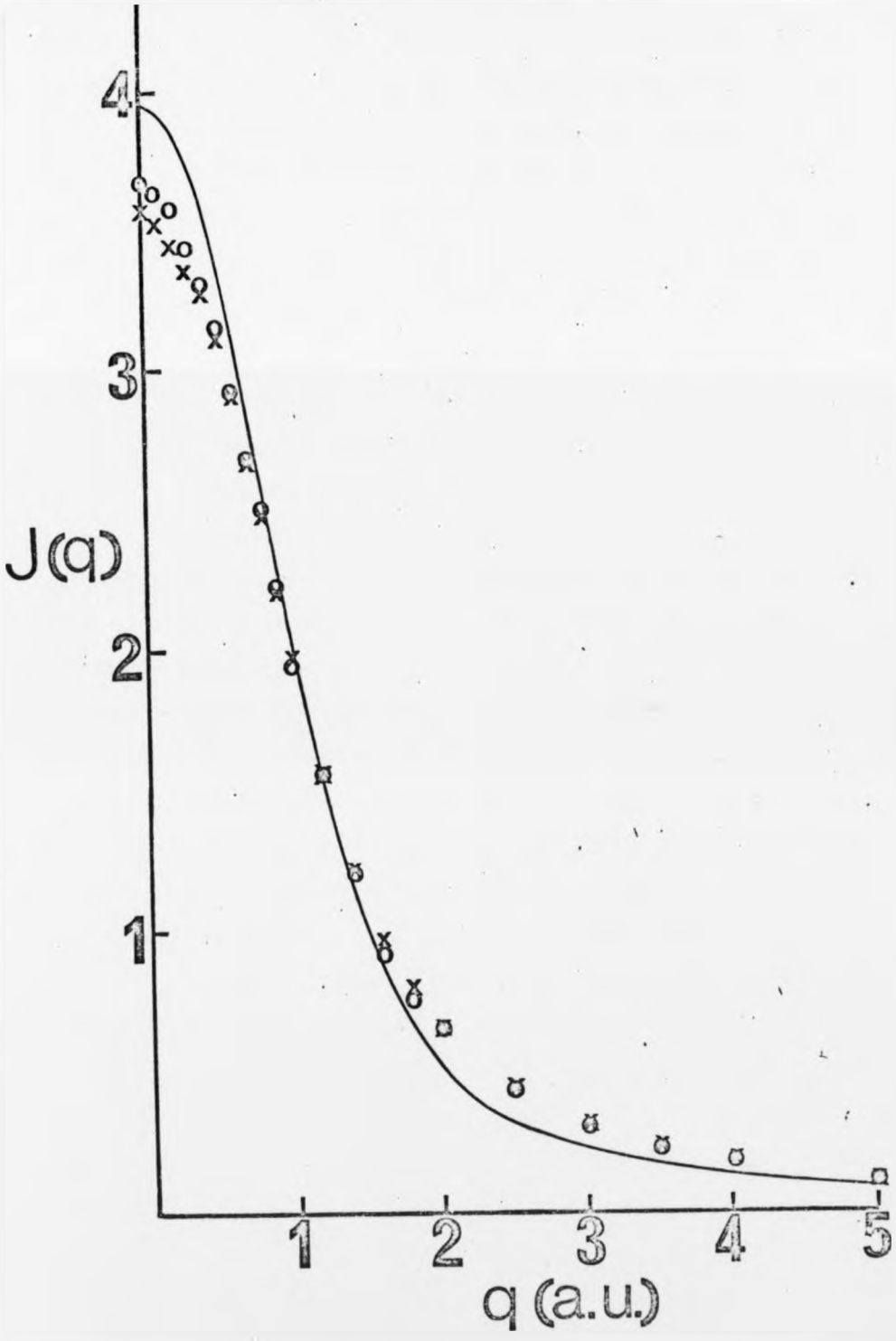

Fig. 4-3: Compton profiles of water. Experimental points are for sample thicknesses of 3 cm (xxxx) and 1 cm (oooo) and are not corrected for multiple scattering. Solid line is NHF theory.

dence upon sample thickness shown in table 4-2 is due to multiple scattering. However, in the procedure described earlier, only stationary electrons were considered. In order to take into account the momenta of the scattering electrons, the energy distribution of the scattered photons, derived initially from the Klein-Nishina formula, was convoluted for each scattering event with the appropriate Compton profile. Since the Compton profile for single scattering, needed for the convolution, is not known exactly (because of multiple scattering), an iterative procedure was used. The experimental Compton profile was taken as a first approximation to the single scattering profile and the contribution of multiple scattering obtained in this way was then subtracted from the experimental Compton profile. This corrected profile, renormalised, served as a new approximation for the iterative procedure. Three or four iterations proved sufficient to obtain self-consistent profiles.

The final energy distributions of the photons which have undergone two or three collisions and leave the specimen at a total scattering angle of $157^{\circ} \pm 2^{\circ}$ are given in fig. 4-4 for both thicknesses. It was assumed that the effect of the sample holder (brass) was to make the cylindrical walls totally absorbing for 60 keV radiation. Table 4-3 gives the final Compton profiles corrected for double scattering, and for both double and triple scattering. It is seen that when the effect of both double and triple scattering is taken into account, the corrected profiles for both thicknesses agree well. Thus, it seems clear that the discrepancy between the experimental profiles shown in table 4-2 is due to multiple scattering effects. Furthermore, it is demonstrated in table 4-3 that the effect of triple scattering is much more significant in the thicker sample and must be included in

Fig.4-4: Calculated energy distributions of multiple scattered photons which emerge in the angular range $157^{o} \pm 2^{o}$ are shown for two sample thicknesses. The distributions include the broadening effect of the electron momenta. The intensity of each distribution is relative to the number of photons which have a single Compton collision, and leave in the same angular range. An experimental profile (dashed line) which is not to scale, is shown for comparison.

ions of
ge in the
wo sample
ude the
enta. The
ative to the
Compton
lar range.
which is

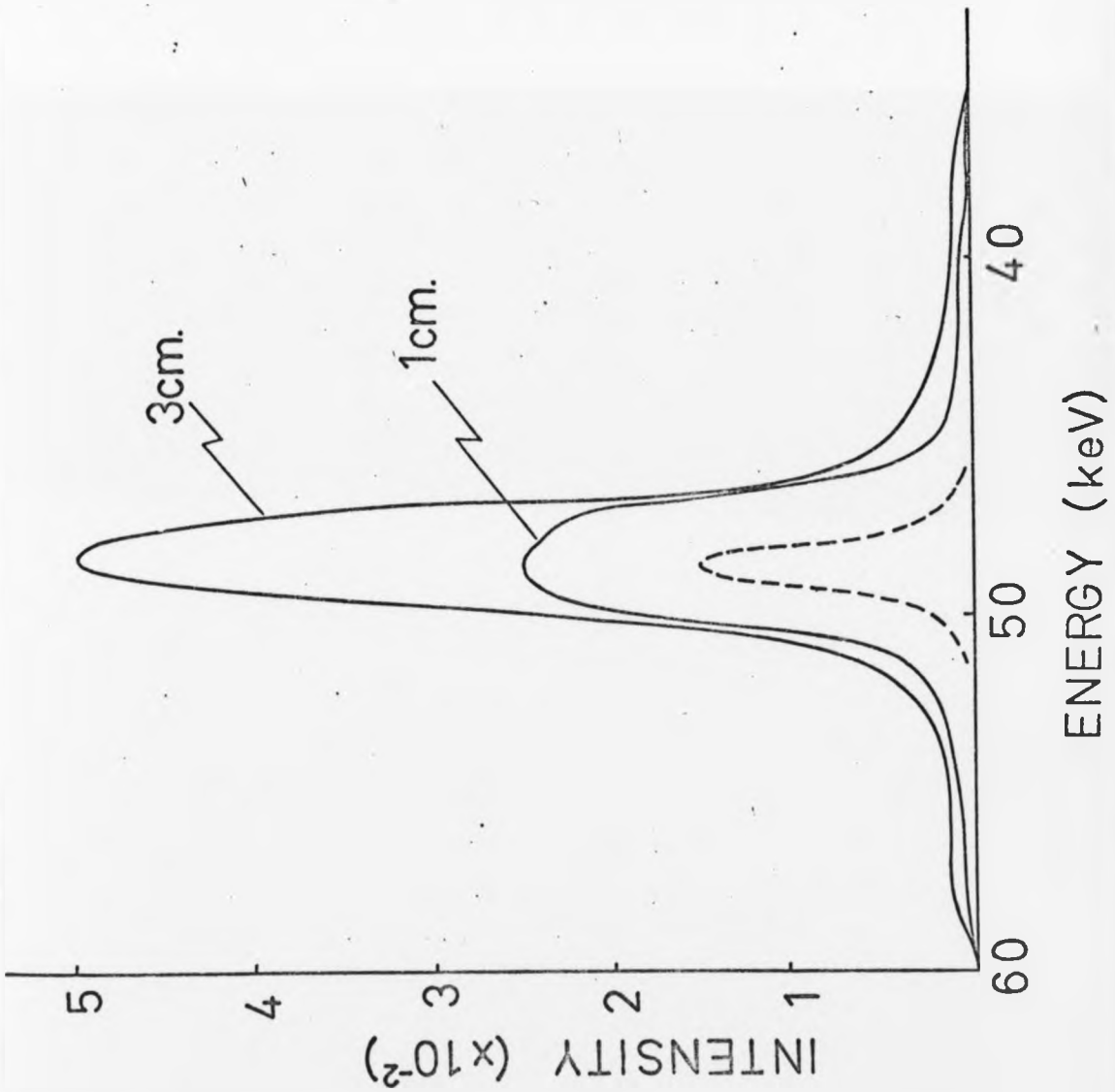

Table 4-3

Experimental Compton profiles of water for two sample thicknesses after correction for multiple scattering. The profiles are normalised to an area of 5.0 in the range 0 -5 a.u.

p (a.u.)	Corrected for double scattering		Corrected for double and triple scattering	
	1 cm.	3 cm.	1 cm.	3 cm.
0.0	3.937	3.883	3.942±1.5%	3.930±1.5%
0.1	3.901	3.820	3.908	3.867
0.2	3.831	3.727	3.837	3.773
0.3	3.670	3.630	3.676	3.674
0.4	3.521	3.529	3.527	3.572
0.5	3.345	3.321	3.350	3.361
0.6	3.096	3.082	3.101	3.117
0.7	2.815	2.818	2.819	2.849
0.8	2.611	2.573	2.615	2.599
0.9	2.298	2.266	2.301	2.286
1.0	1.972	2.004	1.973±3%	2.019±3%
1.2	1.533	1.515	1.534	1.521
1.4	1.140	1.130	1.139	1.129
1.6	0.820	0.861	0.819	0.855
1.8	0.652	0.685	0.651	0.677
2.0	0.551	0.544	0.550±5%	0.534±6%
2.5	0.357	0.369	0.356	0.358
3.0	0.250	0.266	0.248	0.255
3.5	0.208	0.209	0.206	0.198
4.0	0.156	0.168	0.154	0.156
5.0	0.104	0.104	0.103±10%	0.091±12%

order to obtain good agreement between the two profiles. It follows that the triple scattering correction can be neglected only when thin samples are considered. The contribution from scattering of higher order than three was found to be negligible for both thicknesses considered.

Inspection of tables 4-2 and 4-3 indicates an increase in the statistical errors after the multiple scattering correction has been made. A larger number of photons used in the Monte-Carlo calculation would have resulted in a smaller increase in these errors, but this was not practicable in view of the limited computational facilities available. It can also be seen from these tables that the agreement between the NHF theory and experiment has been considerably improved following the multiple scattering correction. This is illustrated in fig. 4-5 where the difference curves between theory and experiment are given.

After applying the Monte Carlo procedure to measured profiles of water, the corrected profiles appear to be independent of sample thickness, within their statistical error. Furthermore, there is now good agreement between the corrected profiles and a NHF theory. The other methods previously employed to correct for multiple scattering involved the measurement of a number of profiles for different sample thicknesses and the subsequent extrapolation of the data to zero thickness. The application of these methods to the experimental profiles given in table 4-2 leads, for example, to values of J(0) of 3.71 for linear extrapolation and of 3.78 for square root extrapolation. Both of these values are still in poor agreement with the value 3.95, given by the NHF theory in table 4-2.

It is clearly wise to minimise multiple scattering by performing measurements on samples as thin as possible. In

order to obtain good agreement between the two profiles. It follows that the triple scattering correction can be neglected only when thin samples are considered. The contribution from scattering of higher order than three was found to be negligible for both thicknesses considered.

Inspection of tables 4-2 and 4-3 indicates an increase in the statistical errors after the multiple scattering correction has been made. A larger number of photons used in the Monte-Carlo calculation would have resulted in a smaller increase in these errors, but this was not practicable in view of the limited computational facilities available. It can also be seen from these tables that the agreement between the NHF theory and experiment has been considerably improved following the multiple scattering correction. This is illustrated in fig. 4-5 where the difference curves between theory and experiment are given.

After applying the Monte Carlo procedure to measured profiles of water, the corrected profiles appear to be independent of sample thickness, within their statistical error. Furthermore, there is now good agreement between the corrected profiles and a NHF theory. The other methods previously employed to correct for multiple scattering involved the measurement of a number of profiles for different sample thicknesses and the subsequent extrapolation of the data to zero thickness. The application of these methods to the experimental profiles given in table 4-2 leads, for example, to values of J(0) of 3.71 for linear extrapolation and of 3.78 for square root extrapolation. Both of these values are still in poor agreement with the value 3.95, given by the NHF theory in table 4-2.

It is clearly wise to minimise multiple scattering by performing measurements on samples as thin as possible. In

Fig. 4-5: Difference curves between experimental Compton profiles of water and the NHF theory.

_____ Before correction for multiple scattering.

-------- After correction for multiple scattering.

The range of statistical uncertainty is indicated by the error bars.

peri-

e NHF

scattering.

scattering.

indicated

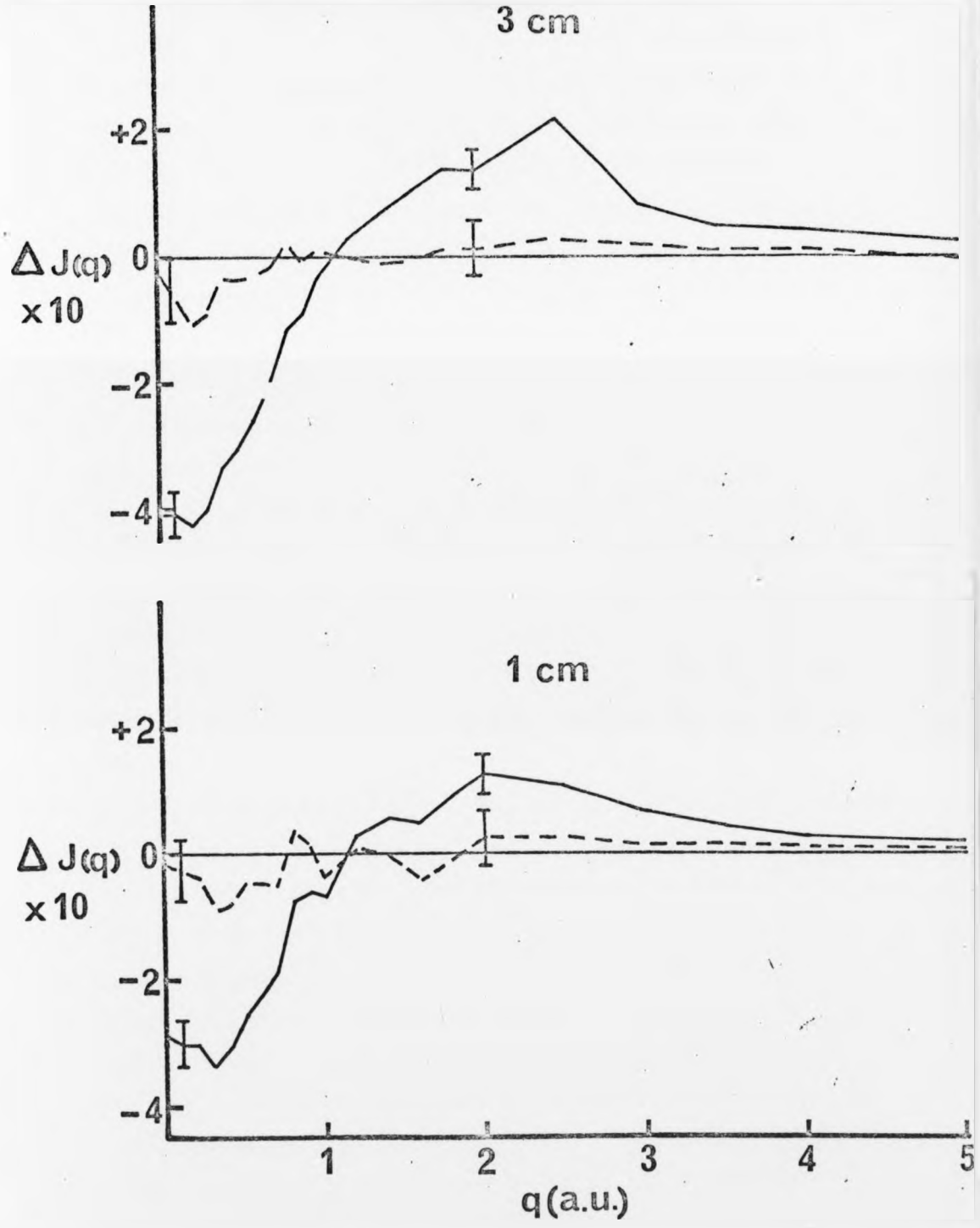

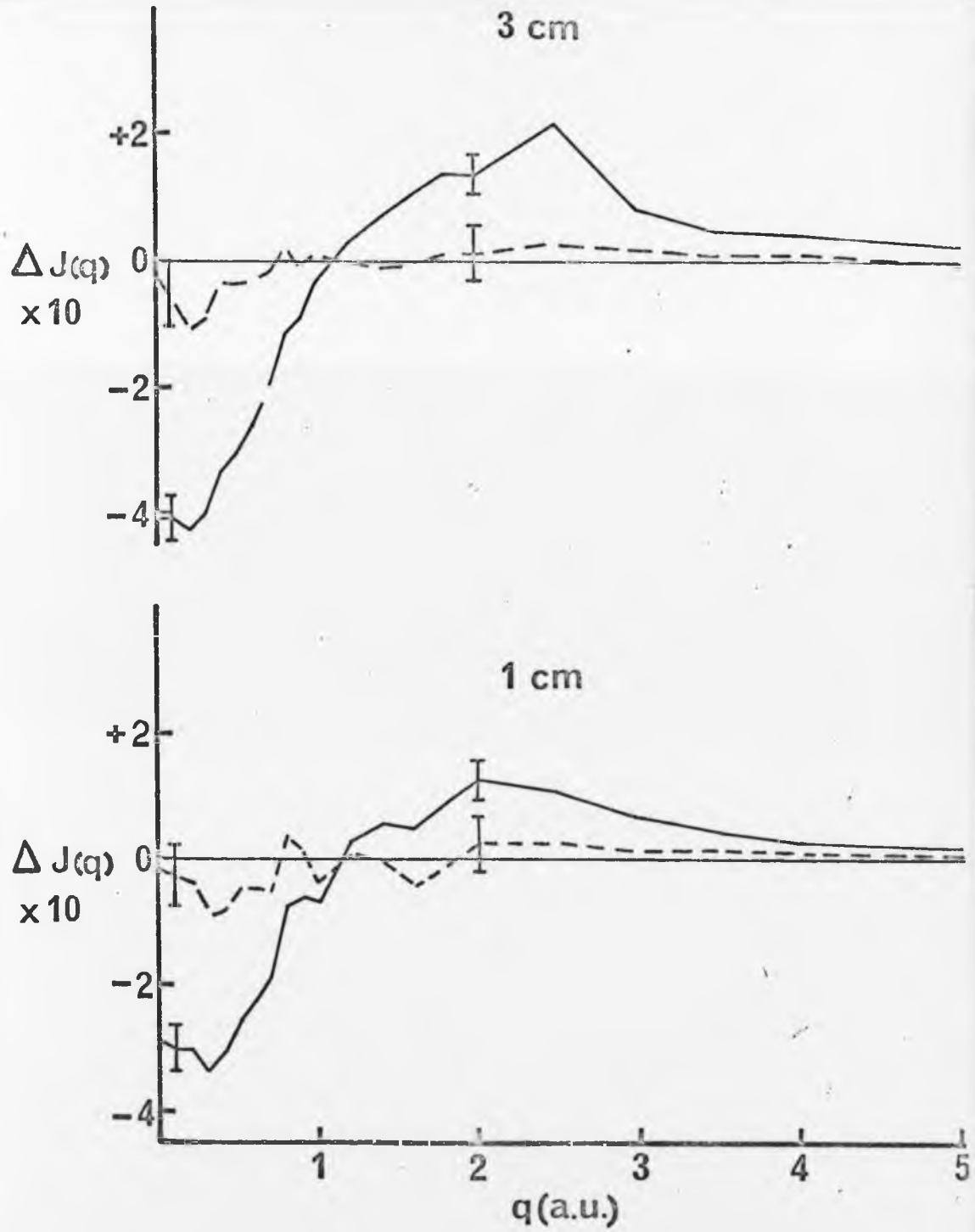

perimental

e NHF

scattering.

scattering.

indicated

practice, however, it is necessary to make a compromise between this requirement and the limitations arising from the low intensity inherent in such an experiment. The results reported above indicate that the Monte Carlo technique can be used successfully to correct Compton profile data, measured on a single sample, for the effects of multiple scattering.

4.3 The Cross Section Ratio

Since it is not possible to isolate the multiple scattered radiation in a Compton profile measurement, no direct check can be made of the spectrum obtained by the Monte Carlo method. However, it is possible to measure the total amount of multiple scattering in a Compton experiment, without changing the scattering geometry. This can be achieved by studying the way in which multiple scattering modifies the observed ratio of the Compton to the elastic cross section.

There have been several experimental determinations of the variation of the Compton cross section with momentum transfer (i.e. as a function of $\sin\Theta/\lambda$) in the x-ray region, see, for example, Laval[5], Walker[6], Currat De Cicco and Weiss[7], and Paakkari and Suortti[8]. In these experiments, which were done in the low momentum transfer region ($\sin\Theta/\lambda < 1.0\ A^{-1}$) the main contribution to the measured incoherent intensity comes from the valence electrons and there is marked disagreement among the predictions of the various theories for the Compton cross section. Experimentally, it is not usually possible to separate the Compton scattering from the elastic, diffuse scattering (TDS) and a calculated TDS contribution must be subtracted from the measurement. The TDS contribution is calculated

from the single atom form factor f_{ii}, modified by inter-atomic lattice effects which depend on the Debye-Waller factor (see e.g. Warren[9]). At low momentum transfer, the lattice effects are important, and the presence of the Debye-Waller factor complicates the calculation.

On the other hand, in the high momentum transfer region ($\sin\Theta/\lambda \sim 5.0$ A^{-1}, say) these problems do not exist. In the experiment the Compton scattering and the elastic scattering are easily separated. The total Compton intensity predicted by the Waller-Hartree theory[10] and by the impulse approximation (Currat, DeCicco and Weiss[7]) is the same. The elastic intensity can be calculated simply from the atomic form factor, since in this region the lattice effects are negligible.

The ratio R of the elastic to inelastic cross sections can therefore be calculated unambiguously provided the scattering occurs at high momentum transfer. Weiss[11] has noted that this provides a basis for normalising Compton profile measurements. However, the validity of such a procedure rests on the assumption that the multiple scattering is negligible. The results of the Monte Carlo calculations given earlier in this Chapter show that in general this assumption is unwarranted. The measured ratio R therefore deviates from its theoretical value by an amount directly related to the multiple scattering contribution. Thus the total intensity of multiple scattering (relative to single Compton scattering) present in a particular Compton profile measurement can be directly measured in that experiment. In the work described below, the measured multiple scattering contribution is found to be in good agreement with the prediction of a Monte Carlo calculation.

4.3.1 Total Cross Sections for Inelastic and Elastic Scattering

In this section the scattering cross-section per unit solid angle, $d\sigma/d\Omega$ is referred to as the total cross-section and the scattering cross-section per unit solid angle per unit energy, $d\sigma/d\Omega d\omega$ is referred to as the differential cross-section.

The two models generally used to describe the total Compton cross-section (i.e. incoherent scattering factor) for many electron systems are (i) the impulse approximation and (ii) the Waller-Hartree theory. In the impulse approximation the cross section per unit solid angle is given by(7)

$$\frac{d\sigma}{d\Omega} = \left(\frac{e^2}{mc^2}\right)^2 K^2 \sum_i \int_{|\varepsilon_i|}^{\omega_1} \frac{\omega_2}{\omega_1} \cdot \frac{m}{|\bar{k}|} \cdot J_i(p_z)\, d\omega \qquad 4\text{-}1$$

where K is the polarisation factor, ω_1 and ω_2 are the initial and final photon energies, $|\bar{k}|$ is the magnitude of the scattering vector $\bar{k} = \bar{k}_2 - \bar{k}_1$ and $\omega = \omega_1 - \omega_2$. $J(p_z)$ is the Compton profile, i.e. the one-dimensional electron momentum distribution, and the momentum component p_z is defined by

$$p_z = -mc\, \frac{\omega_1 - \omega_2 - \omega_1\omega_2(1-\cos\Theta)/mc^2}{(\omega_1^2 + \omega_2^2 - 2\omega_1\omega_2\cos\Theta)^{1/2}} \qquad 4\text{-}2$$

where Θ is the scattering angle. For each occupied orbital i, the integration in eqn. 4-1 is performed from the excitation energy $|\varepsilon_i|$ to the incident energy ω_1.

The corresponding cross-section in the Waller-Hartree theory can be written (Freeman(12), Currat et. al.(7))

$$\frac{1}{c}\frac{d\sigma}{d\Omega} = \left(\frac{e^2}{mc^2}\right)^2 K^2 \left(\frac{\omega_2^\circ}{\omega_1}\right)^2 \left(Z - \sum_i |f_{ii}|^2 - \sum_{i\neq j} |f_{ij}|^2\right) \qquad 4\text{-}3$$

where ω_2° is the final photon energy corresponding to the Compton shift for a stationary free electron, f_{ii} is the usual coherent scattering factor, and the matrix elements

f_{ij} are defined by

$$f_{ij} = \int \psi_i^*(\bar{r})\, e^{i\bar{k}.\bar{r}}\, \psi_j(\bar{r})\, d\bar{r} \qquad 4\text{-}4$$

In a recent work Mendelsohn and Biggs[13] pointed out that the Waller-Hartree theory at low momentum transfer (i.e. at low $\sin\theta/\lambda$) gives incoherent scattering factors which are too high compared with the exact calculations for 1s electrons. This is mainly because for bound electrons ω_2° in eqn. 4-3 can no longer be approximated as the average final photon energy. In contrast, the impulse approximation gave good agreement with the exact total cross section, although there were differences in the differential cross section, and in turn in the shape of the Compton profile, near the binding edge $|\varepsilon_i|$. Nevertheless at high $\sin\theta/\lambda$ both methods were in good agreement with the exact calculation.

The aim of this investigation was to determine the contribution of multiple scattering to the total Compton cross-section of aluminium. The measurements were carried out at high $\sin\theta/\lambda$ ($\theta = 150^\circ$, $\lambda = 0.208$ Å, $\frac{\sin\theta}{\lambda} = 4.6$) for the following reasons: (i) the incoherent scattering factor is well known for each orbital of aluminium, (ii) the interatomic lattice effects on the elastic scattering are negligible, because the Debye-Waller factor $\exp\left(-2B\sin^2\theta/\lambda^2\right)$ is now of order exp(-38). This means that the coherent cross section can be written in the form (see e.g. Weiss[11])

$$\frac{d\sigma}{d\Omega} = \left(\frac{e^2}{mc^2}\right)^2 K^2 \left| \sum f_{ii} \right|^2 \qquad 4\text{-}5$$

The ratio between the coherent and the incoherent cross sections can then be easily calculated from scattering factors f_{ii} and matrix elements f_{ij}. Comparison between the experimental and the theoretical ratio will yield information on

the total amount of multiple scattering in the present experiment.

4.3.2 Experimental

The experimental arrangement for γ-ray measurements has been described in Chapter 2. Gamma-rays from a 300 mCi ^{241}Am source impinged upon a single crystal of aluminium of thickness 7 mm and diameter 24 mm with the [110] zone axis parallel to the scattering vector. After scattering in a vacuum chamber through a mean angle of 150° the spectrum of the scattered gamma-rays was measured with a Ge(Li) detector, with a resolution of 390 eV (FWHM) at 60 keV, coupled to a 4096-channel multichannel analyser. The energy interval between channels was 20 eV and the drift of the apparatus was no more than 5 eV at 60 keV during the measuring period of 12 days. About 500000 counts per channel were accumulated at the Compton peak and 35000 counts per channel at the elastic peak, the peak-to-background ratios being about 1500 to 1 and 100 to 1, respectively.

The subtraction of the background was made in the following way: a separate measurement indicated that there were two different components in the background: (i) an essentially linear part in the region of the Compton distribution, (ii) a small component due to the lead shielding in the scattering system. First the linear part was subtracted by fitting a straight line to the measured points in the linear region of the background. The remaining lead contribution was then subtracted by setting the areas of the lead Kα -fluorescence lines in the background measurement and in the aluminium measurement equal.

Although it is not necessary to apply any deconvolution procedure in order to determine the total area of the Compton

Fig. 4-6: Experimental data from the gamma-ray measurement of the Compton profile of aluminium. The data are shown after background subtraction and tail-stripping. The inset shows the elastic line on a logarithmic scale. A GeKα escape peak can be seen around 39 keV.

COUNTS (x10^5)
1
2
3
4
40
50
60
ENERGY (keV)
LOG SCALE

distribution, it is important to remove the low energy tail, present because of the Ge(Li) detector response, from the measured line shape before applying a correction for the energy dependence of absorption in the sample. The efficiency for total photon absorption in the germanium detector is very close to unity in the range 60 keV - 30 keV, and varies by less than ½% over this range. Therefore no energy-dependent correction for detector efficiency was made to the data.

The resolution function, measured with a low intensity ^{241}Am source, indicated that the tail consisted of linear and exponential parts. The parameters describing these two parts were fitted on the basis of the measured resolution function. After removing the tail the Compton scattering contribution turned out to be negligible below about 30 keV ($\sim$ 28 a.u.) which is consistent with the calculated energy distribution of multiple scattering photons. The measured data after background subtraction and tail stripping are shown in fig. 4-6.

The next stage was the separation of the elastic scattering contribution from the measured data. It should be noted that the elastic line will be broadened by the instrumental resolution function which produces a tail extending into the region of the Compton line shape, making the direct estimation of the integrated intensity impracticable. It is possible to overcome this problem by normalising the height of the resolution function to the same value as the elastic peak. The elastic scattering contribution can be therefore taken as the area of this normalized resolution function. The data were then corrected for absorption in the sample, and the total area under the Compton profile was calculated and the tail contri-

bution included.

4.3.3 Conclusions

The theoretical ratio of the intensities I(single elastic)/I(single Compton) was calculated in the following way. Using eqns. 4-3 and 4-5 the ratio can be written in the form

$$\frac{I(\text{single elastic})}{I(\text{single Compton})} = \frac{\left|\sum f_{ii}\right|^2}{\left(\frac{\omega_2^\circ}{\omega_1}\right)^2\left(Z-\sum|f_{ii}|^2-\sum|f_{ij}|^2\right)_{o-1}} \quad 4\text{-}6$$

In the present experiment the value of $\frac{\sin\Theta}{\lambda}$ is 4.64 A^{o-1}. The value $\sum f_{ii}$ at this $\frac{\sin\Theta}{\lambda}$, taken from relativistic Hartree-Fock scattering factors calculated by Doyle and Turner[14] is 0.344. The factor $\left(Z-\sum|f_{ii}|^2-\sum|f_{ij}|^2\right)$ in eqn. 4-3 has been calculated for aluminium by Taward, Nicolas and Rouault[15]. It should be noted that for inelastic scattering the magnitude of the scattering vector $|\bar{k}|$ is no longer $\frac{4\pi\sin\Theta}{\lambda_1}$, where λ_1 is the incident photon wavelength, as in the case of the elastic scattering, but instead is given by $(k_1^2 + k_2^2 - 2k_1k_2\cos\Theta)^{\frac{1}{2}}$. The value of $|\bar{k}|$ which corresponds to the present experiment is 53.1 A^{o-1} (at the Compton peak), which leads to a value for the factor $\left(Z-\sum|f_{ii}|^2-\sum|f_{ij}|^2\right)$ of 12.91. Here ω_2° = 48.910 keV, ω_1 = 59.537 keV and the value for $\left(\frac{\omega_2^\circ}{\omega_1}\right)^2\left(Z-\sum|f_{ii}|^2-\sum|f_{ij}|^2\right)$ is then 8.71, and from eqn. 4-6 the desired theoretical ratio I(single elastic)/(single Compton) is thus 1.36%.

The elastic and Compton areas, derived from the experimental data as described earlier, gave a ratio of (1.01 ± 0.01)%. This is significantly lower than the figure of 1.36 derived from the Waller-Hartree theory. However, if the ratio is corrected for the effect of multiple Compton scattering, using the Monte Carlo results given in table 4-4 for the total profile, this ratio increases to (1.34 ± 0.03)%.

bution included.

4.3.3 Conclusions

The theoretical ratio of the intensities I(single elastic)/I(single Compton) was calculated in the following way. Using eqns. 4-3 and 4-5 the ratio can be written in the form

$$\frac{I(\text{single elastic})}{I(\text{single Compton})} = \frac{\left|\sum f_{ii}\right|^2}{\left(\frac{\omega_2^\circ}{\omega_1}\right)^2\left(Z-\sum|f_{ii}|^2-\sum|f_{ij}|^2\right)} \qquad 4\text{-}6$$

In the present experiment the value of $\frac{\sin\Theta}{\lambda}$ is 4.64 A^{o-1}. The value $\sum f_{ii}$ at this $\frac{\sin\Theta}{\lambda}$, taken from relativistic Hartree-Fock scattering factors calculated by Doyle and Turner[14] is 0.344. The factor $\left(Z-\sum|f_{ii}|^2-\sum|f_{ij}|^2\right)$ in eqn. 4-3 has been calculated for aluminium by Taward, Nicolas and Rouault[15]. It should be noted that for inelastic scattering the magnitude of the scattering vector $|\bar{k}|$ is no longer $\frac{4\pi\sin\Theta}{\lambda_1}$, where λ_1 is the incident photon wavelength, as in the case of the elastic scattering, but instead is given by $(k_1^2 + k_2^2 - 2k_1k_2\cos\Theta)^{\frac{1}{2}}$. The value of $|\bar{k}|$ which corresponds to the present experiment is 53.1 A^{o-1} (at the Compton peak), which leads to a value for the factor $\left(Z-\sum|f_{ii}|^2-\sum|f_{ij}|^2\right)$ of 12.91. Here ω_2° = 48.910 keV, ω_1 = 59.537 keV and the value for $\left(\frac{\omega_2^\circ}{\omega_1}\right)^2\left(Z-\sum|f_{ii}|^2-\sum|f_{ij}|^2\right)$ is then 8.71, and from eqn. 4-6 the desired theoretical ratio I(single elastic)/(single Compton) is thus 1.36%.

The elastic and Compton areas, derived from the experimental data as described earlier, gave a ratio of (1.01 ± 0.01)%. This is significantly lower than the figure of 1.36 derived from the Waller-Hartree theory. However, if the ratio is corrected for the effect of multiple Compton scattering, using the Monte Carlo results given in table 4-4 for the total profile, this ratio increases to (1.34 ± 0.03)%.

Table 4-4

The relative contributions to the measured Compton profile of various scattering processes are shown as predicted by the Monte Carlo procedure. These contributions are given as percentages of the total incoherent intensity, with statistical errors.

Range	Single	Double	Triple	More than triple
Total profile	75.3±0.5	18.8±0.2	3.8 ± 0.1	2.1 ± 0.2
0-5 a.u.	83.0±1.0	15.6±0.5	1.4 ± 0.1	-

Table 4-5

Experimental and theoretical values for the ratio of elastic to Compton intensities.

Experimental		Theoretical
$\frac{\text{(elastic)}}{\text{(total Compton)}}$	$\frac{\text{(elastic)}}{\text{(single Compton)}}$	$\frac{\text{(single elastic)}}{\text{(single Compton)}}$
(1.01 ± 0.01) %	(1.34 ± 0.03) %	1.36 %

This result is in much better agreement with the Waller-Hartree theory. The correction takes into account all Compton collisions, including cases involving both elastic and Compton events. Multiple elastic collisions were found to be negligible. This was expected since at these energies the cross section for double elastic scattering is lower than the double Compton cross section by a factor of about 10^{-4}. The experimental and theoretical ratios are summarized in table 4-5. The improved agreement between theory and experiment demonstrates the accuracy with which the Monte Carlo technique can describe the effects of multiple scattering.

4.4 Further Developments

The use of the Monte Carlo methods to correct profiles for the effects of multiple scattering is a new and developing technique. The applications described in this Chapter have demonstrated the success of the technique, and have shown the importance of making these corrections to experimental Compton profiles. The Monte Carlo program is used to remove the multiple scattering contribution from each gamma-ray Compton profile reported in this thesis, and has become a standard part of the data processing procedure. The program is written in FORTRAN, and is run on a CDC 7600 computer with a CPU time of 450 seconds.

In all of these Monte Carlo calculations the electrons are treated as free electrons. Therefore the Klein-Nishina (eqn. 3-25), or Thompson (eqn. 3-26) cross sections are used to describe Compton and elastic scattering events respectively. The electron binding modifies the angular and energy distributions of the scattered photons, particularly for high electron binding energies or low energy photons. These modifi-

cations can be taken into account by including the incoherent scattering factors S(q,Z) or form factors f(q,Z) in the differential cross sections (see eqns. 1-4 and 1-6 in section 1.2). For 60 keV radiation these factors may become important for measurements on the transition metals (Z>20). However, since the profile measurements reported here are confined to materials with atomic number $Z \leqslant 13$, the effects of electron binding on the energy distribution of the multiple scattered photons have been neglected.

The Compton profile of aluminium (Z = 13) is the subject of the next chapter. The gamma-ray measurement is shown to be substantially modified by multiple scattering. The corrected profile is in good agreement with a recent measurement on a thin sample (confirming the accuracy of the Monte Carlo method), and a comparison is also made with some theoretical models of aluminium.

Chapter 4 references

(1) Reed, W.A., and Eisenberger, P., (1972), Phys. Rev., B6, 4596.

(2) Paakkari, T., Kohonen, E.L., Aikala, O., Mansikka, K. and Mikkola, S., (1974), Physica Fennica, 9, 207.

(3) Eisenberger, P., and Reed, W.A., (1974), Phys. Rev. B9, 3242.

(4) Tanner, A.C., and Epstein, I.R., (1974), J. Chem. Phys., (to be published).

(5) Laval, J., (1942), C.r. hebd., Seanc. Acad. Sci., Paris, 215, 359.

(6) Walker, C.B., (1956), Phys. Rev., 103, 558.

(7) Currat, R., DeCicco, P.D., and Weiss, R.J., (1971), Phys., Rev., A4, 4256.

(8) Paakkari, T., and Suortti, P., (1974), Phys. Rev., B9, 1756.

(9) Warren, B.E., (1969), X-ray Diffraction (London: Addison-Wesley).

(10) Waller, I., and Hartree, D.R., (1929), Proc.R.Soc., A124, 119.

(11) Weiss, R.J., (1973), Phil. Mag., 28, 1161.

(12) Freeman, A.J. (1959), Phys. Rev., 113, 169.

(13) Mendelsohn, L.B., and Briggs, F., (1973), Inner Shell Ionization Phenomena and Future Applications, Vol. 3., (USAEC Conference - 720404), p. 1142.

(14) Doyle, P.A., and Turner, P.S., (1968), Acta. Cryst. A24, 390.

(15) Taward, C., Nicolas,D., and Rouault, M., (1967), J. Chim. Phys., 64, 540.

CHAPTER 5

THE COMPTON PROFILE OF ALUMINIUM

5.1 Background

There has been considerable interest in the electron density distribution in aluminium ever since the early x-ray form factor measurements by Batterman, Chipman and DeMarco[1] in 1961 indicated big deviations from Hartree-Fock (HF) free atom form factors at all values of $\sin\theta/\lambda$. These results were supported by the more recent measurements reported by DeMarco[2] in 1967. Since the experimental form factors were appreciably less than the HF values for the 'neon core' ($1s^2 2s^2 2p^6$) alone, it was necessary to postulate an expansion of the core electron charge density. However, the binding energies are about 1500 eV for the 1s electrons and 70 eV for the 2s and 2p electrons, while the cohesive energy of aluminium is only 3 eV per atom. Thus, virtually no change can be expected in the core electron wave functions in the metal. The HF free atom form factor for the ten core electrons is plotted in fig. 1-1 (pg. 10) as well as the form factor for the three outer electrons. Apart from the very low angle reflections (111,220) the outer electrons make very little contribution to the Bragg scattered intensity. Therefore it appears that the discrepancy at high $\sin\theta/\lambda$ cannot be attributed to solid state effects, and this was confirmed in a band structure calculation by Arlinghaus[3].

In an effort to establish the source of the discrepancy between the HF free atom theory and the experimental form factors, further diffraction measurements were undertaken by

Raccah and Henrich,[4] and by Inkinen, Pesonen and Paakkari.[5] In common with the previous results, the intensities of the first two reflections were significantly lower than the HF values (lower even than the theoretical values for the neon core alone). However, the results for the other reflections averaged only about 0.5 - 1.0% less than the HF values, well within the experimental errors. Ascarelli and Raccah[6] showed that these results can be explained by changes in the outer electron distribution alone, and the recent work of Brown[7] on beryllium indicates that such a reduction in intensity may arise simply because core and conduction electrons are scattering out of phase as a consequence of the requirement of orthogonality of the two sets of wave functions in the one-electron approximation. Thus it can be concluded that solid state effects do appear in the electron distribution of aluminium, but the effects on measured form factors are confined to the lowest order reflections. It has been pointed out by Suortti[8] that certain factors in the preparation of the specimen can give rise to systematic errors in powder diffraction experiments. The diffracted intensity is reduced by the sample porosity and surface roughness, and this reduction can account for the unexpectedly low values found in the earlier powder measurements[1]. On the other hand, beam extinction is a major source of experimental error in single crystal measurements[2].

The Compton profile is particularly sensitive to the behaviour of the outer electrons. Cooper and Williams[9] have calculated the Compton profile and form factors for aluminium, based on an approximate self consistent local orbital theory by Kunz[10]. Although the form factors differ only slightly from the HF free atom values, there is

a gross discrepancy in the calculated Compton profile. This again demonstrates the relative insensitivity of the form factors to the outer electrons, and suggest that an experimental Compton profile could provide a more stringent test for theoretical models of aluminium.

X-ray Compton scattering measurements of the electron momentum density in aluminium were first published by Phillips and Weiss[11] in 1968. These results were of low accuracy, and formed part of an exploratory study of several metallic systems. After subtraction of a HF free atom core distribution, the conduction electron momentum density appeared to contain a substantial high momentum tail. Alternatively some deviation from free atom behaviour in the atomic core could be responsible for the discrepancy at high momenta. However, gamma-ray measurements by Felsteiner, Fox and Kahane[12] failed to substantiate the hypothesis that there is a high momentum tail on the conduction electron Compton profile. Further x-ray work by Currat, DeCicco and Weiss[13], at improved statistical accuracy, also failed to find any significant deviation from the free atom Compton profile at high momenta (although this work was aimed at investigating the total incoherent intensity, rather than the Compton line shape).

The present work, with both x-rays and gamma-rays, was undertaken to produce data with sufficient statistical accuracy to remove any doubt which may remain about the core electron momentum density, and to investigate the conduction electron density in greater detail than had hitherto been attempted. It is shown that multiple scattering has made a significant contribution to all previous measurements, and the gamma-ray results presented here have been corrected for multiple scattering effects with the Monte Carlo procedure.

At the same time another gamma-ray investigation on aluminium was in progress elsewhere[14] and a detailed comparison with these results is possible.

Since no crystal calculation of the electron momentum density in aluminium is available, the results are first compared with a model consisting of a free atom core plus three free electrons - aluminium is usually thought of as a good free electron metal with a near spherical Fermi surface. Secondly, a more realistic model of an interacting electron gas which includes electron-electron correlations (in the random phase approximation) and the effect of orthogonalising the conduction electron wave function to the core is used.

5.2 The X-ray Measurement

Aluminium has a large photoelectric cross section for Mo Kα x-rays, and the Compton scattered intensity is consequently rather low (2 - 3 counts per second at the profile peak). The long running time for the experiment of about three months places stringent requirements on the stability of the x-ray tube and the electronics of the detection system. These difficulties illustrate the limitations of x-ray Compton scattering, and x-ray measurements are therefore normally confined to materials with lower atomic number. Details of the experiment are given in the next section; a general description of the experimental method was given in Chapter 2, section 2.2.

5.2.1 Experimental

Two single crystal slices of aluminium (each of thickness 7 mm), one cut on (100) and the other on (110), were

irradiated by x-rays from a 2.7 kW molybdenum spectrometer tube at a scattering angle of 146°. The scattered x-rays were detected by a NaI(Tl) scintillation counter, and point by point scans were performed at intervals of 0.02° of $2\Theta_s$. Stability tests on the system showed that its long term stability was better than ½% as measured by the count rate fluctuations at a given angular setting, but even so many short runs over all or part of the profile were taken, and each run compared with the previous runs using a chi-squared test (see Epstein and Williams).[21] No runs were rejected. (This experiment was performed prior to the installation of the monitor system described in Chapter 2.)

In all, 40,000 counts were accumulated at the peak of the Compton profile for each crystal during a three month period. The samples were occasionally interchanged to ensure that spurious geometrical effects had no influence on the Compton profile. Air scattering was checked and found to be negligible. Although the MoKα Compton profile is confined to the wavelength region $0.70\text{Å} - 0.80\text{Å}$ measurements were made over the range $0.60\text{Å} - 0.85\text{Å}$ in order to ensure that a reliable subtraction of the background could be made. The two experimental profiles for 100 and 110 crystal orientations were compared, after the subtraction of the background, by the chi-squared test and no significant difference was indicated.

The resolution function was determined by substituting a molybdenum foil for the aluminium sample. The width of the individual $K\alpha_1$ and $K\alpha_2$ lines was only one-ninth of the width of the Compton profile.

5.2.2 Data Reduction

A linear background was subtracted using points in the

region of 0.60 Å and 0.85 Å to define the zero level. The validity of this procedure was also checked by ensuring that this gave correct values for the MoKβ Compton profile which, being smaller (cf. the MoKα profile), is more sensitive to background subtraction errors. The measured data after background subtraction are shown in fig. 5-1 for one of the crystal orientations. The total number of counts accumulated at each position of the crystal spectrometer is plotted against the analysing crystal Bragg angle.

Analytic corrections were made for the wavelength absorption, polarization and reflectivity of the analysing crystal as described in Chapter 2. The separation of the α_1 and α_2 components of the Compton line was performed initially by the Rachinger method[15] using the experimentally measured $MoK\alpha_2/MoK\alpha_1$ intensity ratio (which was within 1/2% of the accepted value of 0.526). The data was subsequently also separated by the alternative symmetric method in Appendix I. This method has the advantage that it avoids the accumulation of statistical errors characteristic of the Rachinger iterative method, and therefore gives a better separation in the region of the Compton peak and in the long wave-length tail. In this particular case, its use was restricted to the region near the Compton peak, since for $p_z > 2.5$ a.u. the separated line is asymmetric because the $1s^2$ core electron contribution is not excited until the energy transfer exceeds the binding energy of 1500 eV. This asymmetry was clearly visible in the data separated by the Rachinger method. The data was deconvoluted using the method of Lloyd[16] as described in Appendix II. Finally the wavelength scale was converted to the momentum scale and the data normalised.

The normalisation presented certain difficulties because

Fig. 5-1: Raw data for the x-ray measurement of the Compton profile of aluminium. The points are given as a function of the Bragg angle of the analysing crystal.

rement

The

ragg

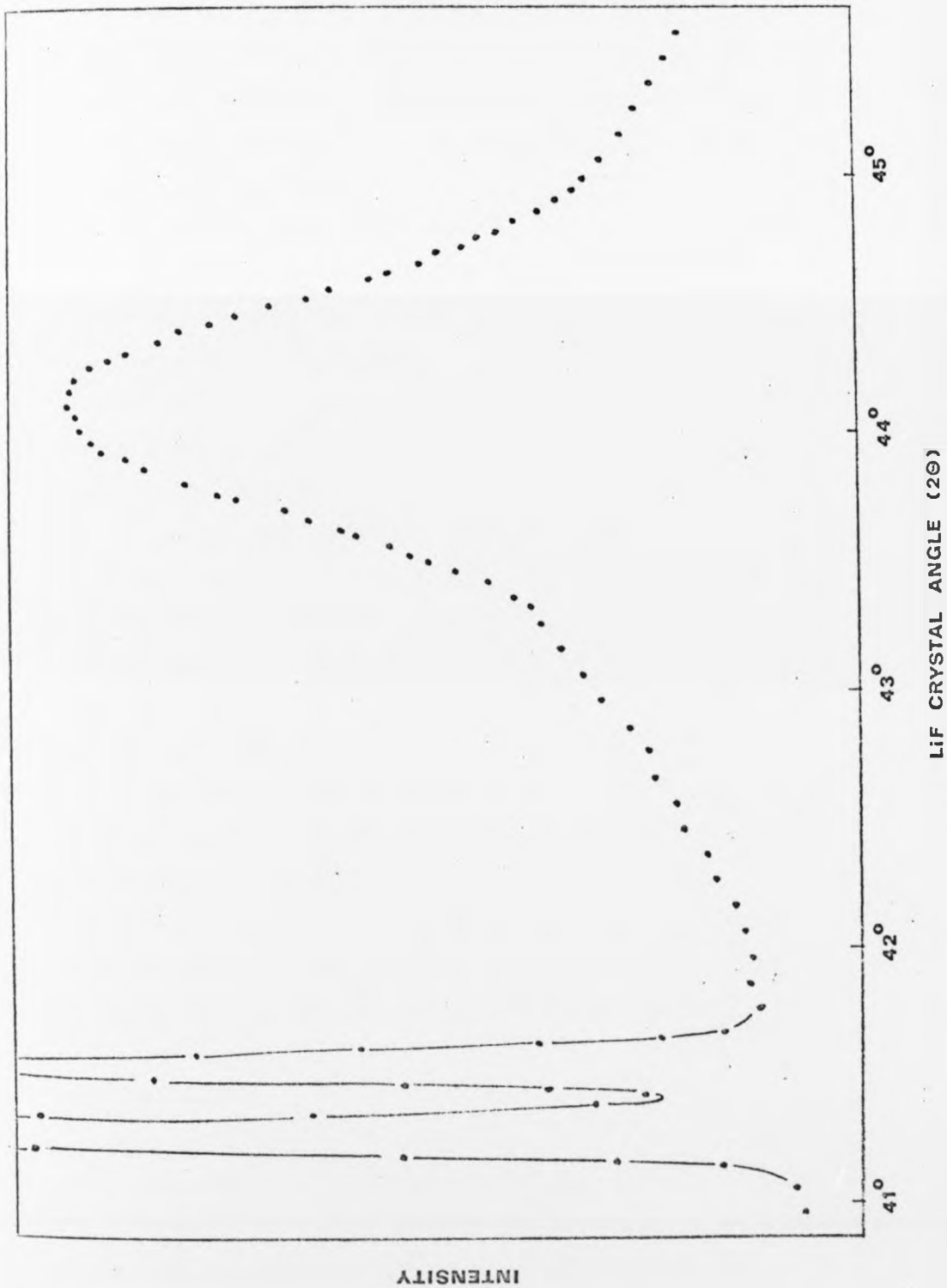

of the nature of the $1s^2$ core contribution. The procedure adopted was to scale the area under the profile, in the region $|p| < 2.0$ a.u., to the value calculated in the impulse approximation from Clementi's Hartree-Fock wave-functions (see Weiss, Harvey and Phillips)[17] for the L and M shell electrons for $|p| < 2.0$ a.u. A $1s^2$ free atom core profile was then added to the experimental results. X-ray data at higher values of p_z cannot be easily interpreted for two reasons; firstly, in the short wavelength tail the profile terminates at the position of the incident wavelength ($p_z \sim 3$ a.u.) and, secondly, on the long wavelength side the profile has a contribution from the K electrons for values of $p_z > 2.5$ a.u.

Following this procedure the experimental results, for $p_z < 2.0$ a.u. are directly comparable with the gamma-ray data of Manninen, Paakkari and Kajantie[14] which are not affected by the K electron binding energy. Both theoretical curves were normalised in the same way, so a direct comparison between experiment and theory is possible.

The processed experimental profiles for both crystal orientations were found to be symmetric about $p_z = 0$ and the results were therefore folded about this origin. Furthermore, as no statistically significant difference was found between the two profiles, the final experimental curve was taken as the average of both folded profiles.

5.2.3 Discussion

The results are presented in fig. 5-2 and in table 5-1. The figure also shows a theoretical profile based on a treatment of an interacting electron gas which includes the effect of electron-electron correlations and the

Table 5-1 (a)

Theoretical Compton profiles of aluminium. The profile for the conduction electrons using the interacting electron gas model is due to Pandey and Lam.[18]

p_z a.u.	$(1s^2 2s^2 2p^6 3s^2 3p)$ free-atom	$(1s^2 2s^2 2p^6)$+3 free electrons	$(1s^2 2s^2 2p^6)$+ interacting electron gas
0.0	5.151	4.183	3.985
0.1	4.999	4.152	3.996
0.2	4.575	4.061	3.944
0.3	3.969	3.907	3.805
0.4	3.325	3.692	3.611
0.5	2.761	3.416	3.356
0.6	2.333	3.078	3.036
0.7	2.037	2.679	2.652
0.8	1.842	2.219	2.207
0.9	1.713	1.698	1.767
1.0	1.623	1.524	1.653
1.2	1.492	1.429	1.513
1.4	1.378	1.325	1.385
1.6	1.261	1.215	1.256
1.8	1.144	1.104	1.134
2.0	1.029	0.996	1.023

Table 5-1 (b)

Experimental Compton profiles of aluminium where Exp. 1 are the present x-ray results and Exp. 2 and 3 are the gamma-ray results of Manninen et al.[14] and Felsteiner et al.[19] respectively.

p_z a.u.	Expt 1	Expt 2	Expt 3
0.0	3.88±0.04	4.00±0.04	3.95±0.15
0.1	3.86	3.95	3.92
0.2	3.82	3.83	3.84
0.3	3.69	3.65	3.66
0.4	3.55	3.41	3.43
0.5	3.17	3.14	3.13
0.6	2.93	2.86	2.85
0.7	2.56	2.57	2.59
0.8	2.22	2.28	2.28
0.9	1.86	2.02	1.98
1.0	1.74±0.03	1.81±0.03	1.75±0.08
1.2	1.54	1.48	1.55
1.4	1.42	1.33	1.43
1.6	1.35	1.23	1.28
1.8	1.17	1.16	1.14
2.0	1.07±0.02	1.06±0.02	1.05±0.06

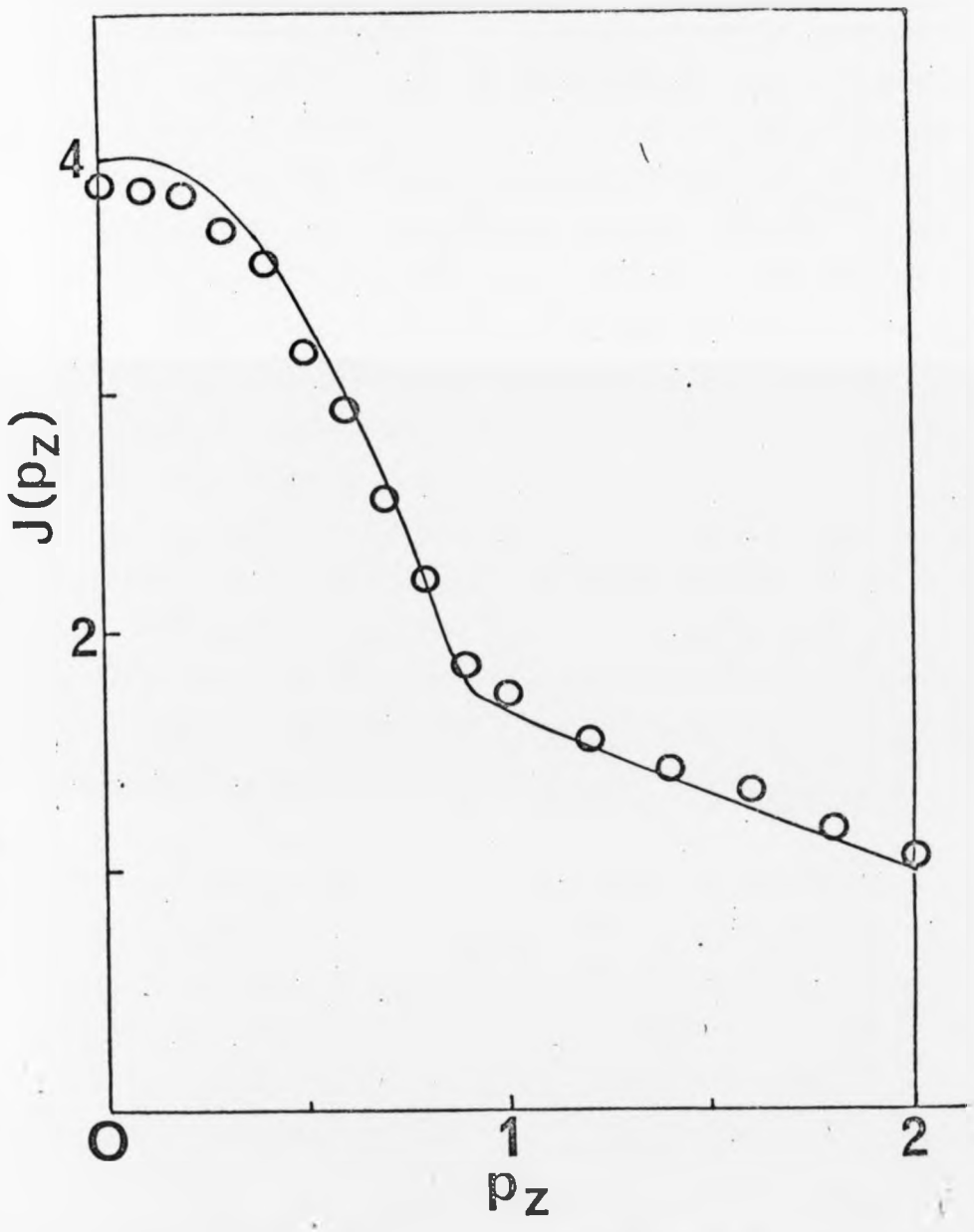

Fig. 5-2: Experimental and theoretical Compton profiles of aluminium. The experimental profile (0 0 0) was measured with MoKα x-rays and the theoretical profile is due to Pandey and Lam[18].

orthogonalisation of the conduction electron wavefunction to the core states (Pandy[18], 1973). As can be seen from the table, this model substantially improves upon the model based upon free atom core states plus three free conduction electrons. The experimental results of Manninen, Paakkari and Kajantie[14] and of Felsteiner, Fox and Kahane[19] show general agreement with this result, but were both obtained at much lower resolution. (In both gamma-ray experiments the ratio of the Compton line width to the instrumental resolution function width was roughly three to one, in the present X-ray experiment the ratio is nine to one). This probably accounts for some of the disagreement between the experiments in the region near the Fermi momentum (p_f = 0.926 a.u.). Even so the x-ray results indicate that the change in slope of the Compton profile at the Fermi momentum is not as abrupt as predicted by the free electron or interacting electron gas models.

However, the experimental data are not corrected for multiple scattering effects. The sample thickness (7 mm) is far greater than the mean free path of the incident x-rays in aluminium, and multiple scattering therefore accounts for almost 10% of the total Compton intensity (see fig. 4-2(b), pg. 76). When this contribution is removed, the resulting profile will be narrower, with a higher peak and a sharper break at the Fermi momentum. There will also be some reduction in the high momentum region of the profile. These changes would each improve the agreement between the experimental profile and the interacting electron gas model.

Unfortunately at these x-ray energies (~17 keV) the angular and energy distributions of the scattered photons are significantly modified by the incoherent scattering

factors and form factors for aluminium. The Monte Carlo method as described in Chapters 3 and 4 cannot be reliably employed to remove the effects of multiple scattering, since in its present form, the electrons are treated as free and binding effects are neglected. However, at the higher gamma-ray energies (~60 keV), these factors have little effect on the multiple scattering. Therefore a gamma-ray Compton profile of aluminium, corrected with the Monte Carlo program, can provide a more reliable experimental profile for comparison with the theoretical profiles given in table 5-1 despite the lower resolution. The results of such an experiment are given in the following section.

5.3 The Gamma-ray Measurement

5.3.1 Experimental and Data Processing

A general description of the gamma-ray experimental method is given in Chapter 2, section 2.3. The gamma-ray Compton profile of aluminium was measured with a 300 mCi Am^{241} source, at a scattering angle of 150^{o}. The sample thickness was 7 mm. The data were first used to establish the effect of multiple scattering on the total Compton cross section of aluminium, as described in Chapter 4, section 4.3. This section also contains details of the experimental procedure. The measured differential Compton cross section from which the Compton profile is obtained is shown in fig. 4-6 (pg. 85).

After the area determination needed for the total cross-section measurement, the data were processed to obtain the Compton profile $J(p_z)$. Lloyd's[16] deconvolution method was used to correct the data for instrumental broadening arising from both detector resolution and beam divergence

(altogether 430 eV at 60 keV). The deconvolution method is discussed in Appendix II. The Compton profile $J(p_z)$ was obtained from the differential Compton cross section using the relativistic relation, eqn. 2-15, and the energy-momentum relation given in eqn. 2-13. After conversion to electron momentum scale the position of the Compton profile peak was checked by integrating the profile in the ranges -0.5 to 0.0 a.u. and 0.0 to 0.5 a.u. These areas were found to agree to within 0.2%. The final profile was then normalised to have the same area as a free atom Hartree-Fock profile in the region 0.0 a.u. to 5.0 a.u. (i.e. 5.89 electrons), using Clementi's wave functions and the impulse approximation[17]. The resulting Compton profile is presented in table 5-2.

5.3.2 Multiple Scattering Correction

The profile measured in this experiment, using a sample of 7 mm thickness, differs appreciably from the results of Manninen, Paakkari and Kajantie[14] for 1 mm thickness. It was shown in Chapter 4 that such a discrepancy can be interpreted as an effect of multiple scattering in the sample. The Monte Carlo programme described in Chapter 3 has been applied here to determine both the total intensity and the spectral distribution of the multiple scattered photons. This spectral distribution (for both two and three photon collisions) was used to correct the experimental Compton profile.

In table 5-2 and fig. 5-3 there is a comparison between the Compton profiles before and after correction. This correction is clearly significant since, for example, the difference at J(0) before and after correction is about four times the statistical error. Also reference to the

Table 5-2

The experimental Compton profile of aluminium (sample thickness 7 mm) before and after correction for multiple scattering.

p_z	Before correction	After correction
0.0	3.657 ± 0.7 %	4.065 ± 1.0 %
0.1	3.630	4.023
0.2	3.559	3.942
0.3	3.443	3.802
0.4	3.258	3.580
0.5	3.059	3.342
0.6	2.733	2.951
0.7	2.438	2.598
0.8	2.168	2.275
0.9	1.930	1.992
1.0	1.753 ± 1.0 %	1.782 ± 1.5 %
1.2	1.508	1.494
1.4	1.404	1.376
1.6	1.306	1.263
1.8	1.203	1.146
2.0	1.095 ± 1.5 %	1.022 ± 3.0 %
2.5	0.856	0.763
3.0	0.660	0.575
3.5	0.499	0.428
4.0	0.388	0.325
5.0	0.247 ± 2.0 %	0.192 ± 6.0 %

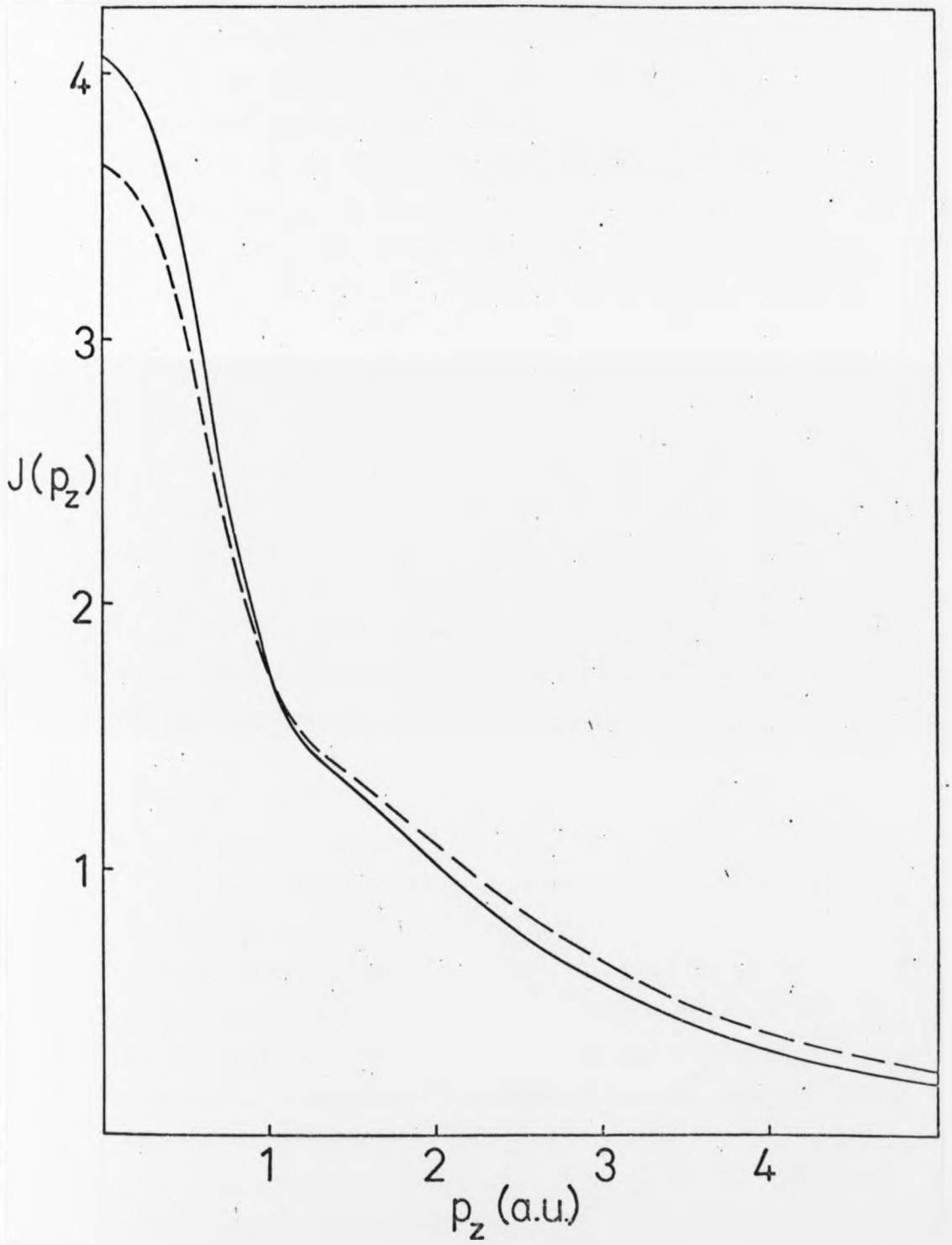

Fig. 5-3: The experimental Compton profile of aluminium measured with 60 keV gamma-rays shown before and after (——) correction for multiple scattering.

result of Manninen et.al.[14] shows that there is now much closer agreement with their measurement on an aluminium sample of thickness 1 mm. A small amount of multiple scattering ($\sim 5\%$) still present in the 1 mm sample is probably responsible for the remaining discrepancy, and this is consistent with the lower value of J(0) reported by Manninen et al. i.e. $3.96 \pm .04$ cf $4.06 \pm .04$ reported here.

The relative contributions of the various scattering events which result in a final photon emerging at a total scattering angle of $150^{\circ} \pm 2^{\circ}$ are given in table 5-3. It is important to note that for the correction of an experimental Compton profile the spectral distribution and relative intensity of each contribution must be known. It is seen in table 5-3 that there is a significant difference between the relative contributions in the total range of the profile, and those contributions in the range of only 0-5 a.u.

5.3.3 Results and Discussion

In section 5.2 of this Chapter an x-ray measurement of the Compton profile of aluminium was reported, and compared with a theoretical profile based on a treatment of an interacting gas. While the agreement between these calculated and measured profiles seemed to be fair, no correction had been made for multiple scattering present in the experiment. Indeed, the present data, which have been corrected for multiple scattering are in much better agreement with the above theory. The inadequency present in any deconvolution procedure (see e.g. Paatero, Manninen and Paakkari[20]) is likely to be responsible for some of the remaining discrepancy, particularly in the region of the Fermi surface

Table 5-3

The relative contributions to the measured Compton profile of various scattering processes are shown. These contributions are given as percentages of the total incoherent intensity, with statistical errors.

Range	Single	Double	Triple	More than triple
Total Profile	75.3 ± 0.5	18.8 ± 0.2	3.8 ± 0.1	2.1 ± 0.2
0-5 a.u.	83.0 ± 1.0	15.6 ± 0.5	1.4 ± 0.1	-

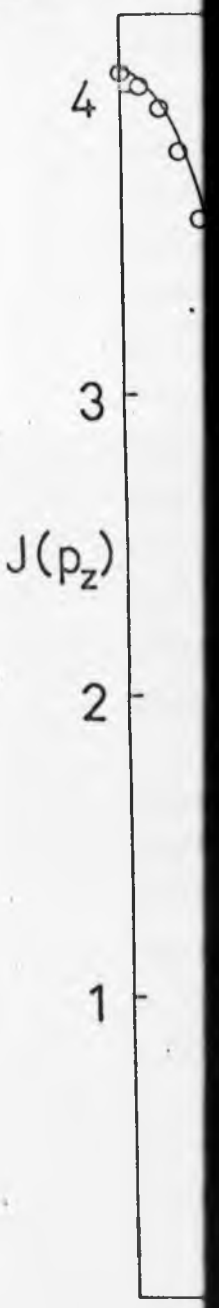

Fig. 5-4: The experimental Compton profile of aluminium measured with 60 keV gamma-rays, after correction for multiple scattering, is compared with the calculated profile given by Pandey and Lam[18]. The calculated profile has been convoluted and then deconvoluted with the experimental resolution function.

file of
ys, after
compared
ndey and
n convo-
perimental

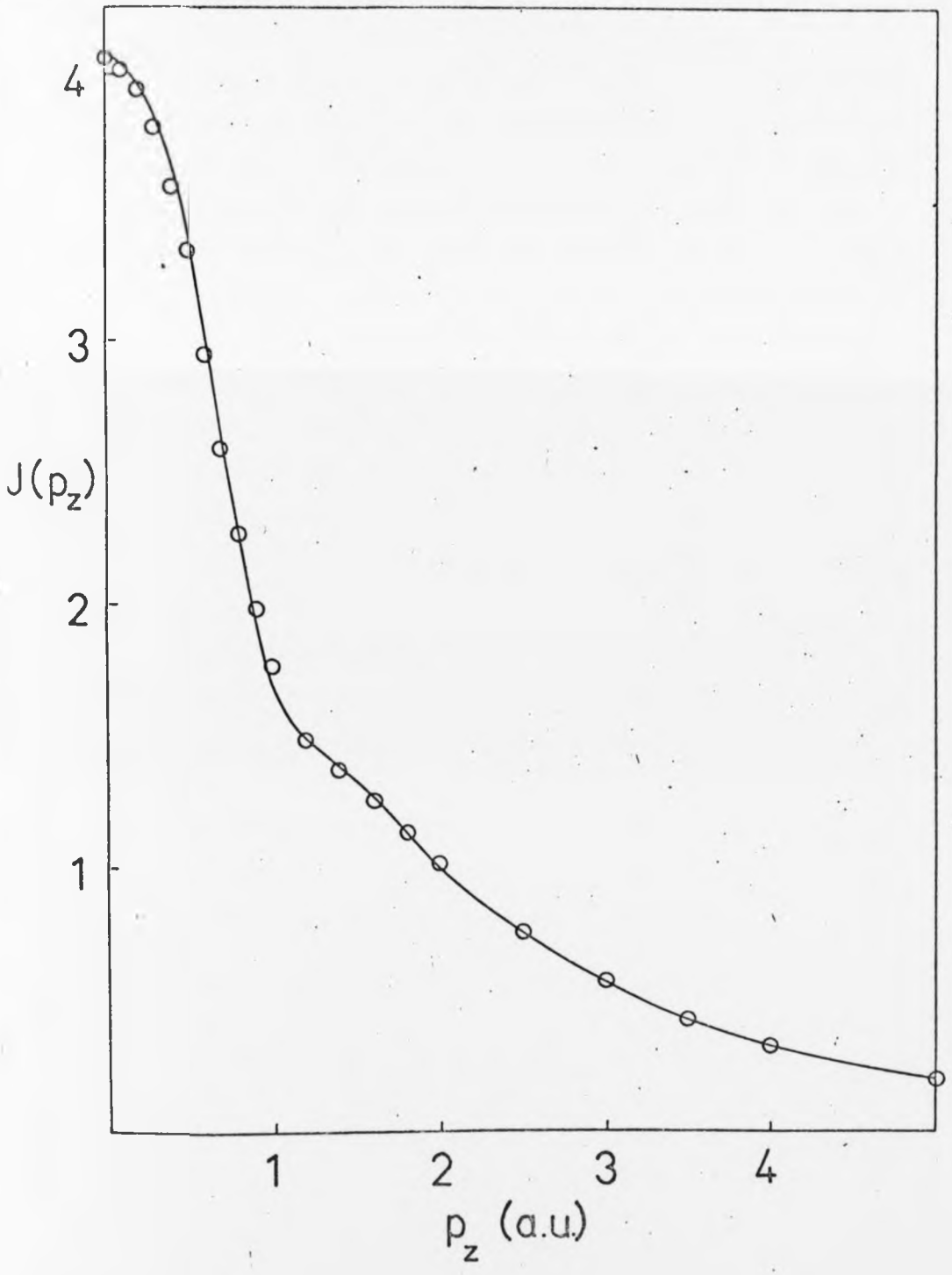

(0.93 a.u.)

In order to overcome some of the errors introduced into any comparison of theory and experiment by imperfect deconvolution, the calculated profile given in table 5-1 has been convoluted with the instrumental resolution function and subsequently deconvoluted in the same way as the experimental data. Although this procedure is 'experiment dependent' the resulting theoretical curve can be reliably compared with the experimental profile. The very good agreement between experiment, (after the multiple scattering correction), and theory illustrated in fig. 5-4 indicates that the electron gas model incorporating correlations and orthogonalisation effects gives a good description of the conduction electron density.

The agreement also found at higher momenta between experiment and values deduced from Hartree-Fock free atom wavefunctions implies that the core electron density in solid aluminium is not appreciably different from that in the free atom, despite the speculation which has existed on this point with regard to the interpretation of earlier x-ray form factor measurements on aluminium.

Chapter 5 references

(1) Batterman, B.W., Chipman, D.R., and DeMarco, J.J., (1961), Phys. Rev., 122, 68.

(2) DeMarco, J.J., (1967), Phil. Mag., 15, 483.

(3) Arlinghaus, F.J., (1967), Phys. Rev., 153, 743.

(4) Raccah, P.M., and Henrich, V.E., (1969), Phys. Rev., 184, 607.

(5) Inkinen, O., Pesonen, A., and Paakkari, T., (1970), Ann. Acad. Sci. Fenn., AVI, 344.

(6) Ascarelli, P., and Raccah, P.M., (1970), Phys.Lett., 31A, 549.

(7) Brown, P.J., (1972), Phil. Mag., 26, 1377.

(8) Suortti, P., (1972), J. Appl. Cryst., 5, 325.

(9) Cooper, M.J., and Williams, B., (1972), Phil.Mag., 26, 1441.

(10) Kunz, R.P., (1971), Phys. Stat. Sol., 46, 385.

(11) Phillips, W.C., and Weiss, R.J., (1968), Phys.Rev., 171, 790.

(12) Felsteiner, J., Fox., R., and Kahane, S., (1971), Sol.St. Commun., 9, 61.

(13) Currat, R., DeCicco, P.J., and Weiss, R.J., (1971), Phys. Rev., B4, 4256.

(14) Manninen, S., Paakkari, T., and Kajantie, K., (1974), Phil. Mag., 29, 167.

(15) Rachinger, W.A., (1948), J. Scient. Instrum., 25, 254.

(16) Lloyd, K.H., (1969), Am. J. Phys., 37, 329.

(17) Weiss, R.J., Harvey, A, and Phillips, W.C., (1968), Phil. Mag., 17, 241.

(18) Pandey, K.C., and Lam., L., (1973), Phys.Lett., A43, 319.

(19) Felsteiner, J., Fox. R., and Kahane, S., (1972), Sol.St. Comm., 11, 635.

(20) Paatero, P., Manninen, S., and Paakkari, T., (1974), Phil. Mag., 30, 1281.

(21) Epstein, I.R., and Williams, B.G., (1973), Phil. Mag., 27, 311.

CHAPTER SIX

Molecular Compton Profiles

6.1 Introduction.

The calculation of atomic and molecular wavefunctions in momentum space has been of considerable interest to theoretical chemists for more than thirty years. So far, however, very few momentum space studies have been reported for molecules containing many electrons. To some extent this is related to the computational difficulties involved in performing accurate self-consistent-field (SCF) calculations of the electronic structure of large molecules. In addition, the scarcity of experimental results for these systems has made comparison of theory with experiment difficult. Moreover, the available experimental results were treated with some scepticism, since there have been serious discrepancies between some reported profiles (e.g. in benzene the peak values of two experimental profiles[1,2] differed by almost 10%). It is now clear that multiple scattering was largely responsible for these anomalous results. In this Chapter experimental profiles, corrected for multiple scattering, are reported for several molecular systems and the results are compared with various theoretical profiles. Several techniques are employed which avoid some of the difficulties associated with the computation of Compton profiles for large molecules.

As pointed out in Chapter 1, attempts to solve the quantum mechanical equations directly in momentum space have met with little success. The most fruitful approach is to solve the familiar Schrodinger equation in the position space representation, and then apply the Dirac transformation to the result. This method was adopted in the first systematic studies of

molecular momentum wavefunctions by Coulson and Duncanson[3] in 1942, although their work was hampered by the lack of accurate molecular wavefunctions in position space. However, through their study of H_2^+, H_2 and some simple hydrocarbons using only elementary wavefunctions they obtained a number of important qualitative results. In particular their analysis in terms of localised molecular orbitals has become the basis for many recent calculations (as described below).

Henneker and Cade[4] made the first momentum space calculations using molecular SCF wavefunctions. They found that for atomic and diatomic systems Hartree-Fock accuracy is necessary to ensure good agreement with experiment. SCF studies of molecules containing more than two atoms have been almost completely limited to minimum basis set (MBS) wavefunctions. Epstein and Lipscomb obtained molecular momentum distributions for boron hydrides[5] and hydrocarbons[6] in this way. These studies show that, in spite of the need for H-F accuracy in calculations of atoms and diatomic molecules, good agreement with experiment on larger systems can be obtained with MBS-SCF calculations.

As the size of the molecule increases the effort in computing accurate SCF wavefunctions becomes prohibitive. One method of circumventing this problem is the use of a localised molecular orbital (LMO) model.[5,7] In this approach the valence electrons of the hydrocarbons, say, are considered to be made up from a combination of C-H, C-C and C=C bond electrons. If these bonds are transferrable it should be possible to 'build up' Compton profiles of large molecules from their constituent LMO's obtained from calculations on small molecules. If reliable large molecule wavefunctions can be synthesised in this way, the LMO method would lead to a considerable reduction in the computational effort (compared

to SCF methods). This effort could be concentrated on extracting the necessary bond units from calculations on small and relatively simple molecules. For the case of the hydrocarbons, strong experimental evidence for the transferability of LMO's has already been presented by Eisenberger and Marra.[2]

Until now calculations based on the LMO method have provided the only means of comparing theory with experiment for the large molecules (apart from a simple superposition of free atom profiles)[2,8] The aim of the present work is to extend the range of experimental data to include larger molecules, and to assess the reliability of the LMO description of these more complex systems. The results are also compared with profiles obtained using an empirical molecular orbital scheme[9] and, in one case, an SCF profile is also available.

Experimental and theoretical Compton profiles are presented for formamide (NH_2CHO), p-benzoquinone ($C_6H_4O_2$) and decaborane ($B_{10}H_{14}$) molecules. The measurements were made with 60 keV gamma-rays, and the Monte Carlo procedure was used to correct the profiles for multiple scattering effects. For the formamide and p-benzoquinone the theoretical profiles are obtained by means of the localised orbital approach and also by the iterative extended Hückel (IEH) method.[10] An ab initio SCF calculation is given for formamide.[10] The decaborane result is compared with an LMO profile,[11] where the constituent LMO's are taken from a calculation on hexaborane (B_6H_{10}).

6.2 Experimental.

A general description of the experimental method is given in Chapter 2. 59.54 keV gamma-rays from a 300 mCi Am^{241}

source were scattered by the sample through a mean angle of 150°. The detection system consisted of a Ge(Li) detector with a resolution of 390 eV at 60 keV, coupled to the 4096 channel MCA. The energy interval between channels was 20 eV.

Formamide: The liquid formamide (98.5% purity) was supplied by Hopkin and Williams Ltd., England. The impurity, mainly water, will make a small contribution to the experimental profile. However, since this contribution will be less than 2% of the total, and moreover will closely resemble the formamide profile, its effect on the experimental result can be neglected. The sample container (diameter 5cm., thickness 0.5cm.) was covered with thin mylar foils. During the measuring period of two weeks some 250,000 counts per channel were accumulated at the profile peak. A separate measurement was made of the empty sample container in order to evaluate the contribution of the background from the foils and from air scattering. The Compton peak-to-background was found to be about 50 to 1.

p-benzoquinone: The powder used in the p-benzoquinone measurement was supplied by Fluka AG, Switzerland. Impurities (in total about 2%) consist mainly of hydroquinone, and their effects on the final profile can be neglected. The sample was constructed by compressing the powder into a cylindrical specimen holder, with a diameter of 3cm. Samples of two thicknesses, 0.3cm. and 0.17cm., were used in order to check the reliability of the multiple scattering correction. About 40,000 counts per channel at the Compton peak were gathered in both measurements, and the peak-to-background ratios were 750 to 1 and 500 to 1 for thick and thin samples respectively.

Decaborane: The compressed powder sample (thickness 0.2cm, diameter 2.0cm.) was kindly supplied by Prof. M.G.H. Wallbridge,

Dept., of Molecular Sciences, University of Warwick. The decaborane was resublimated immediately prior to the measurement in order to remove any effects of hydrolosis which can occur when the material is exposed to air. Over a measuring period of two weeks about 70,000 counts were accumulated at the Compton peak and the peak-to-background ratio was 200 to 1. A small contribution from the sample holder was measured separately.

After subtraction of the background the experimental profiles were corrected for instrumental resolution effects (see Appendix II for a discussion of the deconvolution procedure). The corrections for the energy dependence of absorption in the sample, and the relativistic Compton cross section are given in Chapter 2 (eqns. 2-9 and 2-15). Finally, the results were converted to the electron momentum scale (eqn. 2-13) and normalised to have the same area as the corresponding theoretical profiles in the range 0.0 a.u. to 5.0 a.u.

A correction for multiple scattering was made for each of the measured Compton profiles by employing the Monte Carlo procedure described earlier. The correction increased J(0) by about 4% for formamide, 3% for the thicker and 2% for the thinner p-benzoquinone sample, respectively, and 1% for the decaborane sample. No difference outside the experimental error were found in the two p-benzoquinone results after making the multiple scattering correction. The final results for eadh molecule are given in tables 6-1, 6-2 and 6-3.

6.3 Results and Discussion

6.3.1 Formamide (NH_2CHO) and p-benzoquinone ($C_6H_4O_2$).

The theoretical profiles for formamide (LMO, SCF and IEH) are given in table 6-1 together with the final experimental results and the results for p-benzoquinone are given in table

Table 6-1

Experimental and theoretical Compton profiles of formamide (NH_2CHO)

p_z(a.u.)	LMO	SCF	IEH	IEH[a)]	Exp.
0.0	9.013	9.136	9.246	9.066	9.151 ± 0.092
0.2	8.788	8.904	8.987	8.825	8.946
0.4	8.129	8.249	8.255	8.139	8.183
0.6	7.106	7.253	7.177	7.116	7.109
0.8	5.883	6.026	5.930	5.924	5.907
1.0	4.658	4.728	4.694	4.728	4.589 ± 0.078
1.2	3.582	3.540	3.600	3.653	3.431
1.4	2.716	2.589	2.716	2.769	2.628
1.6	2.068	1.905	2.050	2.091	1.988
1.8	1.590	1.449	1.573	1.602	1.541
2.0	1.272	1.154	1.238	1.266	1.259 ± 0.038
3.0	0.575	0.584	0.550	0.560	0.629
4.0	-	0.353	0.355	0.355	0.373
5.0	-	0.218	0.221	0.221	0.233 ± 0.012

a) Including the effects of convolution with the residual instrumental function.

Fig. 6-1: Difference curves between experimental and theoretical profiles for formamide. In each case the theoretical profiles have been convoluted with the instrumental resolution function, and then deconvoluted in the same way as the experimental data. The difference curves are obtained from the following theories:

LMO (--------)

SCF (••••••••)

IEH (————————)

experi-
formamide.
s have been
olution
he same way
erence curves
ries:

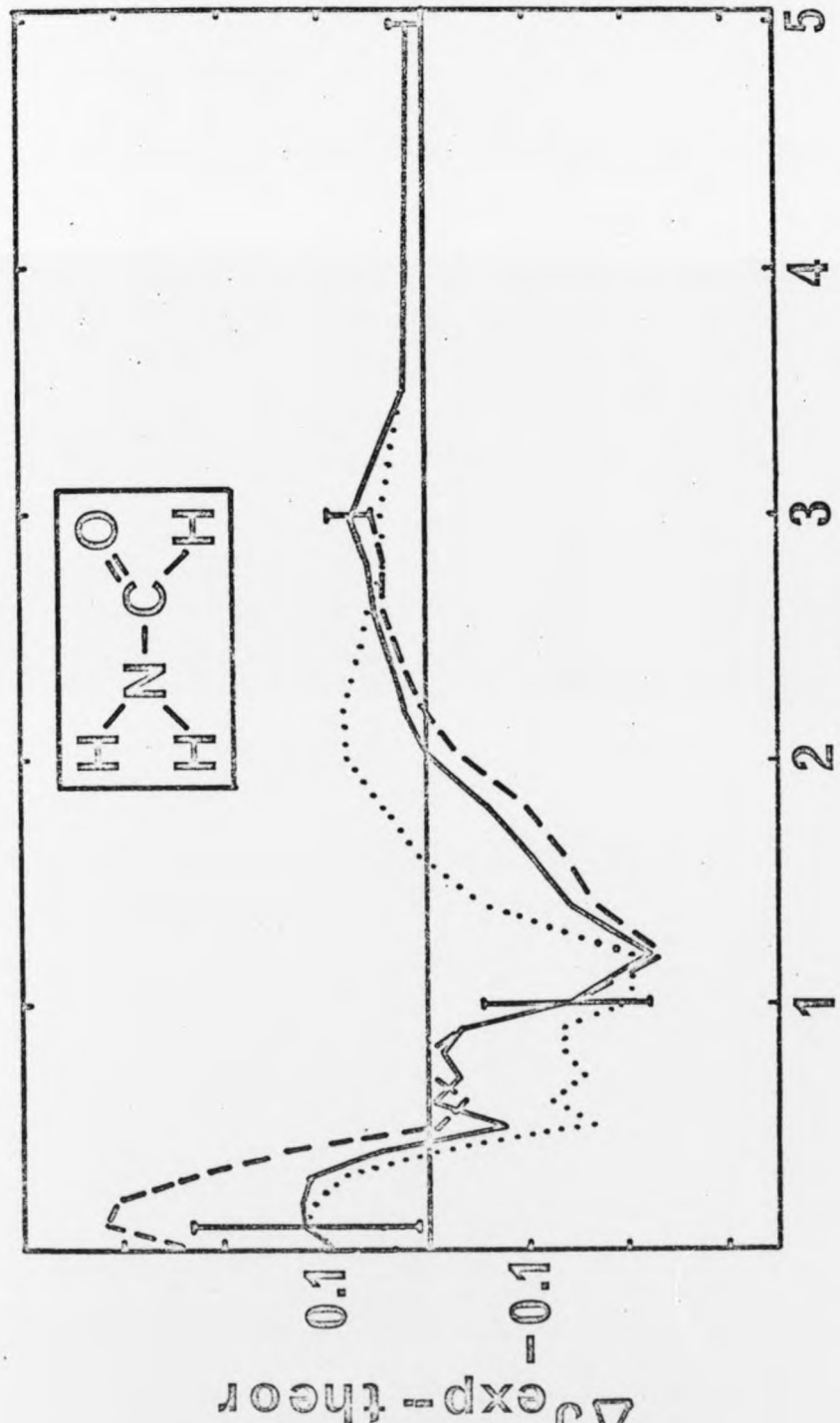

Table 6-2

Experimental and theoretical Compton profiles of p-benzoquinone ($C_6H_4O_2$)

p_z(a.u)	LMO	IEH	IEH[a)]	Exp.
0.0	21.18	21.95	21.61	21.62 ± 0.28
0.2	20.68	21.35	21.03	20.94
0.4	19.19	19.62	19.38	19.13
0.6	16.80	17.01	16.90	16.51
0.8	13.84	13.92	13.95	13.54
1.0	10.81	10.82	10.96	10.56 ± 0.19
1.2	8.16	8.10	8.29	7.79
1.4	6.06	5.97	6.16	5.92
1.6	4.57	4.45	4.60	4.41
1.8	3.53	3.43	3.52	3.55
2.0	2.87	2.76	2.82	3.00 ± 0.08
3.0	1.41	1.34	1.34	1.61
4.0	-	0.86	0.86	0.94
5.0	-	0.52	0.52	0.53 ± 0.03

a) Including the effects of convolution with the residual instrumental function.

Fig. 6-2: Difference curves between experimental and theoretical profiles for p-benzoquinone. In each case the theoretical profiles have been convoluted with the instrumental resolution function, and then deconvoluted in the same way as the experimental data. The difference curves are obtained from the following theories:

LMO (--------)

IEH (————————)

experi-
-benzo-
cal profiles
mental reso-
ed in the same
difference
ng theories:

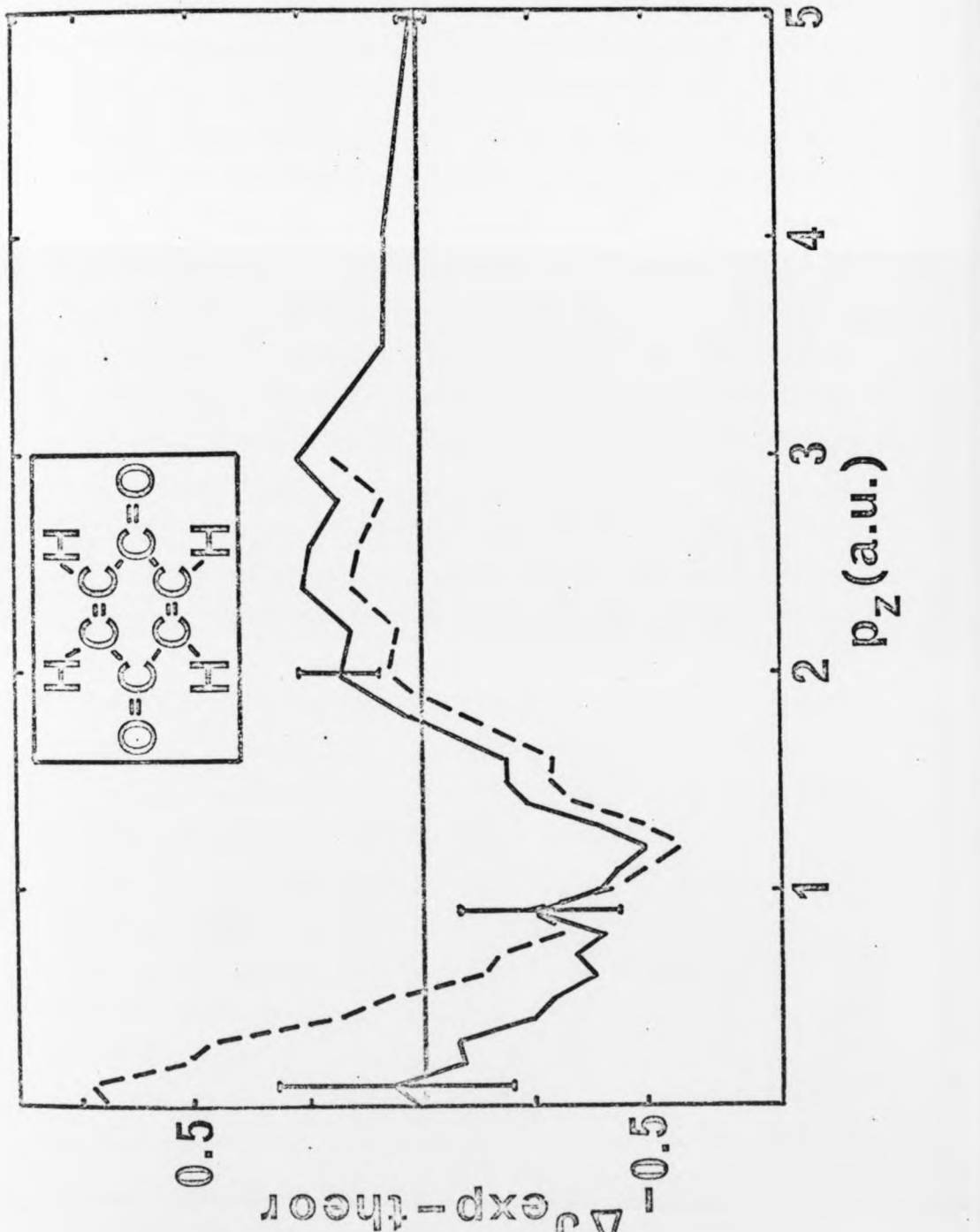

6-2. These tables also include an IEH profile which has been convoluted with the residual instrumental function (RIF). The comparison between theoretical and experimental Compton profiles is more realistic if the effects of imperfect deconvolution are included in this way (see Appendix II). This procedure was adopted for each of the theoretical profiles, and figs. 6-1 and 6-2 show how the resulting profiles differ from the experimental ones for formamide and p-benzoquinone, respectively.

The results of this work as presented in the tables and figures show fairly good agreement between all experimental and theoretical profiles, particularly when the effects of imperfect deconvolution are included in the theoretical curves. In regions of high momentum (> 4.0 a.u.) where the profiles are dominated by contributions from the core electrons, the experimental values are very close to the free atom theory. Since free atom behaviour can certainly be expected for these core electrons, the agreement at high momenta indicates that the various data corrections (including the correction for multiple scattering) have been made in the proper way.

Closer inspection of the results shows that in no case is the agreement between theory and experiment complete. Figs. 6-1 and 6-2 indicate that the LMO model is unsatisfactory at very low values of momenta (< 0.5 a.u.). This behaviour reflects the electron localisation which is assumed in the theory; a consequence of obtaining the constituent LMO's from calculations on small, light molecules[6]. In the larger molecules, particularly formamide, some degree of delocalisation can be expected. The alternative theories (IEH and SCF) include the effects of some delocalisation, and indeed the agreement with experiment at low momentum is improved. Over the remaining momentum range all difference curves show

similar trends.

The qualitative insensitivity of the calculated profiles with respect to the accuracy of the wavefunctions used is not too surprising as the profile is the result of an integration which tends to smooth out the differences between the various wavefunctions. Reasonable agreement with experimental profile can be expected as long as all the major bonding effects are included. The more subtle differences between, say, the ab initio SCF calculation and the experimental data for formamide are difficult to analyze.

More data to elucidate differences between theory and experiment for large molecules with many electrons are desirable. The theoretical methods used here seem, however, to be satisfactory considering the present accuracy of the measurements.

6.3.2 Decaborane ($B_{10}H_{14}$).

Since the material is electron deficient, the bonding in the boron hydrides is particularly unusual. Instead of the normal two-centre bonds, the shortage of electrons leads to the formation of three-centre bonds in which three centres are linked by a single orbital. In this type of bond the electrons may be highly delocalised, with similar characteristics to free electrons in metals. The boron hydrides could therefore provide a good example of metal-like behaviour in a molecular system.

Although no direct evidence for delocalisation in boron hydrides exists, there is much indirect evidence from the unexpected stability of some molecules and the 'fractional bonding' found in the LMO calculations on B_5H_9 and $B_{10}H_{14}$.[12] An effort to establish the valence electron distribution using x-ray diffraction methods was inconclusive owing to the

Table 6-3

Experimental and theoretical Compton profiles of decaborane ($B_{10}H_{14}$).

p_z(a.u)	LMO	LMO[a]	Exp.
0.0	31.104	30.357	30.162 ± 0.30
0.1	30.752	30.021	29.721
0.2	29.792	29.137	28.977
0.3	28.252	27.728	27.481
0.4	26.248	25.825	25.915
0.5	23.888	23.607	23.916
0.6	21.256	21.119	21.534
0.7	18.496	18.509	18.477
0.8	15.744	15.907	15.286
0.9	13.140	13.445	12.983
1.0	10.812	11.172	10.907 ± 0.15
1.2	7.152	7.609	7.516
1.4	4.880	5.191	4.970
1.6	3.636	3.771	3.898
1.8	2.972	3.009	3.220
2.0	2.556	2.565	2.827 ± 0.10
2.5	1.888	1.894	2.122
3.0	1.388	1.388	1.530 ± 0.07

a) Including the effects of convolution with the residual instrumental function.

difficulties in isolating the contribution of the valence electrons to the Bragg scattered intensity. Compton scattering is at present the only technique with sufficient sensitivity to identify the nature of the valence electron distribution. (Compton scattering and x-ray diffraction techniques are compared in Chapter 1).

The results of a preliminary gamma-ray measurement are shown in table 6-3, where a comparison is made with an LMO profile.[11] The constituent LMO's for this theoretical profile were obtained from a calculation on hexaborane (B_6H_{10}). An LMO profile which has been convoluted with the residual instrumental function is also given in table 6-3. Inspection of the profiles shows that the LMO model gives a good description of the Compton profile of decaborane (at least at this level of resolution). This implies that the LMO method can successfully describe the valence bonding even for the three-centre bonds found in the boron hydrides.

The experimental work is now being extended to include high resolution x-ray measurements of decaborane and carborane ($B_{10}C_2H_{12}$) where there are also possible delocalisation effects. The success of the LMO method should simplify the calculations for large molecules or polymers for which SCF calculations are impractical.

The experimental results presented in this Chapter illustrate the way in which the Compton profile can provide a sensitive test of the reliability of theoretical wavefunctions. In particular it is shown that for large molecules the localised orbital and Huckel methods can be employed to produce accurate wavefunctions, and thus avoid laborious SCF calculations. This is in contrast to the results for atoms and diatomic molecules where Hartree-Fock accuracy in the position space wavefunction is necessary.

Chapter Six References

(1) Weiss, R.J., (1970), J. Chem. Phys., 52, 2237.

(2) Eisenberger, P., and Marra, W.C., (1971), Phys. Rev. Lett., 27, 1413.

(3) Coulson, C.A., and Duncanson, W.E., (1942), Proc. Camb., Phil. Soc., 38, 100.

(4) Hennecker, W.H., and Cade, P.E., (1968), Chem. Phys. Lett., 2, 8.

(5) Epstein, I.R., and Lipscomb, W.N., (1970), J. Chem. Phys., 53, 4418.

(6) Epstein, I.R., (1970), Ibid., 53, 4425.

(7) Edmiston, C., and Ruedenberg, K., (1963), Rev. Mod. Phys., 35, 457.

(8) Inkinen, O., Halonen, V., and Manninen, S., (1971), Chem. Phys. Lett., 9, 639; Epstein, I.R., Williams, B.G., and Cooper, M.J., (1973), J. Chem. Phys., 58, 4098.

(9) Ahlenius, T., and Lindner, P., J. Phys. B., (in press).

(10) Lindner, P., (private communication).

(11) Epstein, I.R., (private communcation).

(12) Lipscomb, J. (1972), J. Am. Chem. Soc., 94, 1748.

(13) Brill, von R., Dietrich, H. and Dierks, H., (1971), Acta. Cryst., B27, 2003.

CHAPTER 7

Conclusions and Developments

7.1 General Conclusions.

As early as 1937 the experiments of DuMond and Kirkpatrick[1] successfully demonstrated that the spectrum of x-rays inelastically scattered from atomic electrons can be related to the Compton profile and hence to the electron momentum distribution. However, the development of the technique as a means of measuring electron distributions was extremely slow and indeed it lay completely dormant for about thirty years. The serious experimental difficulties associated with the very low Compton intensity were mainly responsible for the lack of interest during this period. With the availability of more powerful x-ray generators the technique reemerged in 1965[2], and the following ten years has been a time of sustained and expanding interest in both experimental and theoretical aspects of electron momentum distribution.

Much of the recent experimental work has been stimulated by the development of the gamma-ray technique[3]. The use of a solid state detector to analyse the energy spectrum of inelastically scattered gamma-rays leads to a considerable reduction in the length of time taken for a Compton profile measurement. Moreover, the range of systems which can be studied is greatly extended to include materials such as the transition metals where high photoelectric absorption makes x-ray measurements impractical. Therefore the gamma-ray method has effectively replaced the x-ray tube and crystal spectrometer as the principal technique used for Compton profile

measurements. A detailed description of the experimental arrangement and the data processing procedures has been given in this thesis.

In retrospect it can be seen that in the years immediately following the revival of the technique in 1965, the pursuit of qualitative results of general interest took some precedence over efforts to establish and improve the accuracy and reliability of the experimental method. It was not until 1970 that an x-ray measurement of the Compton profile of helium was made by Eisenberger[4] which provided direct confirmation of the claimed experimental accuracy. It is perhaps unfortunate that the long photon mean free paths in a gas leads to a negligible amount of multiple photon scattering, otherwise the problem of multiple scattering might have been recognised earlier. However, it was only with the introduction of the gamma ray technique that the effects of multiple scattering became clear. Experimental profiles with differences an order of magnitude greater than the statistical errors could be observed simply by interchanging thick and thin samples. It was soon established that the largest single factor contributing to the discrepancy between theory and experiment (and between various experiments!) arose from the neglect of multiple scattering effects. A major part of the work reported in this thesis is therefore concerned with the problem of including these effects in the analysis of experimental profiles.

An experimental profile contains a superposition of profiles arising from both single and multiple photon scattering. The task of separating these contributions cannot be accomplished by any practical method without making radical changes to the experimental arrangement. Instead it is

necessary to calculate and subtract the multiple contribution from the measured profile.

A theoretical treatment, with the use of approximate analytical formulae, established some of the general features of the intensity and spectral distribution of multiple scattered photons while also illustrating the limitations of a purely analytical approach. Furthermore it has been shown that the profile from multiple scattered photons can be predicted accurately with the use of the Monte Carlo technique, whereby the passage of a photon through matter is treated as a series of elementary events with each event having a characteristic probability. The Monte Carlo method is used to follow the life histories of a large number of test particles and the result is therefore a simulation of a real experiment. When multiple scattering effects are removed from experimental Compton profiles the resulting curves are seen to be independent of the sample geometry. This was demonstrated with profiles of water measured at different sample thicknesses, and the corrected profile also shows very good agreement with a recent near Hartree-Fock calculation. The predictions of the Monte Carlo program were further confirmed by a measurement of the ratio of the total elastic and Compton cross sections, from which an experimental figure for the total amount of multiple scattering can be obtained. Now that these results have established the reliability of the Monte Carlo procedure, a major source of systematic error can be eliminated from future profile measurements. Several applications of the Compton scattering technique are reported in this thesis, and in each case multiple scattering is shown to play an important role.

The electron distribution in aluminium has been the focus of considerable attention, stemming partly from the conflicting

evidence of x-ray diffraction measurements of the core electron charge distribution[5]. Although the results of a Compton scattering experiment could bear upon this problem, the main advantage of a Compton profile measurement lies in the sensitivity of the profile to the outer, conduction electrons.

Aluminium is generally regarded as a good example of a free electron metal. Although a measurement of the Compton profile made with MoKα x-rays indicated a significant departure from the free electron representation for the conduction electrons, a Monte Carlo analysis showed that multiple scattering was responsible for at least part of this discrepancy. Because a gamma-ray profile which has been corrected for multiple scattering provides a more reliable measurement of the electron momentum distribution, a second measurement was made using gamma-rays from an Am^{241} source. The final, corrected profile indeed shows improved agreement with the free electron gas model. However, if the effects of electron-electron correlations are included and the conduction electron wavefunctions are also made orthogonal to the core electron wavefunctions,[6] then the agreement is excellent. No deviations from free atom behaviour were observed for the core electrons, which is consistent with the latest x-ray diffraction results. This Compton profile measurement highlights the differences between Compton scattering and x-ray diffraction measurements. The conduction electrons make little contribution to the diffraction maxima, and the information from x-ray diffraction experiments is therefore largely limited to the core electron distribution. On the other hand, it has been shown that provided multiple scattering has been taken into account, accurate and reliable distributions for the conduction electrons

can be obtained from a Compton profile measurement.

Gamma-ray Compton profiles were also obtained for several molecular systems. The aim of this work was to extend the range of experimental data to include large molecules in order to assess the reliability of both localised molecular orbital (LMO) and semi-empirical descriptions of the electron momentum distributions in these complex systems. The success of the LMO model for the simpler hydrocarbons has already been demonstrated in the experimental studies made by Eisenberger and Marra[7]. The molecules investigated in the present work were formamide (NH_2COH), p-benzoquinone ($C_6H_4O_2$) and decaborane ($B_{10}H_{14}$). In each case the Monte Carlo procedure was employed to correct for the effects of multiple scattering.

The experimental results were compared with profiles derived from LMO[8] and iterative extended Huckel methods[9] and, in the case of formamide, also an ab initio SCF calculation.[9] Although there is fairly good agreement between theory and experiment for both formamide and p-benzoquinone, in no case is the agreement complete. In particular the LMO model is unsatisfactory at very low values of momenta, and this is probably a consequence of obtaining the LMO's from calculations on small, light molecules where there is none of the delocalisation which can be expected in the larger molecules. For decaborane the simple three-centred bond approach to boron hydride chemistry, quantified through the application of LMO's, has shown itself capable of accurately describing the momentum distribution and Compton profile of at least one boron hydride. The experimental work is being extended to include studies on both the boron hydrides and carboranes with x-ray and gamma-ray techniques.

In conclusion, the work reported in this thesis has shown

that it is essential to take account of multiple scattering effects in experimental Compton profiles. A Monte Carlo approach has been adopted which can be used to calculate and subtract the contribution from multiple scattered photons from the measured profiles. This method was tested in various ways and used to correct several experimental profiles. These experiments show how a technique which is particularly sensitive to the distribution of the outer electrons in an atom can be used in the study of both metallic and molecular systems. In the next section recent developments in the experimental method are discussed and the final section contains some suggestions for future work.

7.2 Developments in the Experimental Method.

Various experimental arrangements can now be employed in Compton profile measurements. The optimum method for a particular experiment depends on the nature of the investigation, and in this section the x-ray and gamma-ray techniques are assessed in the light of the limitations imposed by resolution and intensity. Some alternative methods for measuring electron momentum distributions are also briefly discussed.

7.2.1 X-ray Experiments.

Although the x-ray method can provide the best momentum resolution ($\sim$ 0.25 a.u.), the low Compton intensity which results from photoelectric absorption imposes a severe restriction on the range of materials which can profitably be studied with these low energy photons. Moreover, it is becoming clear that at these energies ($\sim$ 20 keV) the failure of the impulse approximation can give rise to significant systematic errors. Preliminary work by Mendelsohn and Biggs[10] has shown that there are differences between 'exact' hydrogenic and impulse approximation calculations. The exact calculation

uses non-relativistic hydrogenic bound state and continuum wavefunctions, rather than the plane wave states which are the basis of the impulse approximation. For high energy gamma-rays an impulse approximation calculation is satisfactory, whereas for the lower energy gamma-rays an exact calculation is necessary. This results in profiles which vary according to the incident photon energy and implies that the profiles have become 'experiment dependent' at the lower energies. The situation deteriorates further as the atomic number of the scattering material increases.

It is likely therefore that x-ray Compton scattering will mainly become a specialised tool for high resolution studies of light materials for which the impulse approximation is always valid. The boron hydrides provide a good example of materials which are suitable for this type of measurement and such work is now in progress. Crystal anisotropy measurements can provide an alternative application for x-rays. In anisotropy experiments a difference profile is obtained by subtracting profiles which have been measured for two different crystal orientations. This results in the cancellation of the core contributions (which are isotropic) and therefore avoids the errors associated with the failure of the impulse approximation. In these measurements the high resolution which is available with the x-ray technique is invaluable, since the anisotropy may be present only as narrow oscillations in the difference profile.

7.2.2 Gamma-ray Experiments.

The first gamma-ray measurements of Compton profiles were made by Felsteiner, Fox and Kahane[11] in 1970 and 1971 using an Am^{241} source. The technique was soon adopted by several other groups and gamma-rays from both Am^{241} and Te^{123m}

sources were used. Unfortunately, sources which provide a strong, single, isolated line in the energy range 50 - 500 keV are uncommon. Some of the available sources are listed in table 7-1, together with details of their energy and half-life and the momentum resolution which can be attained with each source. For comparison the resolution of the x-ray system is also given.

Several favourable factors make Am^{241} the easiest source to use in Compton scattering experiments. It is available cheaply commercially, has a long half-life and presents few problems for handling and shielding. Unfortunately at 60 keV there can still be a large loss of Compton intensity due to photoelectric absorption, and this limits the range of systems which can be conveniently studied to those containing elements with atomic number below about 30. However, the major drawback of an Am^{241} source is the low momentum resolution which can be achieved at these energies with a Ge (Li) detector. It is necessary to make a careful optimisation of the deconvolution procedure and use a residual instrumental function when making a comparison with a theoretical profile, (the use of a residual instrumental function is discussed in Appendix II). With these precautions the use of Am^{241} source can provide a simple and reliable method for Compton profile measurements, particularly when resolution is not a crucial factor (i.e. where the profile is wide and smooth). For other applications such as anisotropy measurements, where the structure in the profiles may be much narrower than the resolution function, then the information which can be obtained is largely qualitative.

Several profile measurements using gamma-rays from a Te^{123m} source have been reported[12] despite the difficulties

Table 7-1

A selection of sources with strong, single lines in the energy range 50 - 500 keV. The approximate momentum resolution achieved with a Ge(Li) detector is given for each source.

Source	Energy (keV)	Half-life	Momentum Resolution (a.u.)
Am^{241}	60	458 years	0.65
Te^{123m}	159	104 days	0.45
Au^{198}	412	64 hours	0.35
MoKα	17.5	-	0.25

associated with the production of this source. There is a significant improvement in the momentum resolution (see table 7-1) and the use of higher energy photons largely removes any limitations arising from photoelectric absorption. Therefore, provided it becomes more readily available, Te^{123m} will probably replace Am^{241} in most Compton scattering applications.

Au^{198} is the final source shown in table 7-1 and this source has not yet been employed in Compton profile measurements. There are clearly some problems arising from the very short half-life which make it necessary to irradiate the source in a fast neutron reactor every few days to reverse the decay process. However, such facilities are available at the Institute-Laue-Langevin, Grenoble, and Compton profile measurements using Au^{198} are to be performed in the near future by the author.

7.2.3 Alternative Experiments.

There are at least three alternatives to Compton scattering for measuring electron momentum distributions. These are positron annihilation, fast electron scattering and (e,2e) angular correlations. Each of these techniques involves the interaction of a probe with an atomic electron, and the observation of one or both of the products of the interaction. In this section the advantages and disadvantages of the different techniques are outlined.

Positron annihilation angular correlation.

A measurement of the angular correlation of photons produced in a two-gamma annihilation process can be related to the momentum of the electron-positron pair at annihilation, and hence to the electron momentum distribution in the target material[13]. The technique offers considerably better

resolution than Compton scattering and, since the positron samples the outer electrons preferentially, the information about the shapes of Fermi surfaces is particularly good. In angular correlation work the two photons are measured in coincidence and the counting rates are necessarily low. However, the main problem with this technique lies in the knowledge of the positron wavefunction which is required in order to interpret the measured angular distributions. The positron is influenced by its environment, showing preference for the more negatively charged regions, and is also remarkably sensitive to the structural defects in the sample. Although these features can be utilised in various applications their general effect is to throw some doubt on the reliability of the electron momentum distributions which are extracted from angular correlation curves.

High energy electron scattering.

High energy electrons ($\sim$40 keV) are scattered by dilute, well collimated molecular beams and, at some fixed scattering angle, the energy loss spectra of the scattered electrons is measured.[14] The use of an electrostatic velocity analyser to measure the energy spectra leads to a resolution some 20 times better than Compton scattering. Combined with the advantages of low background and high intensity these features make high energy electron scattering an extremely attractive technique. Unfortunately the problem of multiple scattering limits the applications to very dilute gases. Also the exchange and two electron corrections can be quite significant and these effects are difficult to treat theoretically.[15]

(e,2e) angular correlation.

In this technique a beam of electrons are scattered off a sample and the directions and kinetic energies of both

scattered and ejected electrons are measured in coincidence.[16] Information can then be obtained about the electron momentum distribution and the binding energies of the target electrons. Therefore, provided the differences in orbital binding energies are greater than the instrumental energy resolution, it is possible to separate and measure the momentum distribution of an individual orbital. The possibility of obtaining the electron momentum distribution for electrons in a particular orbital is a major development. At present, however, the low resolution (about 4 times less sensitive than Compton scattering), combined with low count rates, result in measured momentum distributions of rather low accuracy.

From these brief comments gamma-ray Compton scattering emerges as the best single technique from the point of view of experimental simplicity, resolution and statistical accuracy. Furthermore, a wide range of systems can be studied with this method. In the following section certain applications of the technique are discussed and some suggestions made for future work.

7.3 Future applications.

Since the revival of the Compton scattering experimental work in 1965, there has been considerable progress both in the experimental method, and in the theoretical understanding of electron momentum distributions. The development of gamma-ray Compton scattering has extended the range of systems within the scope of the experimental technique so that the Compton profile of any material can now, in principle, be measured accurately. Moreover, it is now possible to eliminate the major sources of systematic error, thereby greatly improving the accuracy and the reliability of the experimental results. Although there is

clearly a wealth of potential applications, it is important to select those applications most appropriate to the technique (taking account of the limitations of resolution and intensity) and to ensure that where possible the experimental results are supported by theoretical work. The likely developments in some of the present lines of investigation are discussed below, together with suggestions for future work.

(i) Crystal anisotropy measurements.

In the study of molecular systems described in Chapter 6, it was shown that for these isotropic systems (i.e. liquid and powder samples) the theoretical profiles are somewhat insensitive to the accuracy of the wavefunction used in the calculation. This is not surprising since the profile is the result of an integration over all angles which tends to smooth out the directional nature of the electron density. These results suggest that, when studying solid-state systems, measurements should be made on single crystals in various crystallographic directions in order to obtain both the Compton profile and the anisotropy of the electron momentum density. Indeed several such measurements have already been reported using both x-rays[17] and gamma-rays[18] and these studies have illustrated the sensitivity of the Compton profile anisotropy to the nature of the bonding in various solids.

Although these preliminary results are most promising, there are several reasons for caution before drawing quantitative conclusions from the experimental anisotropy curves. The major problem arises from the low momentum resolution, particularly in the gamma-ray experiment, which limits the observation to those gross features which can generally be explained by qualitative arguments alone. The detail which may be predicted by a full band structure calculation is just beyond the present resolving

power of the apparatus. Moreover, no reported measurements have been corrected for multiple scattering and, as pointed out in Chapter 4, multiple scattering tends to 'wash out' some effects, reducing the degree of anisotropy without changing the qualitative behaviour. Finally there has been a dearth of theoretical results for single crystals which has limited the quantitative information which could be extracted from the available data.

Despite these cautionary comments, the additional information which can be extracted from Compton profiles associated with particular crystallographic directions should encourage further experimental and theoretical work. The limitations of low resolution are now better understood, and a residual instrumental function can be used to determine the effect on any predicted anisotropy. Moreover, the introduction of an Au^{198} source in gamma-ray measurements would lead to a marked improvement in the resolution. Most importantly the problem of multiple scattering can now be overcome with the use of a Monte Carlo procedure of the type described in this thesis. The absence of theoretical support for experimental anisotropy measurements continues to be a problem, but in a few cases, such as the transition metals, some recent calculations are available.(1

(ii) Relativistic Compton profiles.

Mendelsohn, Biggs and Mann[20] have recently calculated Compton profiles from numerical nonrelativistic and relativistic Hartree-Fock wavefunctions for the rare gases and lead. These results predict a flattening of the profiles in the relativistic calculations, reducing J(0) in lead (Z = 82) by over 5%. Experimental results for the heavy atoms are scanty (the intensity decreases rapidly because of photoelectric absorption) and krypton (Z = 36) is the highest atomic number for which a profile

is available for comparison with this theory. Unfortunately the relativistic effects in this case are small and both calculations fall within the experimental error bars. The use of an Au^{198} source with a gamma-ray energy of 412 keV should permit the profiles of heavier atoms to be measured without difficulty and in the case of lead, for example, present levels of accuracy ($\sim 1\%$ at the Compton peak) are enough to provide conclusive results.

(iii) Chemical bonding in molecular systems.

Differential experiments, where attention is focussed on the differences between two profiles which have been measured on related systems under identical experimental conditions, can provide a very sensitive technique for studying the bonding in molecules and solids. The latter case has already been discussed in connection with anisotropy measurements, where profiles are measured along different crystallographic directions in the same material. The use of such an approach can minimise the effects of almost all the systematic errors. There are already a few examples of this technique applied to molecular systems where, for example, the Compton profiles of three isomers of molecular formula $C_4H_8O_2$ (dioxane, isobutyric and n-butyric acids) were compared with one another and also with profiles calculated using localised molecular orbital wave-functions.[21] It is anticipated therefore that the preliminary measurement of a boron hydride reported in Chapter 6 will become part of an extended study of several boron hydrides. The structure of carborane ($B_{10}C_2H_{12}$) is very similar to decaborane ($B_{10}H_{14}$) with carbon replacing two of the hydrogen atoms, and this molecule presents another attractive extension of the boron hydride work.

Summary

The past decade has seen the revival of Compton scattering from obscurity into a powerful research tool. However, it has taken ten years to develop the technique to the point where an experimental accuracy of one per cent can be claimed and accepted. The introduction of gamma-ray Compton scattering has vastly extended the range of applications and the electron momentum distribution in any material can now, in principle, be measured. The work reported in this thesis is concerned primarily with both practical and theoretical aspects of the technique itself, but the applications to metallic and molecular systems demonstrate the potential of Compton scattering in the study of the electron structure of matter and its sensitivity to the behaviour of the outer electrons which are responsible for bonding and cohesion. The technique has far more possible applications than are discussed above and this selection represents only those applications which can be expected to be developed in the near future and at the present level of accuracy and reliability. Experience has shown that the technique is developing, and any improvements will give rise to a host of other fruitful applications.

References for Chapter 7

(1) DuMond, J.W.M., and Kirkpatrick, H.A., (1937), Phys. Rev., 52, 419.

(2) Cooper, M.J., Leake, J.A., and Weiss, R.J., (1965), Phil. Mag., 17, 1079.

(3) Felsteiner, J., Fox, R., and Kahane, S., (1970), Phys. Lett., 33A, 442; Reed, W.A., and Eisenberger, P., (1972), Phys. Rev., A5, 2085.

(4) Eisenberger, P., (1970), Phys. Rev., A2, 1678.

(5) DeMarco, J.J., (1967), Phil. Mag., 15, 483; Raccah, P.M., and Henrich, V.E., (1969), Phys. Rev., 184, 607.

(6) Pandey, K.C., and Lam, L., (1973), Phys. Lett., A43, 319.

(7) Eisenberger, P., and Marra, W.C., (1971), Phys. Rev. Lett., 27, 1413.

(8) Lindner, P., (private communication).

(9) Epstein, I.R., (private communication).

(10) Mendelsohn, L.B., and Biggs, F., (1973), Inner Shell Ionization Phenomena and Future Applications, Vol. 3., (USAEC Conference-720404), p. 1142.

(11) Felsteiner, J., Fox, R., and Kahane, S., (1970), Phys. Lett., 33A, 442; Idem., (1971), Sol.St.Comm., 9, 61.

(12) Eisenberger, P., and Reed, W.A., (1972), Phys. Rev. A5, 2085. Reed, W.A., and Eisenberger, P., (1972), Ibid., B6, 4596.

(13) West, R.N., (1973), Adv. Phys., 22, 263.

(14) Wellenstein, H.F., and Bonham, R.A., (1973), Phys. Rev., A7, 1568.

(15) Bonham, R.A., and Tavard, C., (1973), J. Chem. Phys., 59, 4691.

(16) Hood, S.T., McCarthy, I.E., Teubner, P.J.O., and Weigold, E., (1973), Phys. Rev., A8, 2494.

(17) Phillips, W.C., and Weiss, R.J., (1972), Phys. Rev., B6, 4213; Weiss, R.J., (1974), Phil. Mag., 29, 1029; Currat, R., DeCicco., P.D., and Kaplow, R., (1971), Phys. Rev., B3, 243.

(18) Reed, W.A., and Eisenberger, P., (1972), Phys. Rev., B6, 4596. Eisenberger, P., and Reed, W.A., (1974), Idem. B9, 3242. Paakkari, T.L.P., (1974), Physica Fenn., 9, 185.

(19) Rath, J., Wang , C.S., and Callaway, J., (1973), Phys. Rev., B8, 5139.

(20) Mendelsohn, L.B., Biggs, F., and Mann, J.B., (1974), Chem. Phys. Lett., 26, 521.

(21) Epstein, I.R., Williams, B.G., and Cooper, M.J., (1973), J. Chem. Phys., 58, 4098.

APPENDIX I

The Separation of X-ray Doublets

The most intense x-ray lines, the K lines, are unfortunately not singlets, the Kα is a doublet, and the K_β a complicated multiplet. The $K\alpha_1$, $K\alpha_2$ lines have a typical separation of 5×10^{-3} Å, and an intensity ratio close to 2:1. In x-ray Compton scattering experiments the $K\alpha_1$, $K\alpha_2$ x-radiation is Doppler broadened upon scattering from moving electrons in the sample to produce spectral lines some five times broader than the $K\alpha_1$ - $K\alpha_2$ wavelength separation, i.e. the two line profiles are completely overlapped as is indicated in fig. A-1. (Typical experimental data illustrating the overlapping is given in fig. 5-1, pg. 95.) In nearly all cases the observed, instrumentally broadened, lines are centro-symmetric when analytic corrections have been applied to remedy systematic errors, such as the wavelength variation of absorption in the sample. Moreover, the lines will be of identical shape if, as is usually the case, the apparatus function is significantly broader than the natural x-ray line width.

If a thorough line shape analysis involving deconvolution forms part of the processing procedure the separation of the two components can be achieved as part of the Fourier analysis (see Cheng, Williams and Cooper[1]) but such a full analysis is not always undertaken, and the iterative method of Rachinger[2] which can be performed rapidly 'by hand' is frequently used to separate out the $K\alpha_1$ component. Alternatively the separation can be made by employing a little used technique, first published by Papoulis[3] in 1955, which takes advantage of the

Fig. A-1: The broken line represents an observed spectral line which is composed of contributions from a $K\alpha_1$, $K\alpha_2$ doublet with a wavelength separation Δ .

ts an
posed
ublet

centro-symmetry of the constituent lines. Data taken from the x-ray Compton scattering experiment on aluminium described in Chapter 5 are used to compare the two techniques.

If an observed spectrum $I(\lambda)$ is composed of two similar components (see fig. A-1) $h(\lambda)$ and $rh(\lambda)$ where Δ is their mutual separation, and r the ratio of their intensities, then it is a straightforward matter to obtain an expression for the line shape $h(\lambda)$. The result, first given by DuMond[4] in 1933 is:

$$h(\lambda) = I(\lambda) - rI(\lambda - \Delta) + r^2 I(\lambda - 2\Delta) \ldots r^n(-1)^n I(\lambda - n\Delta) \qquad A\text{-}1$$

The result was also given by Rachinger in a form suitable for iteration, vis:

$$h(\lambda) = I(\lambda) - r\, h\,(\lambda - \Delta) \qquad A\text{-}2$$

The iteration starts at a point in the short wavelength tail of the profile where it can be assumed that $h(\lambda) = I(\lambda)$ if $r < 1$. Calculation is often simplified by taking $r = \frac{1}{2}$ which is a good approximation for most x-ray doublets, for example $r = 0.527$ for MoKα x-rays.

The difficulty encountered with Rachinger's method is that errors accumulate as the iteration proceeds across the profile. These errors can become particularly large on the long wavelength side since the statistical errors associated with the second and third terms in eqn. A-1 may exceed the error in the first term. Spurious "bumps" in the data therefore propagate errors which reappear at intervals equal to the $K\alpha_1 - K\alpha_2$ spacing, unless some smoothing procedure is first applied. Unfortunately smoothing may remove features of physical significance.

The symmetric method described below avoids such difficulties because it produces an expression for the true curve containing only two terms. Referring to fig. A-1, and

letting λ_1, λ_2 represent the wavelengths of the peaks of the $K\alpha_1$ and $K\alpha_2$ profiles, and h_1, h_2 the $K\alpha_1$ and $K\alpha_2$ profiles respectively,

$$I(\lambda_1 - x) = h_1(\lambda_1 - x) + h_2(\lambda_1 - x)$$
$$= h_1(\lambda_1 - x) + rh_1(\lambda_1 - \Delta - x)$$
$$I(\lambda_2 + x) = h_1(\lambda_2 + x) + h_2(\lambda_2 + x)$$
$$= h_1(\lambda_1 + \Delta + x) + rh_1(\lambda_1 + x)$$

then by symmetry $I(\lambda_2 + x) = h_1(\lambda_1 - \Delta - x) + rh_1(\lambda_1 - x)$

Hence $$h_1(\lambda_1 - x) = \frac{1}{1 - r^2}\left(I(\lambda_1 - x) - rI(\lambda_2 + x)\right) \qquad \text{A-3}$$

A point in the true profile is therefore found by using two experimental points only. The error associated with a derived point is $E^2(\lambda_1 - x) + E^2(\lambda_2 + x)^{\frac{1}{2}}$ where E represents the absolute error in the experimental data. Error bars are typically increased by about 60%. The separation process does not "force" the profile $h_1(\lambda)$ to be symmetric, if it is not, since different experimental points are used to deduce $(h_1(\lambda_1 - x)$, and $h_1(\lambda_1 + x)$ in eqn. A-3. A comparison of the separated K_1 data folded about the line $\lambda = \lambda_1$ provides a valid test of the hypothesis that the line is symmetric.

Compton scattering data were taken from the experiment described in section 5.2 in which a single crystal of aluminium was irradiated with $MoK\alpha_1\alpha_2$ radiation. The data were corrected for systematic errors and the results interpolated at equal intervals. The $K\alpha_1$ Compton component was then separated out by Rachinger's method. The results, for the portion of the profile near the peak, are shown in fig. A-2(a). The separated curve is folded about the centre of the Compton shifted $K\alpha_1$ line and the results plotted as percentage differences between points equidistant to the left and right. The discrepancies are much larger than the errors on the original data, ($>1\%$ as compared with $<\frac{1}{2}\%$) and are not

Fig. A-2: The deviation from centrosymmetry for the Compton profile of aluminium. Both sets are derived from the same experimental data, plot (a) by the Rachinger method and plot (b) by the symmetric method.

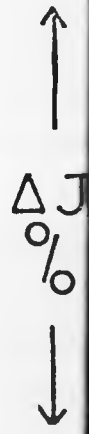

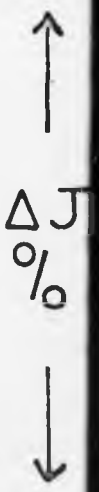

symmetry

. Both

imental

od and plot

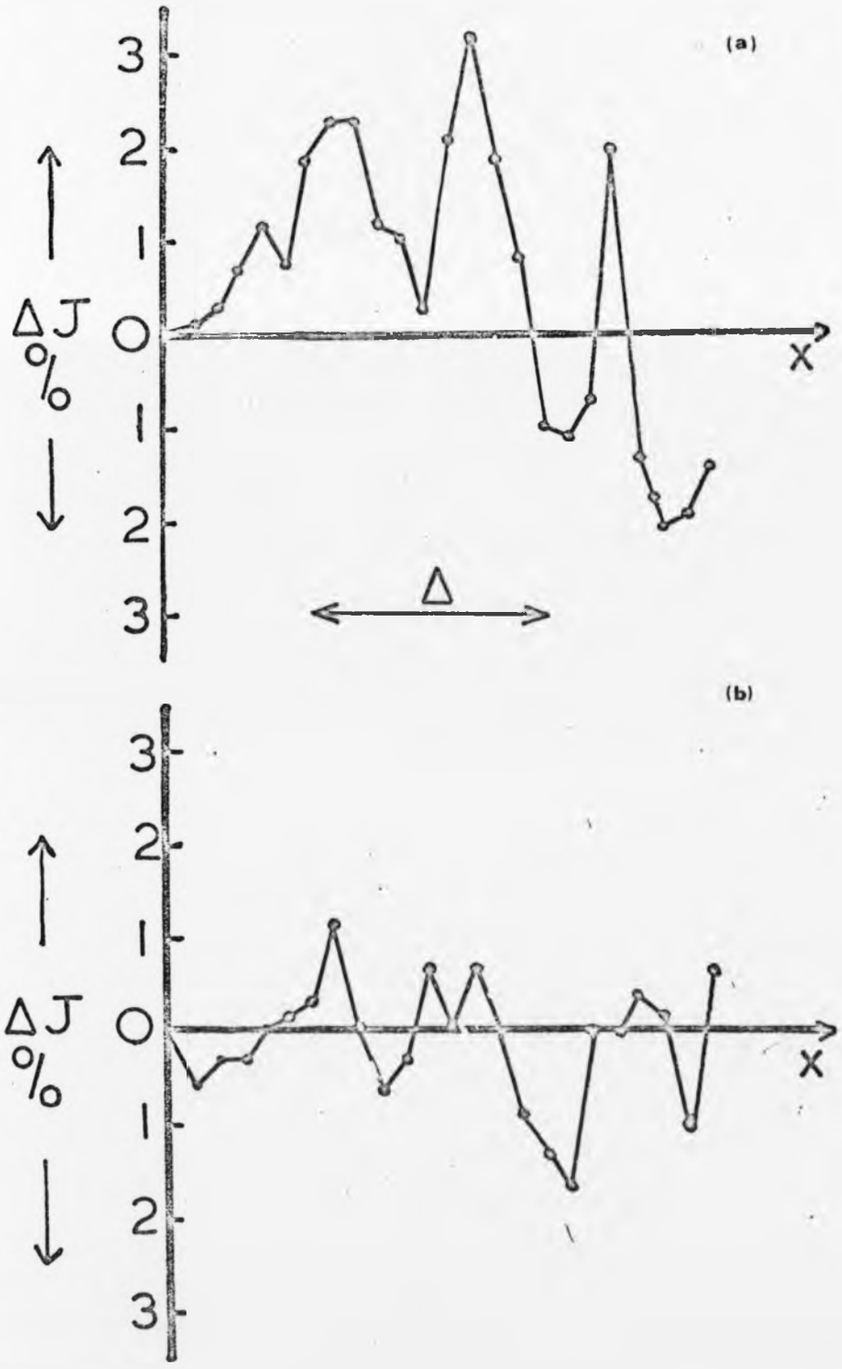

entirely random, reflecting the magnification of errors inherent in the Rachinger process, or the incorrect application of the asymmetric analytic corrections.

Fig. A-2(b) shows the result of separating out the $K\alpha_1$ component from the same data on the assumption that the line is symmetric. The position of the $K\alpha_1$ Compton peak was taken from the result of the Rachinger process - it is necessary to know this position fairly accurately, otherwise a trial and error approach will need to be adopted.

A comparison of figs. A-2(a) and A-2(b) shows that the latter reveals a large improvement. The deviations from centro-symmetry are not statistically significant. Furthermore the computation is just as simple as that involved in the iterative method.

APPENDIX II

The Deconvolution of Compton Profiles

The line shape I(x) observed in an experiment may differ appreciably from the true spectrum F(x) because of the finite resolution of the apparatus. The intensity at some point x_o can be expressed as a convolution process,

$$I(x_o) = \int_{-\infty}^{\infty} T(x - x_o)\, F(x)\, dx \qquad \text{A-4}$$

where $T(x - x_o)$ is the instrumental resolution function, normalised so that

$$\int_{-\infty}^{\infty} T(\delta)\, d\delta = 1 \qquad \delta = x - x_o \qquad \text{A-5}$$

The problem of recovering F(x), the true function, involves a deconvolution procedure which has been the subject of considerable attention. In particular the deconvolution of Compton profiles has been discussed by Cheng, Williams and Cooper[1] where the measured curve was expressed as a sum of basis functions (in this case a finite sine/cosine series) for which the deconvolution can be carried out analytically. In a recent report Paatero, Manninen and Paakkari[5] made a survey of the commonly used deconvolution schemes, and concluded that the method of generalised least squares is the most reliable.

The experimental profiles given in this thesis are deconvoluted by the graphical reconstruction technique described by Lloyd.[6] Here the expression for $I(x_o)$ given in eqn. A-4 is expanded in a Taylor series, and inverted to yield

$$F(x_o) = I(x_o) - S\left\{\tfrac{1}{2}\left[I(x_o + a) + I(x_o - a)\right] - I(x_o)\right\} \qquad \text{A-6}$$

S is called the instrumental factor and is defined by

$$S = \frac{1}{a^2} \int_{-\infty}^{\infty} \delta^2 T(\delta) d\delta \qquad \text{A-7}$$

For a Gaussian resolution function $\frac{1}{2\alpha} \exp\left[-\frac{\pi}{4}\left(\frac{\delta}{\alpha}\right)^2\right]$ the instrumental factor is given by

$$S = \left(\frac{2}{\pi}\right)\left(\frac{\alpha}{a}\right)^2 \qquad \text{A-8}$$

where 2a is the FWHM of the Gaussian.

The application of Lloyd's method of deconvolution increases the error on the final curve by a factor of about 2.5. This increased error arises from the use of three points on the experimental curve ($I(x_o)$, $I(x_o-a)$, and $I(x_o+a)$) to reconstruct the deconvoluted curve at each point x_o. If higher orders in the Taylor expansion are used in the deconvolution there is a further increase in this error factor. From the error factor, a confidence band can be constructed around the deconvoluted profile. However, the confidence band is not an upper and lower bound for the true unknown function F(x), but for the deconvolute which would be obtained if the measurement could be performed without error, and the deconvolution procedure applied to this error-free result.

A more reliable comparison between a deconvoluted experiment and a theoretical prediction for the profile can only be achieved with the use of a residual instrumental function (RIF). No deconvolution of an experimental profile can remove all of the resolution effects, and the RIF is the residual smearing which remains after the deconvolution procedure has been applied. The RIF can be obtained by deconvoluting the resolution function itself. The result is shown in fig. A-3 where (a) is the resolution function, and (b) is the residual function left after deconvolution. Thus when a measured result is to be compared with a theory which predicts a

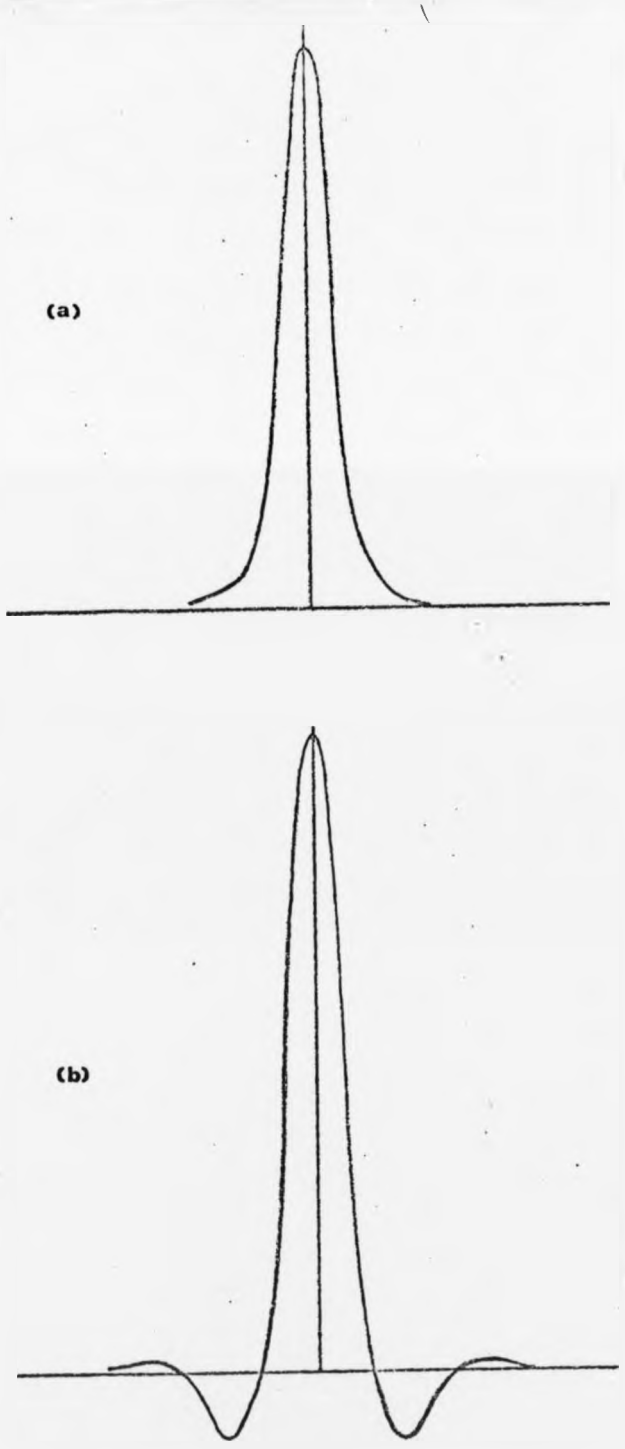

Fig. A-3: (a) The instrumental resolution function and (b) the residual instrumental function (RIF) after deconvolution.

certain F(x), the convolute of this F(x) with the RIF should be compared with the deconvolute of the experimental profile. This procedure has been followed in all comparisons with gamma-ray profiles reported in this thesis. The effects of convoluting the theoretical profile with the RIF are most significant where there is a sharp break in the profile (e.g. at the Fermi momentum in aluminium, Chapter 5), or where the profile is very narrow (e.g. $B_{10}H_{14}$, Chapter 6).

References for Appendix I and II

(1) Cheng, R., Williams, B.G., and Cooper, M.J., (1971), Phil. Mag., 23, 115.

(2) Rachinger, W.A., (1948), J. Sci. Instrum., 25, 254.

(3) Papoulis, A., (1955), Rev. Sci. Instrum., 26, 423.

(4) DuMond, J.W.M., (1933), Rev. Mod.Phys., 5, 1.

(5) Paatero, P., Manninen, S., and Paakkari, T., (1974), Phil. Mag., 30, 1281.

(6) Lloyd, K.H., (1969), Am. J. Phys., 37, 329.